ALMA MATER STUDIORUM - UNIVERSITÀ DI BOLOGNA

SCHOOL OF SCIENCE
Department of Industrial chemistry "Toso Montanari"

Corso di Laurea Magistrale / Master

Advanced Spectroscopy in Chemistry

Classe LM-71 - Scienze e Tecnologia della Chimica Industriale

Investigation of the reactivity of metal oxide catalysts for the gas-phase phenol methylation

Experimental Master Thesis

Candidate:
Dauren Zhambakin

Supervisor:
Prof. Fabrizio Cavani

Co-supervisors:
Dr. Carlo Lucarelli
Dr.Tommaso Tabanelli

Academic Year 2013-2014

CONTENTS

CHAPTER 3 – RESULTS AND DISCUSSIONS

OBJECTIVES

Alkylphenols are essential chemicals and intermediates which are used in a wide range of applications such as agrochemical, pharmaceutical, polymer industries and other. Cresols and xylenols are fundamentally used as intermediates in the manufacturing of a multiple products such as pharmaceuticals, disinfectants, dye stuffs, antioxidants, pesticides, phenolic resins and others.

Nowadays synthetic cresols and xylenols could be produced by methylation of phenol with methanol in the presence of catalysts. The process consists of only one reaction step, but is relatively expensive, due to costly separation of products from the reaction mixture.

Therefore, one of the central problems is selectivity and conversion of catalysts. Also, according to the literature, for successive methylation of phenol, major role is assigned to methanol conversion to formaldehyde. There are a lot of discussions on these themes. Hence, the aim of this research work is a deeper understanding of the reaction pathways, activity of catalysts, interaction of reactants with surface of the catalysts, with all the possible intermediates and products.

The particular interests represent the redox type catalysts, with different ratio of iron and aluminum in vanadate phase. The list of studied catalysts include $FeVO_4$, $AlVO_4$, V_2O_5 and $Fe_xAl_{1-x}VO_4$ (x= 0.2; 0.6; 0.8). The coupling of catalytic tests with spectroscopic investigations was important for full coverage of the process research.

Uses of spectroscopic techniques were essential to obtain information that could be helpful for understanding the processes on surface of catalyst, changes concerning catalysts and reactants from the molecular level. X-ray diffraction and in-situ Raman spectroscopy was used in order to investigate behavior of the catalyst while Diffuse reflectance infrared spectroscopy coupled to mass spectrometry (DRIFT-MS) and in-situ infrared spectroscopy in vacuum were used to study the way of adsorption, transformation of reactants, intermediates and desorption of products on the surface of the catalysts at reaction conditions.

CHAPTER 1 - INTRODUCTION

1.1 Overview of alkylphenols

1.1.1 Properties of phenol and alkylphenols

Phenol is a white amorphous material at ambient temperatures. It has a melting point of 40,9^{o}C. In the molten state phenol is a clear and colorless liquid. When exposed to air, phenol rapidly changes to a pink color due to certain trace impurities like iron and copper that are present in its production process or during storage. The melting and solidification temperature is lowered considerably by traces of water - approximately 0.4^{o}C per 0.1 wt% water. Phenol is soluble in aromatic hydrocarbons, alcohols, ketones, ethers, acids, and halogenated hydrocarbons. [1]

The chemical properties of phenol are unique. They are due to the presence of a hydroxyl group and an aromatic ring which are complementary to each other in facilitating both electrophilic and nucleophilic type of reactions. The unshared electron pair located on the hydroxyl group is delocalized over the aromatic ring leading to an electron excess at the ortho and para positions. [2,3]

Phenol's unique ability to react with formaldehyde under acidic or basic conditions leading either to novolaks resins (via acid conditions) or resole resins (basic conditions), were the resin reactions that fostered the commercialization of phenolic resins. [2, 3]

Alkylphenols are phenols with one or more of the aromatic hydrogens being replaced by an alkyl group. Cresols are monomethyl derivatives of phenol. Xylenols are dimethyl derivatives.

Cresols only slightly less acidic than phenol. The cresols together with phenol are labeled as hazardous air pollutants (HAPs). The presence of the methyl group on the ring increases the boiling point compared to phenol. The boiling points of *m*- and *p*-cresols are very similar which makes separation through distillation impossible. Due to hydrogen bonding between the two adjacent functional groups on the ring, *o*-cresol has a much lower boiling point at 191.0°C and is readily separated from the other two isomers and in high purity. [4]

Xylenols or dimethylphenols are available as six isomeric forms, see Table 1. They are all crystalline materials at room temperature. Compared to cresols, xylenols are less soluble in water, but can still be extracted from organic mixture with aqueous caustic soda. Xylenols can be recovered from the same natural sources as cresols and phenol.

In Table 1.1, the main physical properties of these various phenols are summarized.

Table 1.1 Physical properties of selected phenols [4,5]

Name		MW	MP(^{o}C)	BP(^{o}C)	pK_a 25^{o}C
Phenol	Hydroxybenzene	94,1	40,9	181,8	10,0
o-Cresol	2-methylphenol	108,1	31,0	191,0	10,32
m-Cresol	3-methylphenol	108,1	12,2	202,2	10,09
p-Cresol	4-methylphenol	108,1	34,7	201,9	10,27
2,3-xylenol	2,3-dimethylphenol	122,2	72,6	216,9	10,54
2,4-xylenol	2,4-dimethylphenol	122,2	24,5	210,9	10,60
2,5-xylenol	2,5-dimethylphenol	122,2	74,9	211,1	10,41
2,6-xylenol	2,6-dimethylphenol	122,2	45,6	201,0	10,63
3,4-xylenol	3,4-dimethylphenol	122,2	65,1	227,0	10,36
3,5-xylenol	3,5-dimethylphenol	122,2	63,3	221,7	10,19

1.1.2 Uses and applications of alkylphenols

Alkylphenols are important chemicals and intermediates which are used in a wide range of applications such as agrochemical, pharmaceutical and polymer industries. Alkylphenols are largely used as intermediates in the manufacturing of a variety of products such as disinfectants, dye stuffs, antioxidants, optical brighteners, flavours and fragrances. [6]

o-Cresol (ortho-methylpehnol) is processed to epoxy-*o*-cresol novolak resins. Also it is used to modify phenol-formaldehyde resins [1[sp]]. In agricultural chemicals *o*-Cresol is used for manufacturing of *p*-chloro-*o*-cresol, which is in turn used in the production of phenoxyacetic acid (MCPA) and phenoxy propionic acid (MCPP) herbicides. [6] *o*-Cresol is used in the production of coumarin, which is used in the flavour and fragrance industry. *o*-Cresol is used in the production of *o*-cresotinic acid, which is weighty in the pharmaceutical industry.[4]

m-Cresol could be converted to *m*-phenoxytoluene, which is oxidized to *m*-phenoxybenzyl alcohol and traded to manufacturers of pyrethoid insecticides. In fabrication of antioxidants *m*-Cresol is used to produce 6-*t*-butyl -*m*-cresol (TBMC), an intermediate in the manufacturing of hindered phenolic antioxidants. *m*-Cresol is used to make several fragrances and flavours. For instance thymol (5-methyl-2-isopropropylphenol), which could be synthesized by Friedel -Crafts alkylation of *m*-cresol with propylene, is used in some liniments, balms and antiseptics, and as a precursor in the synthesis of L-menthol. One of the largest use of *m*-cresol is in the production of vitamin E where it is methylated to form trimethylhydroquinone (TMHQ), followed by the reaction with isophytol to yield d-alpha-tocopherol (synthetic vitamin E). Synthetic vitamin E also produced from trimethylphenols. Other uses of trimetylphenols such as 2,3,6- and 2,4,6-trimethylphenol in fields of antioxidants and plastics. [4]

p-Cresol (para-methylphenol) is a significant intermediate in the production of antioxidants and preservers for plastics, foods and motor oil. [7] *p*-Cresol, pure or mixed with *m*-cresol, is used to produce 2,6-di-*t*-butyl-*p*-cresol (BHT), a non-staining and light-resistant antioxidant with a wide range of applications. *p*-Cresol is used as an intermediate to make *p*-methylanisole (p-cresol methyl ether), for the production *p*-anisaldehyde, which is used in the fragrance industry. 6-methylcoumarin, another flavour and fragrance chemical, could be manufactured by the addition of fumaric acid to *p*-cresol. [4]

2,6-xylenol (*2,6*-dimethylphenol) is used largely as monomer for poly(phenylene oxide) (PPO) which is used to make Noryl - thermoplastic resin distinguished by high impact resistance, thermal stability, fire resistance, and dimensional stability. Oxidation of *2,6*-xylenol gives *2,6*-xylenol dimer, a specialty monomer to produce epoxy resins for encapsulating advanced semiconductors. Other applications are mainly as phenolic resins, disinfectants and antioxidants. [4]

1.1.3 Sources of Alkylphenols

The oldest source of alkylphenols is a coal tar, which is obtained during the production of metallurgical coke by the coking of bituminous coal between 900 and 1300ºC. The crude coal tar is distilled into four types of oil and in the light and middle oil fractions cresylic acid is primarily present. Washing of these fractions with caustic soda solution removes the sodium cresylates, from which undesirable components can be removed by steam distillation. Cresylic acid recovered from coal tar contains usually 45% phenol, 35% cresols, 15% xylenols, and 5% other phenolic homologues. [8]

Refinery spent caustic method of alkylphenol separation is mostly employed in the United States. The cresols and xylenols are obtained from the naphtha fraction produced in catalytic and thermal cracking processes in the petrochemical industry. The phenolic compounds are extracted during the removal of sulphur compounds that contained in these fractions, by scrubbing with concentrated alkaline solutions. The phenols are then precipitated from the alkaline phase in a packed column with a countercurrent stream of carbon dioxide and decanted. A typical composition of the phenol mixture obtained is approximately 20% phenol, 18% *o*-cresol, 22% *m*-cresol, 9% *p*-cresol, 28% xylenols and 3% higher phenols. [8]

Specific cresol and xylenol isomers have been produced synthetically since 1965. These processes are based on either phenol or toluene and are, therefore, more expensive compared to the isolation of cresol and xylenol as co-products. The synthesis of methylated phenols offer some control over regioselectivity and can lead to the synthesis of high purity products.

Sulfonation of toluene, followed by neutralization, sodium hydroxide fusion and hydrolysis, is used to produce mainly *p*-cresol. This process is analogous to the production of phenol from benzene through sulfonation, except that the rate of toluene conversion is far greater. A typical isomer distribution of 80- 85% *p*-cresol, 6-12% *o*-cresol, and 6-12% *m*-cresol is obtained. Milder reaction conditions can reduce the *m*-cresol content, while *o*-cresol is easily separated by distillation. Generally, *p*-cresol of up to 90% purity can be produced in this manner. Sulfonation processes had been operated in the USA, Japan and the United Kingdom. Overall yields are typically around 80% and can be improved by altering the temperature and acid strength during the sulfonation step, and by using a higher concentration of base (NaOH) in the fusion step. [4, 8, 9]

A mixture of cresol isomers can be obtained by the chlorination of toluene and subsequent hydrolysis in the presence of sodium hydroxide at elevated temperature and pressure. The basic reaction is analogous to the production of phenol from chlorobenzene. This process results in larger amounts of byproducts compared to the previous processes, including such compounds as dimeric and polymeric ethers, small amounts of toluene, phenol, benzoic acid, and methane and hydrogen gas. Here yields are not higher than 70%. The resulting cresol mixture classically contains 60% of *m*-cresol, the rest being *p*- and *o*-cresol in an approximate 1:1 ratio. Different cresol mixtures had been produced according to this process in the United States, Japan, India and the United Kingdom. [4, 8, 9]

Commercial processes based on the acid cleavage of cymene hydroperoxide produce cresol mixtures containing approximately 60% *m*-cresol and 40% *p*cresol.

3,5-Xylenol is produced in the United Kingdom by demethylation of isophorane. The reaction can yield up to 80% 3,5-xylenol, depending on the catalyst used. Side products include toluene, 1,3-xylene, mesitylene, *m*-cresol, 2,4- and 2,5-xylenol, and 2,4,6-trimethylphenol. After work-up, 3,5-xylenol is obtained in 99% purity. [4, 8, 9]

Analogous to the large-scale industrial process for the direct hydroxylation of benzene to form phenol, toluene can be hydroxylated with hydrogen peroxide to form cresols. Acid and transition metal catalysts could be used for this transformation. Side-chain oxidation occurs in competition with ring hydroxylation. However, the use of shape selective microporous catalysts like clays, and titanium zeolites can result in largely controlled ring-hydroxylation reactions. Alcoholic media tend to favor *para*-selectivity. Although not yet optimized for large-scale application, this reaction can yield cresols with 80% selectivity (typically 1.33:1 *p*-:*o*-isomers) at 58% conversion of toluene in butanol. [10-17]

The use of Vanadium-based catalysts in acidic media for the hydroxylation of aromatics had been reported. [18] In this system, hydrogen peroxide is generated *in situ* by the air oxidation of hydroquinone. The hydrogen peroxide subsequently oxidizes the vanadium species to an active oxide, which acts as the hydroxylating agent.

1.2 Gas phase methylation of phenol

The alkylation of phenols is a very important industrial reaction. Olefins, alcohols and alkyls halides might be used as alkylating agents. Preferred alkylating agents for industrial purposes are methanol and dimethylcarbonate. More conventional reactants, such as methylchloride and dimethylsulphate, although still employed industrially, are less attractive nowadays due to environmental concerns [19].

Phenol methylation process is alkylation of phenol with methanol. It is used to produce mainly *o*-cresol, 2,6-xylenol and trace amounts of 2,4,6-trimethylphenol. Reaction conditions can, in some cases, be adjusted to promote the selectivity for one of the products.

Industrially the phenol methylation process is carried out by means of three main types of processes: i) liquid-phase methylation; ii) fixed-bed liquid-phase methylation; iii) gas-phase methylation. When the reaction is carried out in the liquid phase it gives numerous products and their separation is very difficult and complicated. In opposite gas-phase alkylation is simpler, more selective and doesn't require complicated separation of products.

Classically gas phase methylations produce mainly 2,6-xylenol, while liquid phase methylations yield *o*-cresol as the main product, The other products being *p*-cresol, 2,4- and 2,6- xylenols in a typical 7:5:2 ratio, respectively. Yields of up to 98% (based on phenol) have been reported for the gas phase reaction. Common side products include water, methane gas, carbon monoxide and carbon dioxide. This process is currently used worldwide to produce almost the entire supply of 2,6-xylenol. [4,8,9]

General Electric of USA had been producing 10,000 tpa o-cresol and 70,000 tpa 2,6-xylenols, in USA, and in Holland further, 4000 tpa o-cresol and 16,000 tpa 2,6-xylenols. Synthetic Chemicals, UK (later on taken over by Inspec and now Laporte) had been producing 8000 tpa o-cresol and 2,6-xylenols in UK. There has been production of o-cresol and 2,6-xylenols in Japan, Russia, and Czech Republic. [20]

1.3 General types of catalysts in a gas phase methylation of phenol

Generally and historically it is accepted that there are two types of catalysts for phenol methylation process.

Depending on the catalysts and on the reaction conditions the process can be chemoselective to C-methylated (ring methylated) or O-methylated (ether) phenols and regioselective to ortho-methylated or para-methylated phenols.

1.3.1 Catalysts possessing acid characteristics

Among catalysts having Bronsted-type acid characteristics, the most studied are (i) phosphates (e.g., $AlPO_4$, Re phosphates, BPO_4) [21-33], (ii) γ-Al_2O_3 or doped with alkali or alkaline earth metal ions, to possess some basic-type characteristics [34-41], and (iii) zeolites, similarly in this case sometimes exchanged with alkali or alkaline earth metal ions [42-52].

Catalysts with Bronsted-type acid characteristics are highly active, and great conversions of the aromatic substrate can be reached at relatively moderate temperatures (300-350°C). The main characteristics of these catalysts are preferred formation of the product of O-methylation (etherification), especially for less acid catalysts. It is in general accepted that C-alkylation requires stronger acidic sites than for O-alkylation [25,31,53-55], and without a doubt less acid zeolites are more selective to anisole than to cresols [42,56,57]. With relatively weak acidic sites anisole itself may then act as a methylating agent at higher reaction temperature, and support the formation of cresols, which become the dominant products for higher reactant conversion (and temperature), together with polymethylated phenols and polymethylated anisoles. The direct formation of cresols may instead occur with more acid catalysts, in competition with the O-methylation reaction. [58]

Therefore, the acid strength and control of reaction parameters, especially temperature, are key parameters to obtain high selectivity to desired product. Among cresols, the orthoisomer is the preferred one, against classical rules which govern the electrophilic substitution in aromatics. A slight enhancement of the para/ortho-C-alkylated selectivity ratio can be obtained through exploitation of the shape-selectivity effects in zeolites, but nevertheless this ratio remains lower than the expected one.

1.3.2 Catalysts possessing basic characteristics

With catalysts having basic characteristics and using methanol as alkylating agent the ortho-C-methylation reaction is preferred. Industrially these catalysts are used for the production of o-cresol and 2,6-xylenol. Catalysts are made of either (i) supported and unsupported alkali and alkaline-earth metal oxides, or (ii) transition or post-transition mixed metal oxides, or (iii) mixed oxides containing both alkaline-earth metals and transition metal ions. [19]

The basicity of catalysts is fundamentally related to the properties of the O^{2-}anion, and therefore to the covalent character of the Me-O bond in the oxide. The strongest ones are alkali and alkaline-earth metal oxides, which however may deactivate by some interaction with acid molecules such as carbon dioxide and water. For that reason from the industrial point of view, preferred catalysts are those based on either supported V/Fe mixed oxides [59], or Mn oxide-based systems [60], or doped MgO [61].

These catalysts may also possess Lewis-type acid characteristics towards the aromatic ring; this interaction further enhances the selectivity to the products of ortho-C-methylation, with negligible formation of the product of O-methylation and of that of para-C-methylation [62-65]. Therefore, general characteristics of catalysts possessing basic features are: (i) the very high regioselectivity in C-methylation, where the ortho- to para-C-methylation ratio, though being in all cases largely higher than 2, is yet affected by catalyst characteristics, and (ii) a O-selectivity to C-selectivity ratio, which is a function of the basic strength of catalysts, which in general is low, and becomes close to zero for catalysts having bifunctional properties.

1.4 The Mechanism of the methylation of phenol through phenol activation

The very high regio-selectivity in basic-catalyzed phenol methylation, if compared to acid-catalyzed methylation, is explained through the commonly accepted Tanabe's model [58,66]. This model describes the vertical adsorption of the phenate anion over the oxide surface, because of the repulsion between highly nucleophilic O^{2-} anions and the aromatic ring. Consequently the para position becomes less accessible for attack by adsorbed methanol, while the ortho positions, closer to the surface, are readily available.

A pioneer in the study on the mechanism of alkylation of hydroxyarenes was Klemm [67-73], who was the first to point out the importance of the geometry adsorption on the regioselectivity of phenol and 1-naphthol methylation. In 1-naphthol methylation catalyzed by alumina [68] the products found were naphtyl ethers, methylated naphtols (especially at T lower than 350°C, amongst which the most important one was 2-methyl-1-naphthol, followed by 4-methyl-1- naphthol; the yield to these compounds fell to zero at high T), and methylated naphthalenes (the prevailing products a t T > 350°C, were dimethyl, trimethyl and tetramethylnaphthalene), and small amounts of 1-oxo-2-methyl-1,2- dihydronaphthalene and 1-oxo-2,2-dimethyl-1,2-dihydronaphthalene at low temperature. The necessary presence of the arenolic group for effective ring methylation was established, which also oriented the regio-selectivity.

Tanabe [58,66,74] demonstrated that in solids having acid characteristics, an interaction also develops between the aromatic ring of the phenolate anion and the catalyst surface, while the same did not occur in the case of catalysts having basic characteristics, such as MgO. As a consequence of this, in the former case, the plane of the benzene ring is close to the surface, and any position can be methylated, while in the latter case only the ortho position is close to the surface, and can be methylated. Therefore, the model attributes to a geometric factor the high regioselectivity typical of the basic catalysis. This model has been invoked by the vast majority of papers dealing with the reaction of phenol or diphenols methylation with catalysts having basic characteristics, to justify the high regioselectivity to the product of ortho-C-methylation. An alternative explanation has been provided by Grabowska et al [75,76], to justify the high ortho-C-methylation selectivity in the basic-catalyzed reaction between 1-naphthol and methanol, for the production of 2-methyl-1-naphthol, intermediate for the synthesis of vitamin K3 with the Vikasib technology. The authors hypothesized that the coordinative properties of Fe^{3+} might favour the adsorption of both naphthol (after abstraction of the proton) and methanol over the same site; as a consequence of this, the ortho position is in close proximity of methanol. Also in this case, the model is essentially adsorbitive/geometric. Gopinath et al [63] also identified by means of IR study the development of formaldehyde, dioxymethylene, formate species by feeding methanol over Cu/Co/Fe/O catalysts, with decomposition at above 300°C, but due to the competition of phenol for adsorption on the same sites responsible for methanol oxidation, the latter did not apparently occur in the contemporaneous presence of the two compounds. Therefore, the authors proposed a mechanism in methanol is adsorbed on

protons released by phenol, and the protonated methanol interacts with the ortho position of phenol. The same authors obtained spectroscopical evidences about the perpendicular orientation of phenol and phenolate [77,78], and attributed to this the high selectivity to the product of ortho methylation. However, while in the alkylation of alkylbenzenes (e.g., toluene) with methanol it is possible to obtain high selectivity to the para-C-alkylated compound, even in the case of the acid-catalyzed alkylation of activated arenes, such as phenol and diphenols, and aniline as well, with olefins or with alcohols, the product of para-electrophilic substitution is obtained with lower selectivity than the expected one, even with zeolites catalysts [79]. On amorphous acid catalysts, the selectivity to o-cresol can even approach 100% [27,48,80]. The thermodynamic equilibrium ratio between para and ortho-cresol at 380°C is close to 0.43 (the statistical kinetic ratio is instead 0.5), but experimental ratios are usually lower than these values, and only in a few cases values higher than 0.7 have been reported [81] thanks to the exploitation of shape-selectivity effects, and to the enhancement of diffusional effects in larger crystalites.

In general, an interaction between the alkylating agent and the O atom of phenol, which favours the alkylation at the ortho position [44,45,48] Beltrame et al [48] formulated the hypothesis of a reaction between adsorbed anisole, which acts as the alkylating agent, and gas-phase phenol, in which the interaction between the two O atoms puts the methyl group of anisole closer to the ortho position of phenol. It is relevant the observation that even in homogeneous acid electrophilic substitution on phenols, usually ortho/para ratios higher than the statistic value 2/1 are found [79]. This implies that adsorbitive/geometric effects are not the main reason for the regioselectivity observed. So, the overall mechanism for the acidcatalyzed methylation of phenol [79] includes direct C alkylation at the ortho and para positions (in confined environments the direct para-C-alkylation can be preferred), and O-akylation to yield anisole, the ratio C/O-alkylation being a function of the catalyst acid strength. The consecutive intramolecular rearrangement of anisole to o-cresol makes the final ortho/para-C-alkylation ratio to become very high, especially in less acid catalysts (i.e., on amorphous materials).

Most models described in literature refer to the Tanabe's one, and thus are primarily centred on the mode of adsorption of phenol. Methanol is assumed to adsorb on surface, develop the methoxy species or simply be activated by interaction with the acid-base pairs, but in most cases no specific role is attributed to methanol concerning the

reaction pathway or mechanism. Nevertheless, various literature demonstrated that methanol undergoes different transformations, depending on the catalyst surface properties [82-84].

1.5 The role of methanol in the gas-phase methylation of phenol

One of the major problems of the industrial process of phenol methylation is that due to decomposition of methanol there is a low yield with respect to it. Consequently a big excess of methanol is usually fed in order to reach satisfactory per-pass conversion of phenol. Numerous solutions have been proposed to minimize this side reaction [85], among which the co-feeding of water appears as the most effective [59, 86]. This aspect, however, is often forgotten in some scientific literature, and only few papers take into consideration the methanol decomposition [87-91] and the transformations that take place with the alkylating agent. On the other hand, a various literature demonstrates that methanol undergoes different transformations on metal oxides, depending on the catalyst surface properties [82-84].

In the 1960's infrared spectroscopy studies have verified that the chemisorption of methanol on alumina leads to the formation of methoxide in the 35-170 °C range; its transformation at higher temperatures into formate-like surface compound [92, 93] is supplemented by evolution of H_2, with the likely intermediate formation of formaldehyde [67].

Some reviews have studied the nature of the species that develop by interaction between methanol and redox-type solid oxides [90, 91]. The interaction with cations having Lewis-type acid characteristics yields non-dissociated CH_3OH*ads, bonded species [94]. Dissociated methoxy species are favorably formed over basic oxides (Bi_2O_3, Fe_2O_3, NiO, ZnO, ZrO_2). The covalent and Lewis-type acid oxides (WO_3, SiO_2, V_2O_5, Nb_2O_5, MoO_3) and amphotheric oxides (CeO_2, TiO_2) produce both non-dissociated and dissociated terminal methoxy species. [95]

The interaction of methanol with non-reducible metal oxides has been the object of some investigations as well. MgO is known to catalyze the dehydrogenation of methanol to formaldehyde [96]. Methanol undergoes to physisorption, chemisorption or heterolytic dissociation [97] *via* acid-base mechanism, with formation of the CH_3O^- species. [98] The development of the adsorbed formate species occurs through a Cannizzaro-type reaction with intermolecular disproportionation. Nucleophilic attack of

the O^{2-} surface species to the carbonyl (with development of the formate), is accompanied by a hydride transfer to a second molecule of adsorbed formaldehyde, which is converted to a methoxy species. [99, 100] The formate may finally decompose to CO and H_2, without any supply of O^{2-} from the solid.

An overview of the interactions that formaldehyde may be developed by metal oxides has been described in the review of Barteau [84]. Over redox-type oxides (ZnO, CuO, etc.), formaldehyde gives rise to adsorbed formates, with incorporation of the O^{2-} species. The nucleophilic attack on the carbonyl moiety happens with the concomitant abstraction of an H^+ by a second O^{2-} species. A nucleophilic attack of surface O^{2-} at the carbonyl produces a dioxymethylene complex, further evolved to the formate species. Desorption of HCOOH, or its decomposition, leads to the reduction of the metal ion. Formic acid on alumina may decompose either through a dehydrative path to H_2O + CO, or through a dehydrogenative path to H_2 + CO2 [100-102], *via* intermediate surface formate species [103]. The formation of methylformate from methanol may occur through different mechanisms, depending on the nature of the oxide (either easily reducible or non-reducible), the conditions (temperature, pressure, presence of H_2O), and the surface concentration of formaldehyde, the latter being predominantly a function of the dehydrogenative properties of the oxide. Methylformate decomposes to yield either CH_4 + CO_2 or CH_3OH + CO, or gives back formaldehyde through a reverse Tischenko reaction [90]. In the presence of water, methylformate decomposes to formic acid and methanol. Concluding, some examples exist in literature describing that methanol go through several transformations on metal oxides, depending on redox characteristics of the cation and on the “basicity” of the oxygen anion.

Concerning acid catalysts, one of the main points regarding methanol mechanism was discovered by feeding formaldehyde to different acid catalysts and obtaining the same products with similar yield as feeding methanol in presence of basic catalysts. Thus, the role of formaldehyde as real active alkylating agent was proved. [19]

1.6 Redox type catalysts

Since activation of alkylating agent plays huge role in methylation of phenol some search on methanol to formaldehyde transformation literature was done. From previous sections it could be obvious that some redox type catalysts activate both methanol and phenol.

In the area of alternative catalysts that are used for the production of formaldehyde from methanol and air, several studies have been reported on vanadia-based catalysts including pure vanadia, mixed oxides, and supported vanadia. [104-107] In particular, vanadates with Ni, Fe, Co, Mg, Cr, Mn, Al, Ag, Cu, and Zn have been found to have selectivities >90% to formaldehyde at high methanol conversion. [108-112] According to Wachs et al. [111], the vanadium in bulk metal vanadates is not volatile in methanol oxidation, although XPS analysis before and after use of the samples in methanol oxidation indicated some structural changes in the surface and near surface layers during catalysis. Besides the surface structure, such changes may involve the formation of new phases; in oxidation catalysis on bulk metal oxides, not only the surface, but also the catalyst bulk structure may change under the influence of the catalytic reaction until steady state is reached. [113]

Consequently, in the work of Häggblad et al. [114], in more detail the performance and the stability of a $Fe_{1-x}Al_xVO4$ series of catalysts with x varying from 0 to 1 was investigated. Their findings indicate that catalysts prepared in the form of phase pure triclinic $Fe_{1-x}Al_xVO4$ phases with 0 - x -1 were active and selective for methanol oxidation to produce formaldehyde. Compared with pure vanadia, the vanadates were less active per vanadium atom and per unit surface area, but more selective to formaldehyde (~90% vs 87%). Substituting Al for Fe gave slightly improved activity but had no notable effect on the selectivity to formaldehyde. The activity data indicate that the electron density on a bridging V–O–M (M = V, Al, Fe) oxygen determined the activity, with increasing activity expressed per V atom decreasing the electronegativity of the M metal. The improved selectivity to formaldehyde of the vanadates compared with pure vanadia suggests that the Al and Fe in the structure create isolation of V and decrease the number of less-selective V–O–V sites. XRD and XANES showed that the triclinic $FeVO_4$ phase was unstable under the reaction conditions and formed a cationvacant spinel-type $Fe_{1.5}V_{1,5}O_4$ phase. Substituting Al for Fe in the catalyst gave more stable bulk structures. [114]

$FeVO_4$ is known not only as methanol oxidation catalyst but also as catalyst for the alkylation of phenols. Redox catalysts that are already available for gas phase methylation of phenol are described in some Japan, British and US patents. Inventions refer basic and redox type oxides of the metal known to exist such as V_2O_5, V_2O_4, V_2O_3, VO, Fe_2O_3, Fe_3O_4, FeO, MgO, TiO_2, MnO_2, MnO, Mn_3O_4 and to mixtures of these various oxides. [59-61, 115]

1.7 Introduction to Infrared and Raman spectroscopy techniques

One of the first modern spectroscopic techniques that found its wide application in catalysis is infrared spectroscopy. The furthermost and contemporary use of the technique in heterogeneous catalysis is to identify adsorbed species on the surface of the catalyst. Additionally, the procedure is useful for understanding the way of chemisorption and identifying phases that are present in the precursor stages of the catalyst. Infrared spectra of known adsorbed molecules could offer important information about the adsorption sites of the catalyst. [116] Moreover, one of the foremost benefits of infrared spectroscopy is that the technique could be applied to study catalysts in-situ.

Infrared spectroscopy exploits the fact that molecules absorb specific frequencies that are characteristic of their structure. These absorptions are resonant frequencies, i.e. the frequency of the absorbed radiation matches the transition energy of the bond or group that vibrates. The energies are determined by the shape of the molecular potential energy surfaces, the masses of the atoms, and the associated vibronic coupling. In order for a vibrational mode in a molecule to be “infrared active”, it must be associated with changes in the dipole. A permanent dipole is not necessary, as the rule requires only a change in dipole moment. A molecule can vibrate in many ways, and each way is called a *vibrational mode.* For molecules with N number of atoms in them, linear molecules have 3N – 5 degrees of vibrational modes, whereas nonlinear molecules have 3N – 6 degrees of vibrational modes. [117]

The infrared spectrum of a sample is recorded by passing a beam of infrared light through the sample. When the frequency of the IR is the same as the vibrational frequency of a bond, absorption occurs. Examination of the transmitted light reveals how much energy was absorbed at each frequency (or wavelength). [117]

Diffuse Reflectance IR Spectroscopy (DRIFTS), which will be used in this work, is very important tool to investigate adsorbates on the surface of the catalysts. In external reflectance, the energy that penetrates one or more particles is reflected in all directions and this component is called diffuse reflectance. In the diffuse reflectance (infrared) technique, commonly called DRIFT, a powdered sample is mixed with KBr powder. The DRIFT cell reflects radiation to the powder and collects the energy reflected back over a large angle. Diffusely scattered light can be collected directly from material in a sampling cup or, alternatively, from material collected by using an abrasive sampling pad. [118]

In diffuse reflectance spectroscopy, there is no linear relation between the reflected light intensity (band intensity) and concentration, in contrast to traditional transmission spectroscopy in which the band intensity is directly proportional to concentration. Therefore, quantitative analyzes by DRIFTS are rather complicated. The empirical Kubelka-Munk equation relates the intensity of the reflected radiation to the concentration that can be used for quantitative evaluation. To obtain reproducible results, particle size, sample packing and dilution should be carefully controlled, especially for quantitative analysis. [119]

Raman spectroscopy is a spectroscopic technique used to observe vibrational, rotational, and other low-frequency modes in a system. It relies on inelastic scattering, or Raman scattering, of monochromatic light, usually from a laser in the visible, near infrared, or near ultraviolet range. Light from the illuminated spot is collected with a lens and sent through a monochromator. Wavelengths close to the laser line due to elastic Rayleigh scattering are filtered out while the rest of the collected light is dispersed onto a detector. [120]

The Raman effect occurs when light impinges on a molecule and interacts with the electron cloud and the bonds of that molecule. For the spontaneous Raman effect, which is a form of light scattering, a photon excites the molecule from the ground state to a virtual energy state. When the molecule relaxes it emits a photon and it returns to a different rotational or vibrational state. The difference in energy between the original state and this new state leads to a shift in the emitted photon's frequency away from the excitation wavelength. The Raman effect, which is a light scattering phenomenon, should not be confused with absorption (as with fluorescence) where the molecule is excited to a discrete (not virtual) energy level. [120]

CHAPTER 2 – EXPERIMENTAL PART

2.1 Catalysts preparation

$FeVO_4$ catalyst were prepared by co-precipitation from an aqueous solution containing the corresponding metal nitrates.

In order to obtain atomic ratio of iron to vanadium in the catalyst 1:1 appropriate calculating were done. To obtain 20 g of $FeVO_4$, 47,32 g of $Fe(NO_3)_3*9H_2O$ (Sigma Aldrich, 99% purity), 13,70 g of NH_4VO_3 (Sigma Aldrich, 99% purity), 105 ml *2 =310 ml of distilled water were prepared.

Ferric nitrate ($Fe(NO_3)_3*9H_2O$) was dissolved in distilled water. Aqueous solution of ammonium metavanadate (NH_4VO_3) dropwise and under stirring was added to the solution. To the resulting solution dropwise and under stirring a solution of ammonia 14% was added, following the change of pH, until it reaches pH 6,8. Under these conditions the precipitation of $FeVO_4$ occurred. After 1h of stirring the precipitate was separated by filtration, washed with excess amount of water and dried overnight at 110^{o}C. The dried mass is crushed to powder and heated 3 hours at 650^{o}C under passing air. Catalyst particles were prepared by pressing the calcined powder to obtain pellets that were then broken into smaller granules and sieved to average 30-60 mesh size.

$Fe_xAl_{1-x}VO_4$ catalysts, where x=0.2, 0.6, 0.8, were supplied by laboratory of prof. Trovarelli. To prepare the metal vanadates of the general formula $Fe_xAl_{1-x}VO_4$ (with x= 0.8, 0.6, 0.2) the calculated stoichiometric amount of iron(III) nitrate nonahydrate and aluminium nitrate nonahydrate (both Aldrich ACS reagent, 98+%) were dissolved in deionized water to yield a mixed nitrate solution. A second aqueous solution was prepared by dissolving ammonium metavanadate (NH4VO3 Aldrich ACS reagent, 99+%) in deionized water at 80°C. The two solutions were then mixed under continuous stirring and the pH value was adjusted to 4 by adding ammonia solution. The precipitate so formed was stirred, filtered, washed with deionized water and dried at 120°C overnight. The samples were thermally treated at 630°C 20h in a muffle furnace under static air atmosphere. The calcined powder was pelletized and sieved between 30 and 60 mesh sieves.

$AlVO_4$ catalyst was prepared by similar method to $FeVO_4$. It was prepared by precipitation from a homogeneous water solution containing dissolved V and Al. The homogeneous solution was prepared from two separate water solutions, NH_4VO_3 (Sigma Aldrich 99% purity) solution and a solution of $Al(NO_3)_3 \cdot 9H_2O$ (Sigma Aldrich 99% purity). Ammonium metavanadate was dropwise added to ferric nitrate under vigorous stirring. At the same time 3M HNO_3 was added dropwise in order to achieve pH1.0. By these procedures solution was mixed together and homogenised. A solid precipitate then was obtained when the pH was rapidly raised to 4.0 by the addition of 3 M NH3. The particles were separated by vacuum filtration and then washed to remove excess of anions with 3 l of water. Finally, the samples were dried for 16 h at 110^{o}C and then calcined for 3 h at 650^{o}C. The calcined powder was pelletized and sieved to an average particle size of 30-60 mesh.

As **V_2O_5** catalyst was used industrial V_2O_5 bought in (Sigma Aldrich with 98% purity). Powder samples were pelletized and sieved to particles 30-60 mesh.

2.2 Catalytic tests

2.2.1 Characteristics of the plant

The plant on which the experiments were carried out could be divided into three zones: i. feeding area of the reactants; ii. reaction zone; iii. sampling zone (Figure 2.1).

In the feeding zone there are devices able to set the conditions of control supply as the input flow rate of reagents and the flow of inert gas. The elements constituting this area are listed below. Mass flow meter, which regulates and maintains a constant flow rate of the carrier gas. The inert nitrogen is used in the system. Bubble flowmeter, in order to control the flow of inert pre-set to match the flow actually delivered. High precision infusion pump, Kd Scientific 100, used to adjust the input flow rate to the reactor of the reaction mixture placed in the syringe fixed appropriately on that pump. Pressure gauge, can detect any increase in pressure within the system. Line thermostat consists of a steel tube that connects the point of mixing of the reagents with the inert gas to the input line of the reactor, maintained at a constant temperature of 250°C by means of heating bands.

The reaction zone is constituted by a glass reactor with a diameter of 1.5cm and 46.5cm long; inside the reactor is inserted a thermocouple door glass reveals that the temperature of the catalytic bed; the catalytic bed is constituted by 1cm^3 of catalyst in the form of pellets of particle size from 30 to 60 mesh, and is positioned approximately 20cm from the reactor bottom. The reactor is in turn inserted inside a tubular heating furnace, model of Carbolite MTF 12/25/250.

The output from the reactor is maintained at a temperature of 250 ° C by a band heater to prevent condensation of high boiling products prior to the collection area and sampling. The sampling area is constituted by a glass bubbler containing iso-propyl alcohol (2-propanol) in which the reaction products are solubilize, which can then be periodically analyzed by gas chromatography.

The temperature control of the heating bands placed in different zones of the system is done through a temperature controller which, when connected to thermocouples inserted between the bands, regulates the output current and maintains the set temperature.

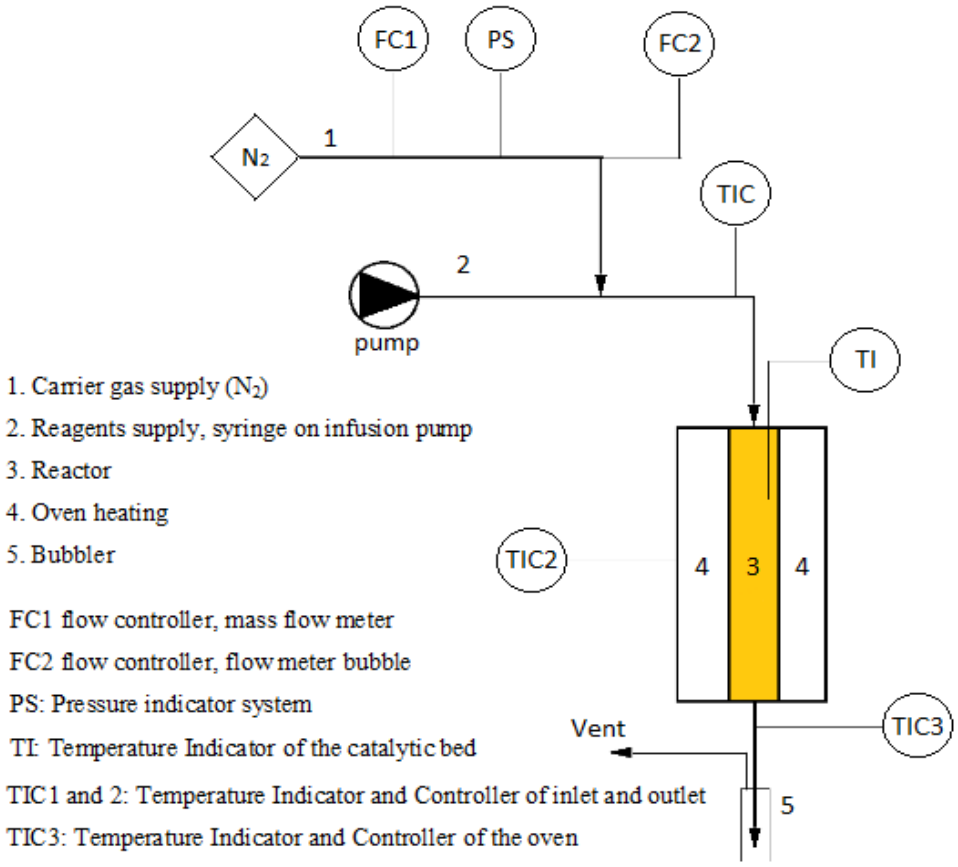

Figure 2.1 Scheme of the plant

2.2.2 Catalytic test procedure

For each catalytic test data collection is performed as described below.

Catalytic test were carried out in a downstream tubular glass reactor. Liquid reagent solutions were fed using a syringe pump, vaporized and carried by a nitrogen flow. The reactor temperature was maintained at the desired temperature by an electric furnace (MFT122525/301 Carbolite) surrounding the reactor that directed by a temperature controller connected to a thermocouple placed within the catalyst bed. In a typical reaction, the pelletized catalyst was loaded into the reactor tube to form a catalyst bed in amount of 1 ml. The reactor was purged with flowing N_2 and then heated to the reaction temperature after which the liquid organic feed (mix of methanol and phenol) was introduced. Condensable downstream were collected in a bubbler containing pure iso-propanol (2-Propanol).

Sampling accumulations are performed every hour. Ceased the accumulation time, the bubbler is removed and repositioned it immediately to another in order to immediately restart the reaction. The solution contained in the flask is poured into a 25mL volumetric flask, brought to volume and finally adding 20 μl of decane as an internal standard. At this point the solution is ready for analysis.

Optimal residence time for phenol methylation reactions were assumed as $1s^{-1}$, thus residence time was calculated for each reaction from following: catalyst volume, temperature, inert flux, syringe flux and weight percentage of phenol. Some values were maintained constant; syringe flux speed 0,46 ml/hour, catalyst volume $1cm^3$; and some values changed as needed.

2.2.3 Products analysis

The compounds accumulated in isopropanol solution during the reaction, were analyzed by a gas chromatograph (GC), Thermo Focus GC model. When necessary, recourse was made also to a gas chromatograph with attached mass detector (GC-MS).

Specifications of Gas chromatograph used for this work:

Non-polar column Agilent HP-5 (5% Phenyl - 95% methylsiloxane), 320 mM dimensions 25m X X 1:05 m; Carrier gas, nitrogen; Flame ionization detector at a temperature of 280 ° C; Injector maintained at a temperature of 280 ° C in split mode

(30:1); Nitrogen flow 36mL/min dispensed; Volume of solution injected for each analysis is 0.5 μL; Programmed temperature (30min): the oven remains in the isotherm at 50 ° C for two minutes, then starts the ramp of 10 ° C / min to reach 280 ° C where it stays isothermally for five minutes.

GC-MS specifications that were used:
Technoligies Agilent 6890 GC coupled with a mass spectrometer Agilent Technologies 5973; Non-polar column (5% Phenyl - 95% methylsiloxane), 250 mM dimensions 30m X X 1:05 m; Helium carrier gas at a flow rate in the column equal to 1ml/min; Injector maintained at a temperature of 250 ° C in split mode (50:1); total flow of 23.9 mL / min; Volume of solution injected 0.5 μL; Temperature program: isotherm remains in the oven at 50 ° C for 5 minutes, then starts the ramp of 10 ° C / min to reach 250 ° C where it stays isothermally for 10 minutes.

2.2.4 Yields, conversion and selectivity

Molar yields were calculated as follows (*n* is the molar flow).

$$\text{Yield of phenolic products} = \frac{n^{in}_{prod}}{n^{out}_{phenol}}$$

where “product” stands for *o*-cresol, 2,6-xylenol, polyalkylated phenols and others.

Conversions are expressed as follows:

$$\text{Conversion of phenol: } \frac{n^{in}_{phenol} - n^{out}_{phenol}}{n^{in}_{phenol}}$$

Selectivity to product is expressed as the ratio between the corresponding yield and the phenol conversion.

$$\text{Selectivity to product "x"} = \frac{\text{yield of product "x"}}{\text{conversion of phenol}}$$

2.2.5 Decomposition of Methanol tests

The tests were carried out by feeding on the catalyst only methanol, in order to obtain information about the decomposition which the methanol goes to meet on such catalytic surfaces to the reaction temperature (320 °C).

The plant used for these tests is substantially similar to the system previously described (Figure 2.1), with the difference that the reactor downstream is directly connected continuously with a micro-GC Agilent 3000 A. The latter is a system automated line which picks a defined amount of reaction mixture to load a loop and individually injects the mixture into three different columns.

Column A - PlotQ type, carrier N2, separates CH4, CO2, H2O, Ethanol

Column B - OV1 type, carrier N2, separates CO2 and oxygenated products C2 and C3

Column C - Molecular sieve 5 A type, carrier Ar, separating H2, O2, N2, CH4, CO.

Last column also has a pre-column PlotU type which serves to block compounds such as CO2 and H2O.

2.3 Catalyst characterization

2.3.1 X-ray diffraction

In the present research Powder X-ray diffraction (XRD) analysis of the synthesized catalysts were determined by performing Ni-filtered CuKa radiation (l = 1.54178 A) on a Philips X'Pert vertical diffractometer equipped with a pulse height analyser and a secondary curved graphitecrystal monochromator.

2.3.2 Raman spectroscopy

Using Raman spectroscopy is possible to observe the differences in the vibrational modes of the samples with respect to the composition which causes local distortions that are not seen by x-ray diffraction.

Laser Raman spectra under static conditions were recorded at room temperature using a Renishaw 1000 spectrometer equipped with a Leica DLML microscope (50X lens was used), CCD detector. Samples were excited with a diod laser beam 782 nm,

with 25 mW power. Spatial resolution is 0,5µm, spectral resolution is 1cm^{-1}. For each sample 10 second exposure and 5 accumulations were done.

2.3.3 Raman In-Situ analysis

By means of same instrument that was described above in-situ Raman analysis for adsorption of methanol on different catalysts were performed. In order to carry out reaction on higher temperatures Raman cell LINKAM Instrument TS1500 was used.

Catalyst was loaded in the cell, heated to 320^{o}C and purged with nitrogen and methanol under calculated speed. While heating and adsorbing Raman spectra was taken.

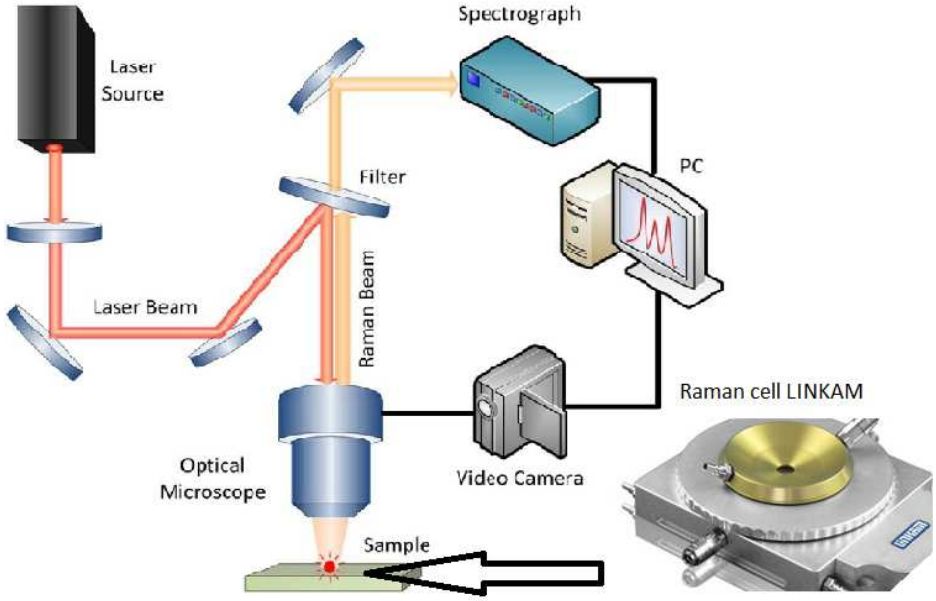

Figure 2.2 Scheme of Raman Spectrometer and image of Raman cell for in-situ investigations

2.3.4 Diffuse Reflectance Infrared Fourier Transform Spectroscopy (DRIFTS) equipped with Mass spectrometer

The in situ IR spectra were recorded using a Bruker IFS 88 FT-IR spectrometer equipped with an in situ flow cell. Methanol was vaporized in a He stream and fed to the cell. Spectra was subtracted from spectra of pure catalysts taken after heating and while cooling.

Figure 2.3 demonstrates the apparatus for the DRIFTS measurement. The infrared beam is focused by a series of mirrors on the surface of the sample, which is placed in a

sample holder. Diffuse radiation through the powder is collected by other mirrors and sent to the detector. An inlet and outlet are provided to send the gasses into the dome and through the sample. Figure 2.3 shows the path of the gases inside the dome. The gases pass through the sample from the bottom upward. This flow direction offers the advantage of thermostatically controlling the gases and tracking the surface reactions at the desired temperatures.

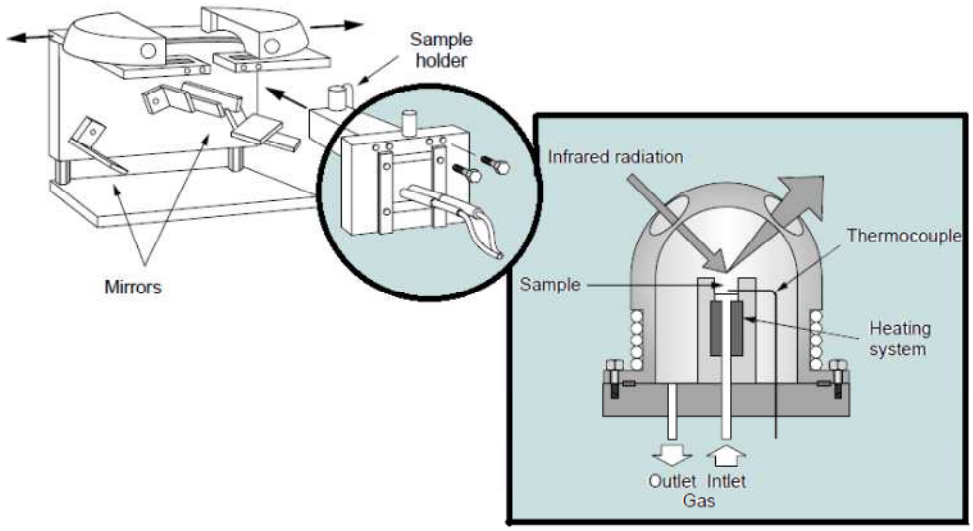

Fig. 2.3 Apparatus for diffuse reflection measurements [121]

Among the different experimental setups for infrared spectroscopy, diffuse reflectance is maybe the one giving the easiest access to the study of the surface of materials. One of the main advantages of this technique is an ease of sample preparation and the ability to analyze nontransparent materials, which could not be analyzed by transmission infrared spectroscopy. Besides, since the spectra are recorded *in situ*, one can “see” the catalyst working by monitoring the changes of species on its surface. However, the information that can be obtained by diffuse reflection infrared spectroscopy remains qualitative, because the technique does not allow high quality quantitative measurements. But, a number of methods can be considered for quantitative analysis of the gases leaving the DRIFTS cell: gas chromatography if permitted by the type and quantity of the gases to be analyzed, or mass spectrometry.

In-situ DRIFT-MASS instrument was used to study the interaction of the methanol with the different catalysts. The experimental setup is depicted on Figure 2.4 DRIFT-MASS scheme. First the sample is loaded in the sample holder and the cell is

closed and inserted into the DRIFT apparatus. Then pretreatment up to 320-450^{o}C were done, in order to remove molecules eventually adsorbed on the material, mainly carbon dioxide and water. While cooling up to 85 ^{o}C spectra of pure catalysts which were used later as a background was taken. First experiment was done under 85^{o}C adsorption. In order to feed the methanol a system was adapted to the apparatus where the alcohol is loaded in a syringe which is pushed by a pump at the desired constant rate. Subsequently, methanol is vaporized in the heating jacket and mixed with the carrier gas flow (He); finally, this gas mixture reaches the inlet of the diffusion reflectance cell and passes through the catalysts. The outlet in this case is connected to a quadrupole mass analyzer. After adsorption of methanol on the surface of catalysts, until saturation was reached (as seen by IR and MS, around 30 min) desorption at the same temperature was analyzed by DRIFT and MASS spectra. He flow was left to flow through the sample till the weakly adsorbed methanol removed. While increasing temperature up to 320 ^{o}C step by step at 125 ^{o}C, 175 ^{o}C, 225 ^{o}C, 275 ^{o}C IR spectra of desorption of physisorbed species was taken. Adsorption for 30-40 min and desorption spectra also was taken at 320 ^{o}C.

The adsorption of methanol over mixed metal oxides can lead to different kind of adsorbed species depending on the surface properties of the material under study.

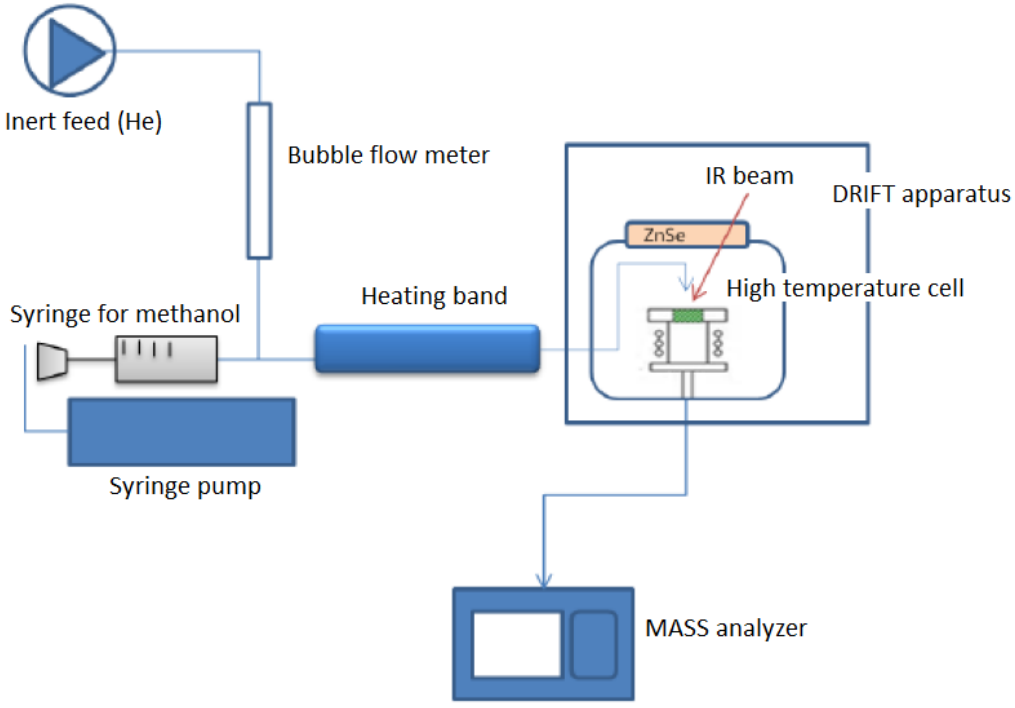

Figure 2.4 Scheme of DRIFT-MASS instrument

2.3.5 In situ Infrared spectroscopy in vacuum

The IR range is investigated between 4000 and 200cm-1 (NIR Near Infra Red).

The IR spectra discussed in this thesis have the distinction of having been derived from a sample of catalyst placed inside an instrument that serves to maintain the sample under vacuum in order to first pretreat the sample favoring the desorption of impurities and water adsorbed on the surface; subsequently adsorb the reagent of interest (phenol in our case); and then perform the desorption. The instrumentation that was used is shown in Figure 2.5 and then followed by the order of operation.

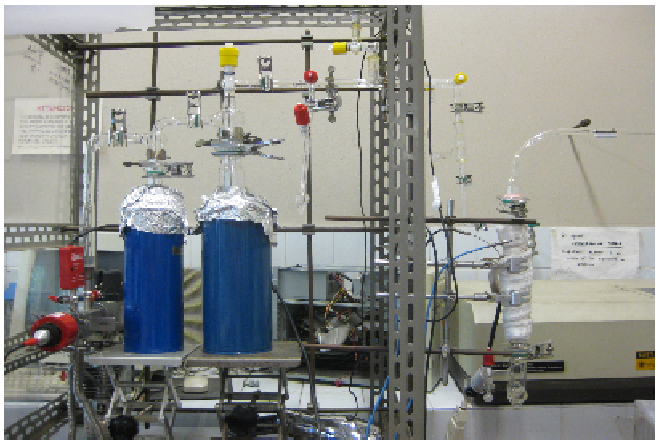

Figure 2.5 Image of a plant for in-situ infrared study of adsorption of reactants on catalysts in vacuum

To perform the IR test described in this thesis, work was operated as described below:

1) The catalyst to be examined, in powder form, was assembled in a thin rectangular tablet placed in a “slide” of quartz;

2) Such “slide” is situated in a cylindrical tube of quartz, wrapped in a heating band to its central part and terminating with a window consisting of two tablets of KBr through which pass the beam of incident radiation of the instrument. The “slide” is skated appropriately depending on where is desired that the catalyst intercepts the optical path, or both at the level of the heating bands;

3) Such a cylindrical tube of quartz is an extreme of the vacuum line, which by means of suitable fittings and taps glass seal, is provided with ampoules in which introduce reagents to be adsorbed. There are also two glass traps immersed in liquid

nitrogen during the operational phase, which protect the pump from the diffusive contact with the chemical species that are progressively desorbed from the catalyst;

4) The vacuum line as a whole is placed on a cart that allows you to place the sample to be analyzed within the instrument properly so as to intercept the optical path of the IR source. The vacuum line upstream is connected with two vacuum pumps: a mechanical pump that serves to push the vacuum up to values around 10^{-3} mbar and a diffusive pump which allows to reach the high vacuum up to 10^{-6} mbar .

5) After reaching a vacuum of between 10^{-5} and 10^{-6} mbar, and after suitably positioning the trolley with the vacuum line on the optical path, we can start the pre-treatment of the sample by heating the sample and verify, via IR, that all the impurities deposited on the surface are removed.

6) Then we cool the sample and proceed with the adsorption of the molecule of interest

7) When the IR spectra confirm the achievement of a significant evidence of the presence of reagent adsorbed, we start the desorption part, by heating the sample and recording the IR spectra at intervals of regular temperature, in order to obtain an overview of the changes that occur while increasing temperature.

CHAPTER 3 – RESULTS AND DISCUSSIONS

3.1 Catalytic tests

$FeVO_4$ is a well-studied catalyst of the (oxi)dehydrogenation of methanol to formaldehyde. As it was described in the introduction part, the properties of the catalyst to form formaldehyde plays one of the most important roles of phenol methylation, as formaldehyde is proved to be the real alkylating agent.

$FeVO_4$ catalyst was obtained as described in Chapter 2. It was found in literature and then experimentally shown that under 320°C temperature with residence time 1s we obtain successful results.

In Figure 3.1 results of the experiment carried out at optimal conditions, referring to the literature, are demonstrated.

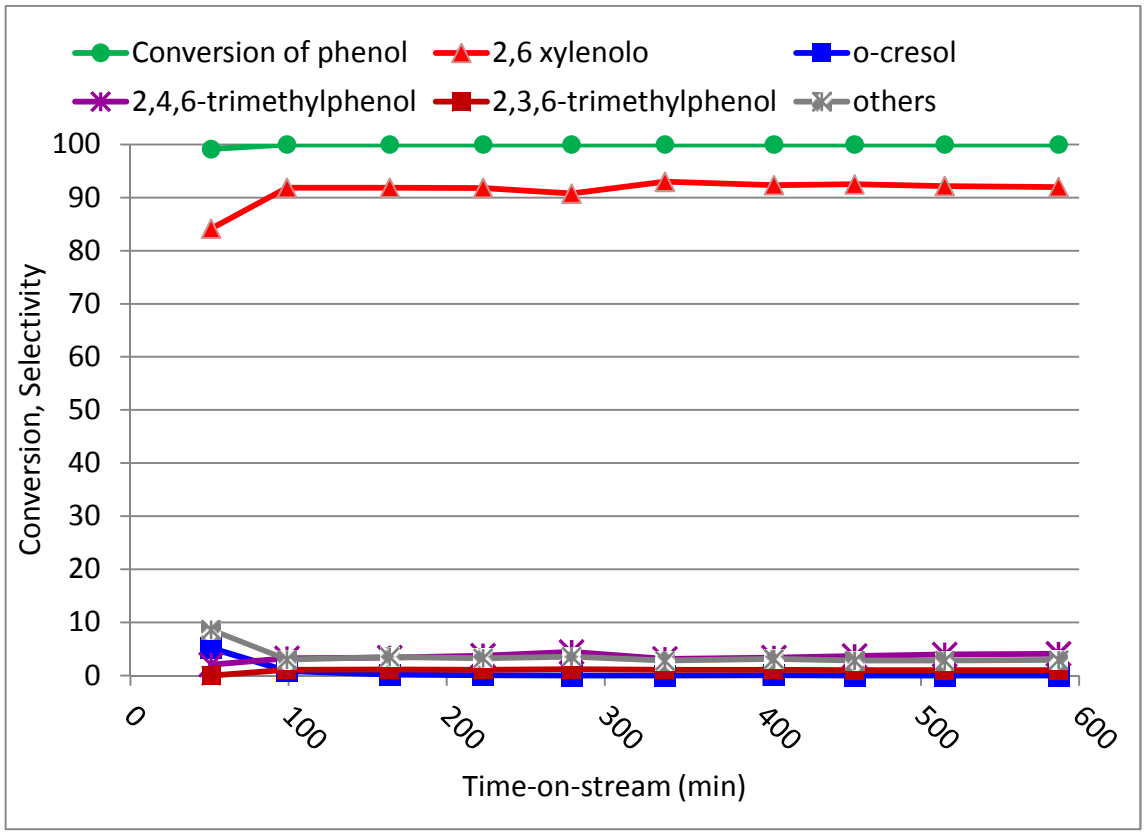

Figure 3.1 Catalytic performance in phenol methylation on $FeVO_4$ in function of time-on-stream at 320°C, residence time 1s; phenol to methanol ratio 1:10

From Figure 3.1 we see that with $FeVO_4$ as a catalyst at 320 °C a principal product of the reaction between methanol and phenol was 2,6-xylenol, with negligible

formation of o-cresol at the very beginning of the reaction and disappearance after 2 hours. The selectivity to 2,6 xylenol was very high during the experiment.

It is worth mentioning that at this conditions minor formation of 2,4,6-trimethylphenol was formed. The very high selectivity to 2,6-xylenol is proving the high selectivity to C-methylation.

From results obtained (Figure 3.1), interesting behavior of the catalyst was noticed in the beginning of the reaction. There is a slightly lower conversion, minor but noticeable change in selectivity to both mono- and di-methylation. This character hypothesized to be due to some transformation or modification of the catalyst.

In order to prove that methylation of both ortho positions are due to high coverage of the surface by adsorbed methanol species, tests with higher phenol to methanol 1/2 ratio was performed. Figure 3.2 demonstrates that using same $FeVO_4$ catalyst with higher phenol to methanol 1/2 ratio the main product is o-cresol which is a product of methylation of only one ortho position. Also in the case when less methanol amount is fed, lower conversion of phenol and resulting lower yield of products are observed.

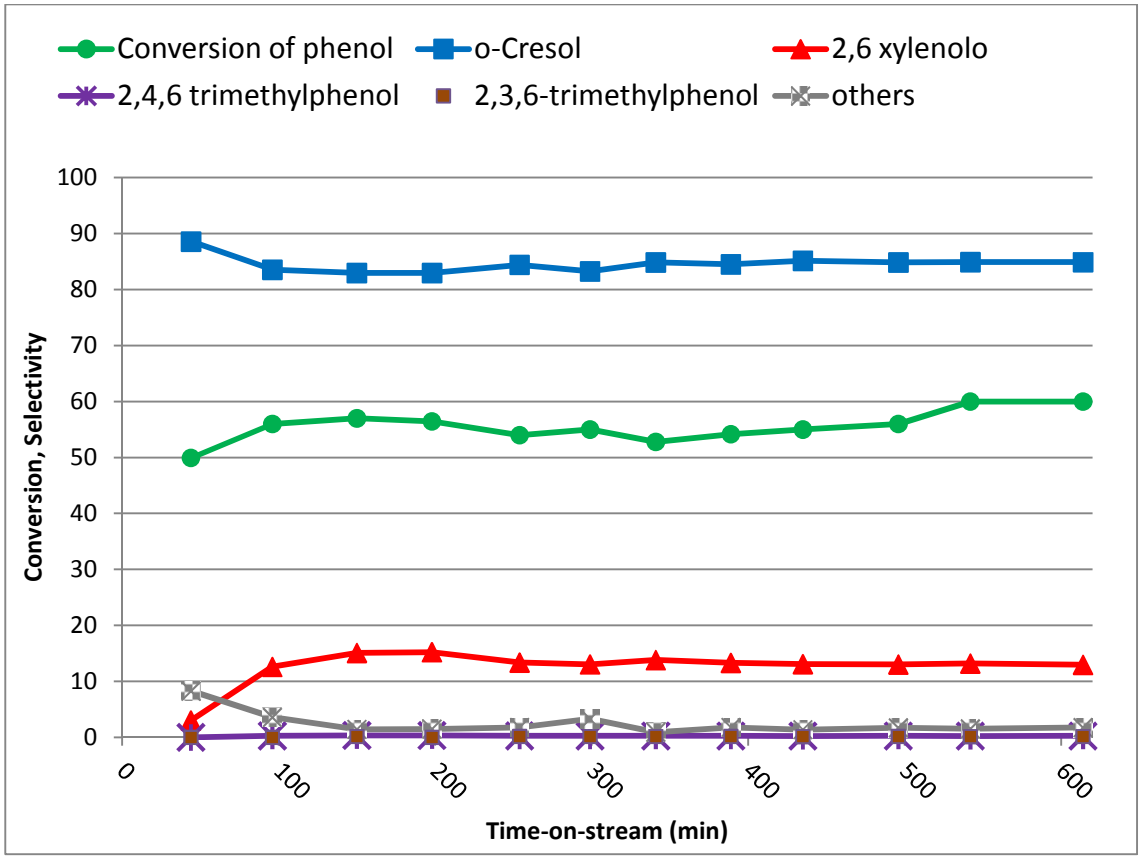

Figure 3.2 Catalytic performance in phenol methylation on $FeVO_4$ in function of time-on-stream at 320°C, residence time 1s; phenol to methanol ratio 1:2

Tests at 380°C (Fig. 3.3) and 450°C (Fig. 3.4) were carried out to prove that optimal temperature for $FeVO_4$ and similar catalysts is 320°C.

In Figure 3.3 there was some significant differences from the test at 320°C, with slight formation of highly alkylated and naphthol like products (shown in the figure with the "others"). Selectivity to main products didn't differ much.

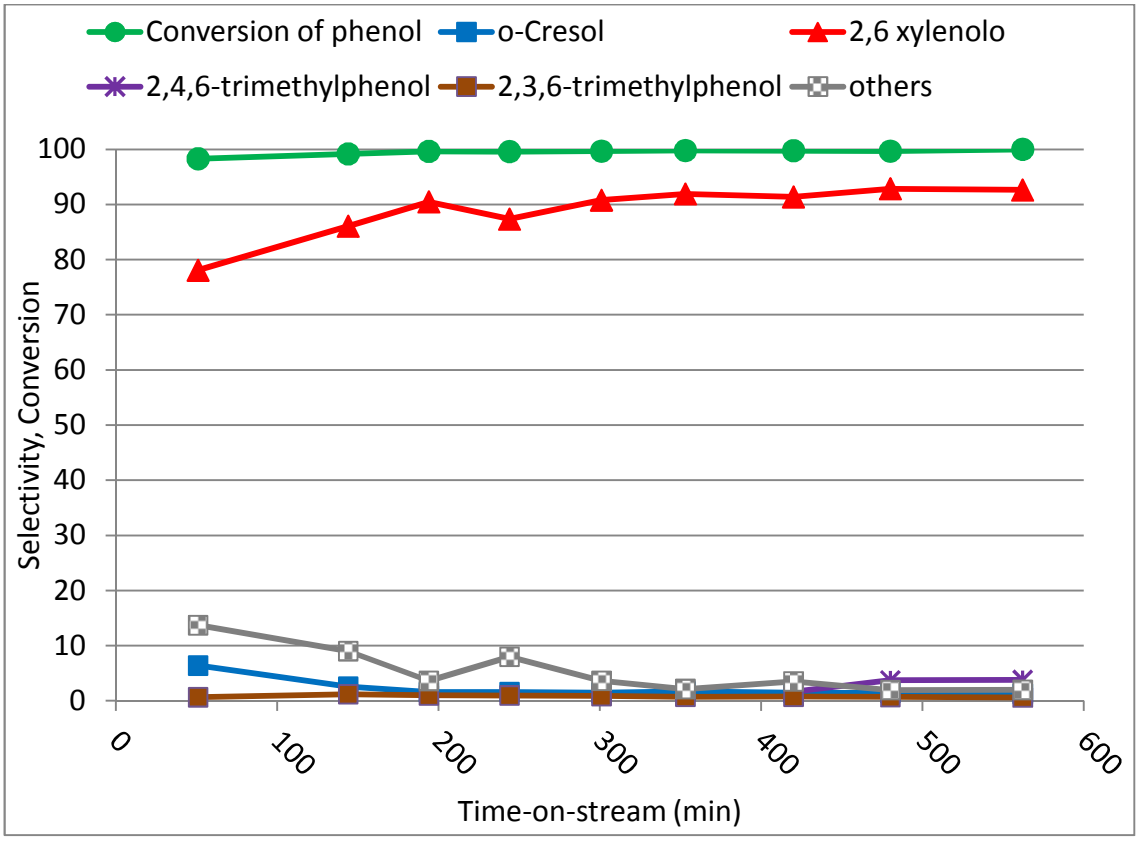

Figure 3.3 Catalytic performance in phenol methylation on $FeVO_4$ in function of time-on-stream at 380°C, residence time 1s; phenol to methanol ratio 1:10

In case of 450°C the formation of highly alkylated and naphthol like products (pointed at figure 'others') are much more significant. Same deviations we could notice in the situation of deactivation of the catalyst, at higher temperature deactivation of the catalyst probably due to formation of the coke occurs much more rapidly. Selectivity to methylation of both ortho position to form 2,6-xylenol was much lower than previous test while selectivity to o-cresol was increasing with time-on-stream constantly; it is also a prior factor to prove the deactivation of $FeVO_4$ catalyst.

It is important to note that at higher temperature there is also a minor contribution of dehydroxilation reaction that leads to the formation of xylenes and toluene.

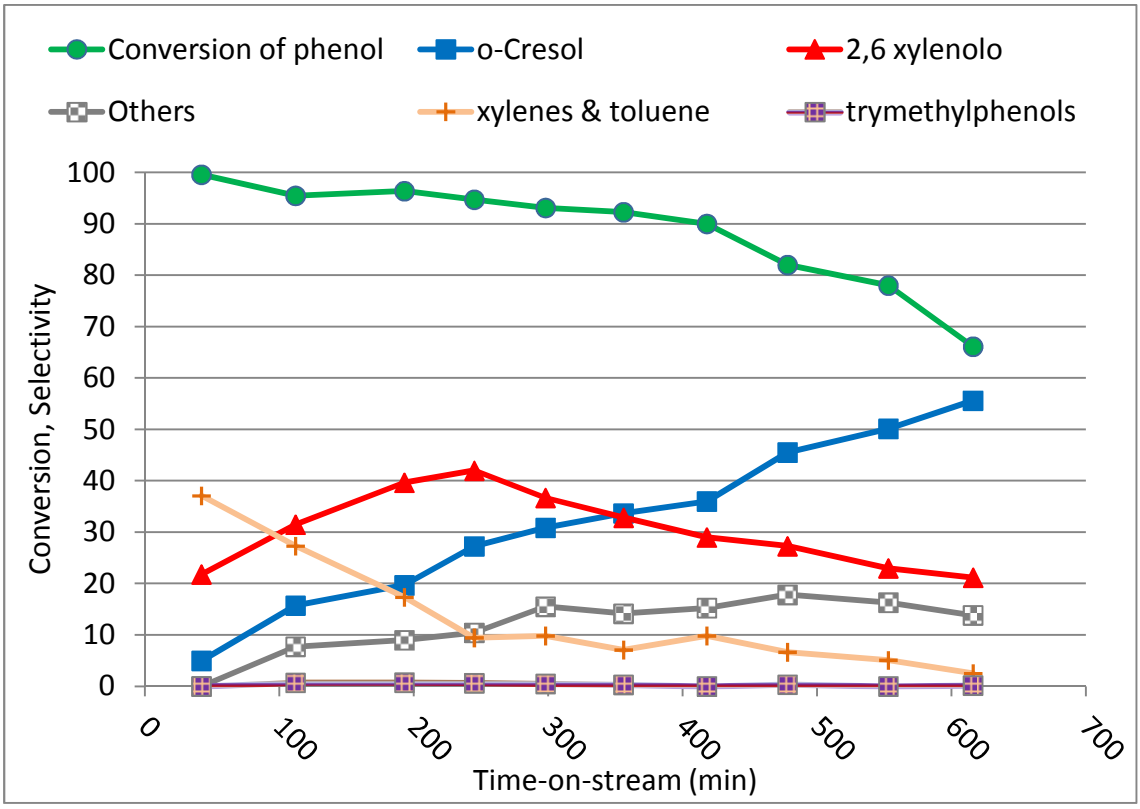

Figure 3.4 Catalytic performance in phenol methylation on $FeVO_4$ in function of time-on-stream at 450°C, residence time 1s, phenol to methanol ratio 1:10

The very high regio-selectivity in basic-catalyzed phenol methylation, if compared to acid-catalyzed methylation, is explained through the commonly accepted Tanabe's model [58,66]. This model describes the vertical adsorption of the phenate anion over the oxide surface, because of the repulsion between highly nucleophilic O^{2-}

anions and the aromatic ring. Consequently the para position becomes less accessible for attack by adsorbed methanol, while the ortho positions, closer to the surface, are readily available.

High regio-selectivity was observed with redox type catalyst $FeVO_4$ in tests that are demonstrated above. In order to prove this behaviour of the $FeVO_4$ catalyst some tests were performed.

Figure 3.5 compiles the results of gas-phase 2,6-xylenol methylation with methanol over the $FeVO_4$ displaying the conversion of 2,6-xylenol, yield sum and the selectivity to the reaction products. Selectivity of the catalyst to 2,4,6-trimethylphenol are very high but the yield of this product is the same as the yield when feeding phenol instead of 2,6-xylenol. The low conversion of 2,6-xylenol also shows that the catalyst favor the ortho-methylation, and if both ortho positions are occupied there is a low conversion of the reactant. It worth noticing that there is a slight formation of 2,3,6-trimethylphenol (both ortho and one meta) with lower selectivity, and almost same amount of 2,6 dimethylanisol formed.

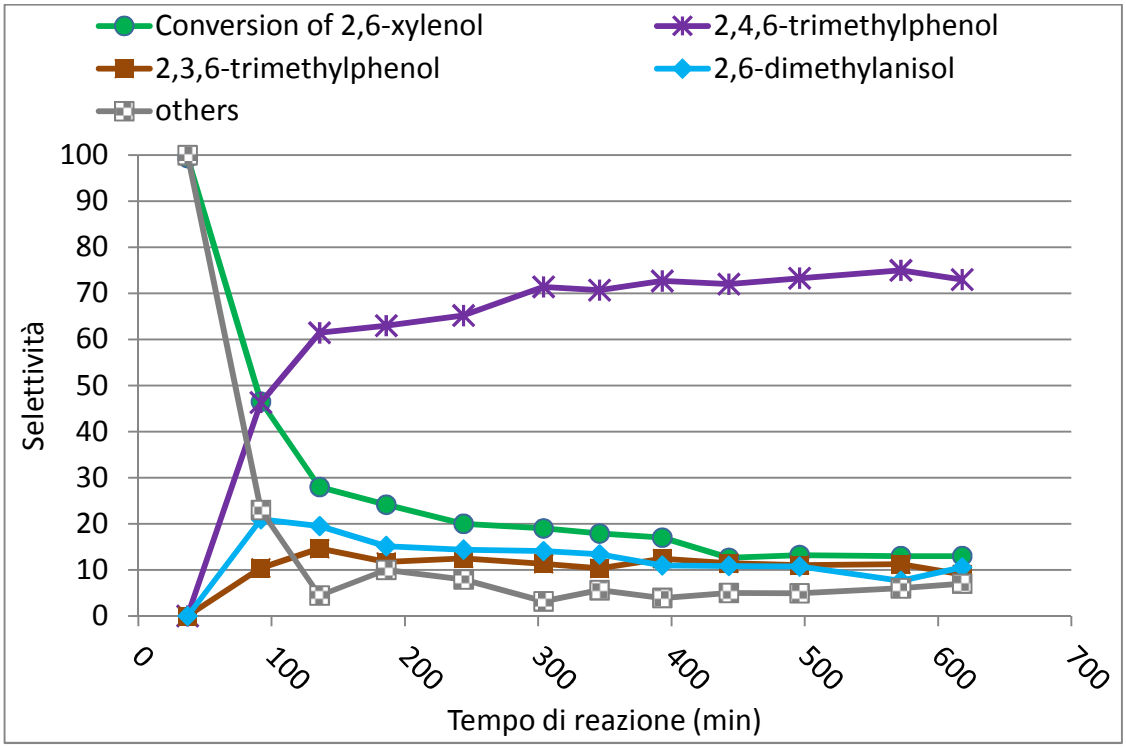

Figure 3.5 Catalytic performance in 2,6-xylenol methylation on $FeVO_4$ in function of time-on-stream at 320°C, residence time 1s; phenol to methanol ratio 1:10

In Figure 3.6 results of the catalytic gas-phase methylation of p-cresol with methanol are shown. In the case when p-cresol was fed both selectivity and yield of 2,4,6-trimethylphenol are very high because para position is already occupied on the reactant. There is a slight formation of 2,4-xylenol and others (complex naphtol like compounds)

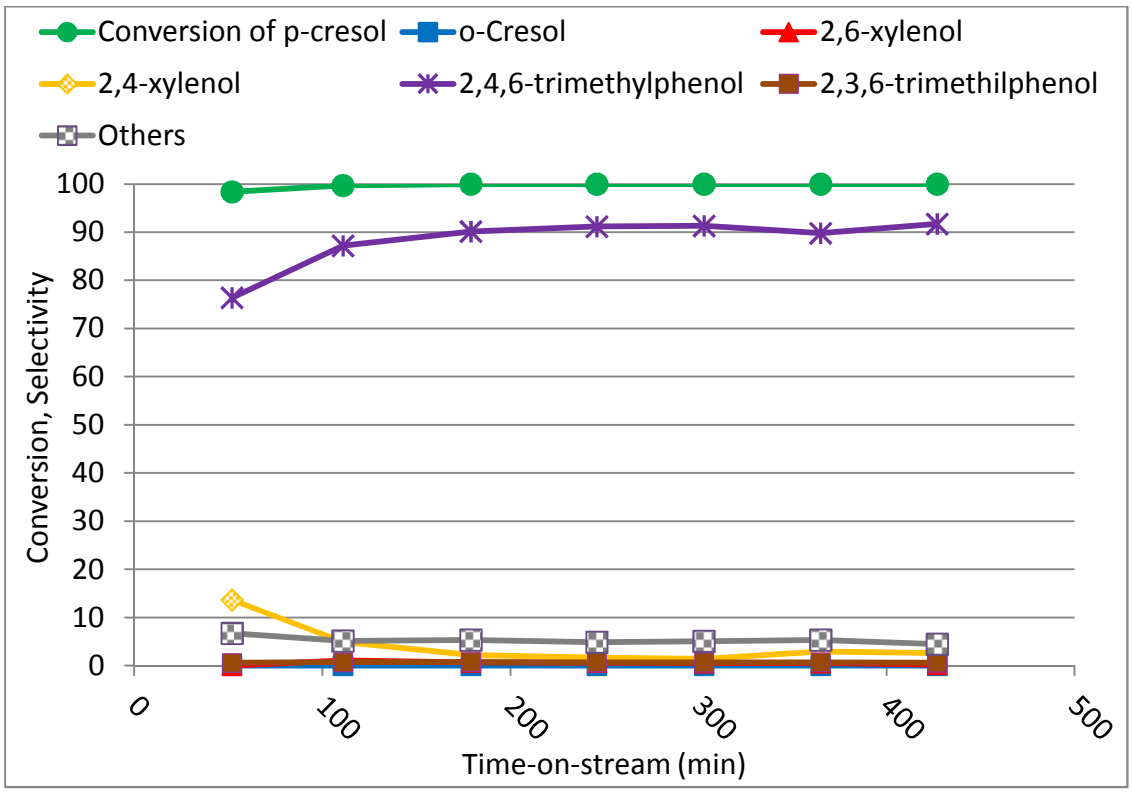

Figure 3.6 Catalytic performance in phenol methylation on $FeVO_4$ in function of time-on-stream at 320°C, residence time 1s; phenol to methanol ratio 1:10

The catalytic tests confirm the great regio- (ortho) and chemoselectivity (C-methylation) of the phenol methylation reaction with $FeVO_4$. We could assume that phenol adsorbs orthogonally on the surface of the redox catalysts as in catalysts with basic characteristics.

With the intention of determining the real active phase of $FeVO_4$ catalyst in the gas phase phenol methylation, as a first step it was decided to compare FeVO4 with behavior of individual oxides. In previous works of our laboratory Fe_3O_4 and V_2O_3 were tested in phenol methylation reaction. Fe_3O_4 catalyst shows low yield, low conversion and low selectivity to di-methylated product, while V_2O_3 has a higher conversion, slightly higher selectivity but deactivates rapidly. In this work catalytic test was performed using commercial V_2O_5 as a catalyst, pelletized and sieved (30-60 mesh).

In Figure 3.7 results of gas phase methylation on V_2O_5 applying same conditions of the reaction that were optimal for $FeVO_4$ catalyst are shown.

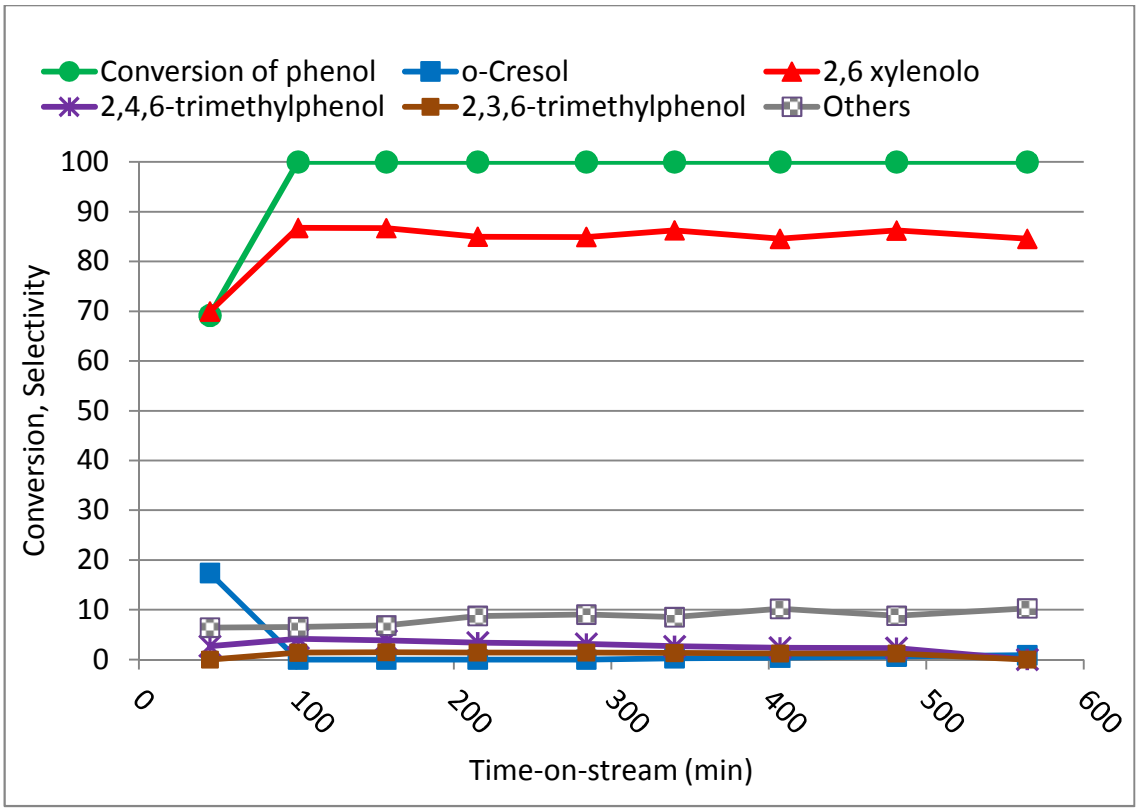

Figure 3.7 Catalytic performance in phenol methylation on V_2O_5 in function of time-on-stream at 320°C, residence time 1s; phenol to methanol ratio 1:10

As it is demonstrated in Figure 3.7 main behavior when using V_2O_5 as a catalyst is same as with $FeVO_4$. Slight differences in results are a bit lower selectivity to 2,6-xylenol and higher selectivity to formation of different complex heteroaromatics similar to benzofuran (Figure 3.7 – see “others”).

Results of the tests carried out shows that in $FeVO_4$ catalyst the main active catalyzing phase is due to vanadium.

It was demonstrated that the real active species in phenol methylation are vanadium sites and it was also shown that the insertion of other elements in vanadium phase improve the catalytic activity. It is known from the literature that in one row together with $FeVO_4$, there are $AlVO_4$ and mixed $Fe_xAl_{1-x}VO_4$ also known as very active catalysts of methanol to formaldehyde conversion. It is worth mentioning that some acid character of Al could change the overall catalyst behavior in gas phase phenol methylation.

Results of the test using $AlVO_4$ in gas phase methylation, under the same conditions that were optimal for $FeVO_4$ and V_2O_5 catalysts, are reported in Figure 3.8.

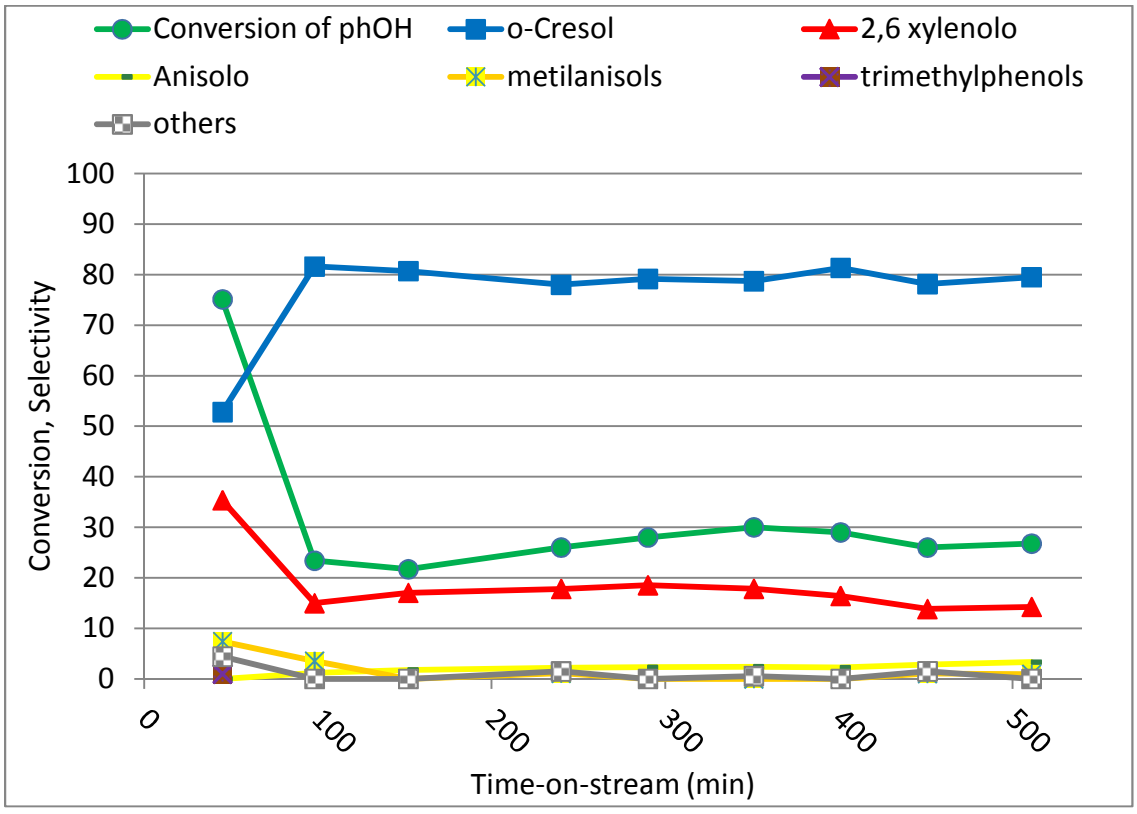

Figure 3.8 Catalytic performance in phenol methylation on $AlVO_4$ in function of time-on-stream at 320°C, residence time 1s; phenol to methanol ratio 1:10

The prevailing products of the reaction with $AlVO_4$ catalytic systems (as shown in Fig. 3.8) are ortho-C-alkylated compounds, in particular high selectivity to o-cresol which is mono- ortho- methylated compound, and lower selectivity to 2,6-xylenol which is di-methylated. Nevertheless high conversion of phenol and high selectivity to di-

methylated 2,6-xylenol which were characteristic in $FeVO_4$ and V_2O_5 are not the case with $AlVO_4$ as a catalyst. Here the low conversion and selectivity might be due to acidity of the Al, despite there was only negligible presence of anisole and methylanisole.

From the previous experiments it is well seen that $FeVO_4$ is very active for the gas phase methylation of phenol with high conversion, yield and selectivity to di-methylated products, when the AlVO4 is selective to mono-methylated compounds with low conversion and yield. To have a complete view it was worth to test compositions in the middle, between Fe and Al: mixed $Fe_xAl_{1-x}VO_4$ catalysts, which also show high activity and selectivity to formaldehyde in different methanol to formaldehyde reactions.

In Figure 3.9 results of gas-phase methylation with $Fe_{0,8}Al_{0,2}VO_4$ catalyst reported. The reaction conditions are same as optimal conditions when using catalysts in previous tests.

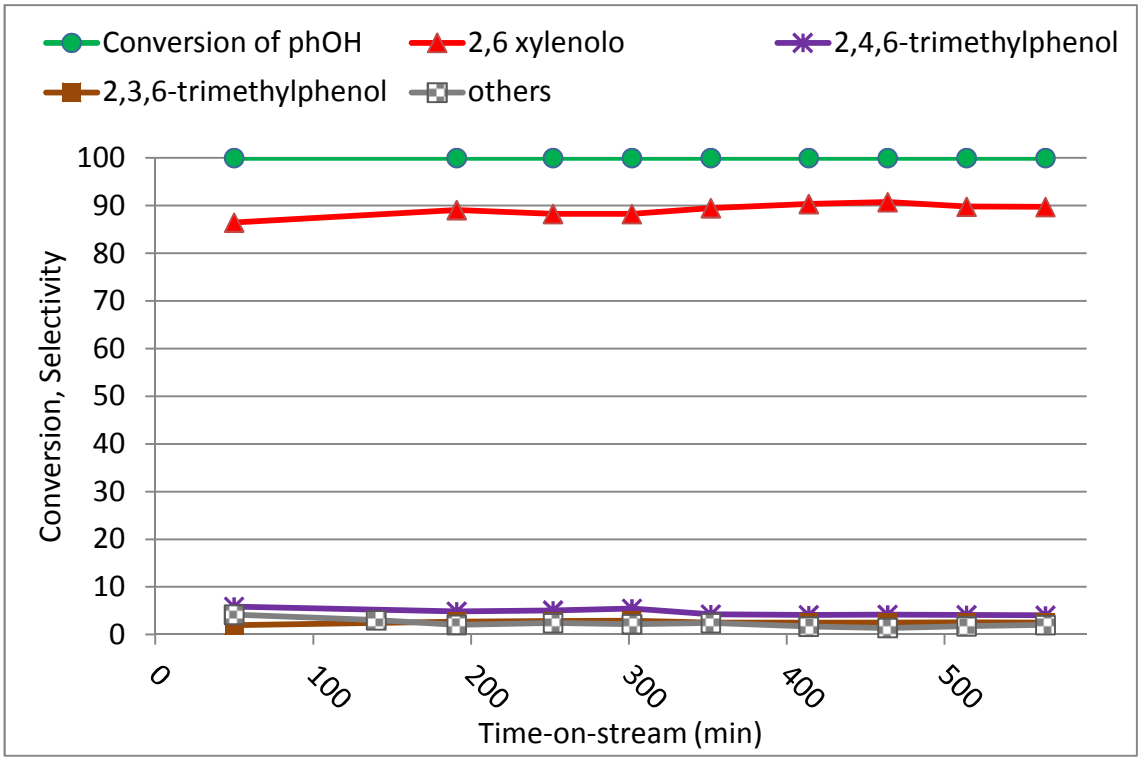

Figure 3.9 Catalytic performance in phenol methylation on $Fe_{0,8}Al_{0,2}VO_4$ in function of time-on-stream at 320°C, , residence time 1s; phenol to methanol ratio 1:10

Figure 3.9 shows that 2,6-xylenol is a principal product of the reaction between methanol and phenol with $Fe_{0,8}Al_{0,2}VO_4$ catalyst. Some minor formation of 2,4,6-trimethylphenol and of 2,3,6-trimethylphenol are noticeable. The selectivity to 2,6-

xylenol is a bit lower, but around 100% conversion of phenol and all the other characteristics of this catalyst was very similar to $FeVO_4$.

Results of gas-phase methylation of phenol with $Fe_{0,6}Al_{0,4}VO_4$ as a catalyst are shown in Figure 3.10. The reaction conditions are same as optimal conditions with previous catalysts.

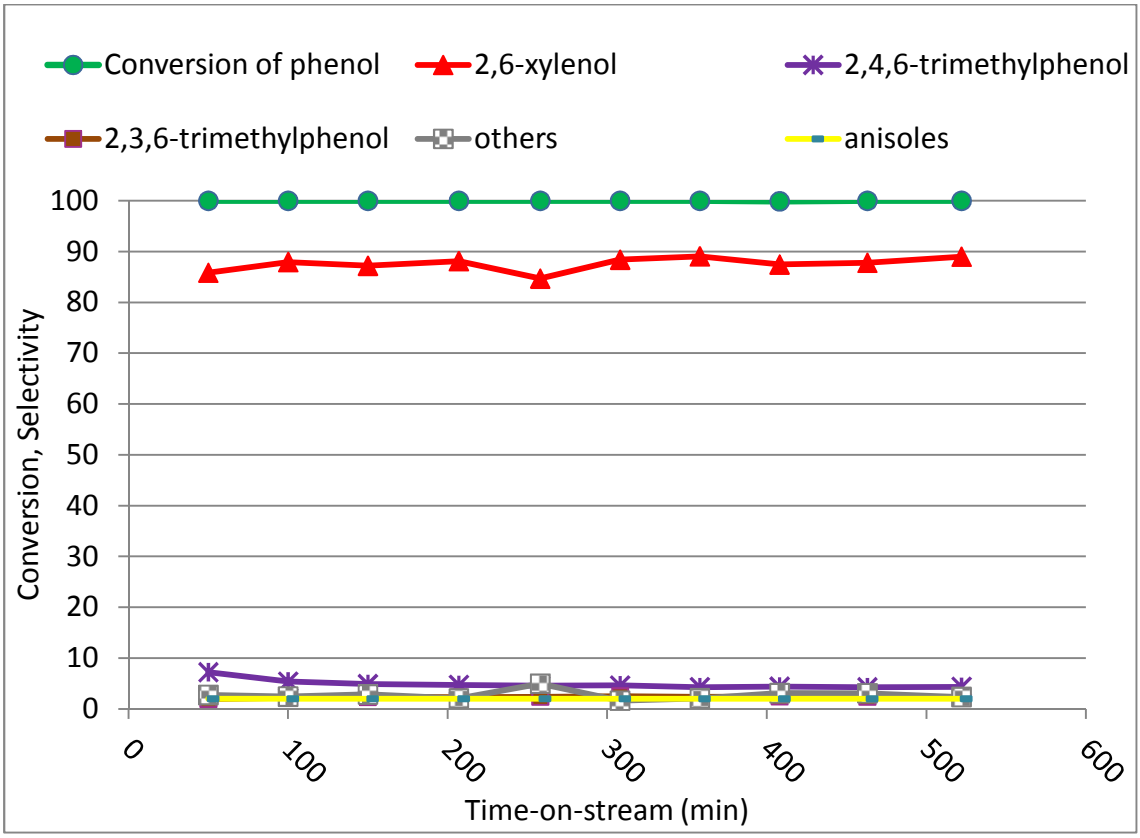

Figure 3.10 Catalytic performance in phenol methylation on $Fe_{0,6}Al_{0,4}VO_4$ in function of time-on-stream at 320°C, , residence time 1s; phenol to methanol ratio 1:10

Slight, almost negligible decrease of selectivity to 2,6-xylenol when using $Fe_{0,6}Al_{0,4}VO_4$ comparing with previous ($Fe_{0,8}Al_{0,2}VO_4$) catalyst is very nearly all the difference. Also very insignificant decrease of selectivity to 2,4,6-trimethylphenol and to 2,3,6-trimethylphenol.

The prevailing products of the reaction with $Fe_{0,2}Al_{0,8}VO_4$ catalytic system (see Figure 3.11) are ortho-C-alkylated compounds, in particular 2,6-xylenol and o-cresol. There was very significant decrease of selectivity to 2,6-xylenol and increase of selectivity to o-cresol. From the time-on-stream decrease of the conversion and increase of mono-methylation (o-cresol) while decrease of dimethylation (2,6-xylenol) demonstrates deactivation of the catalyst.

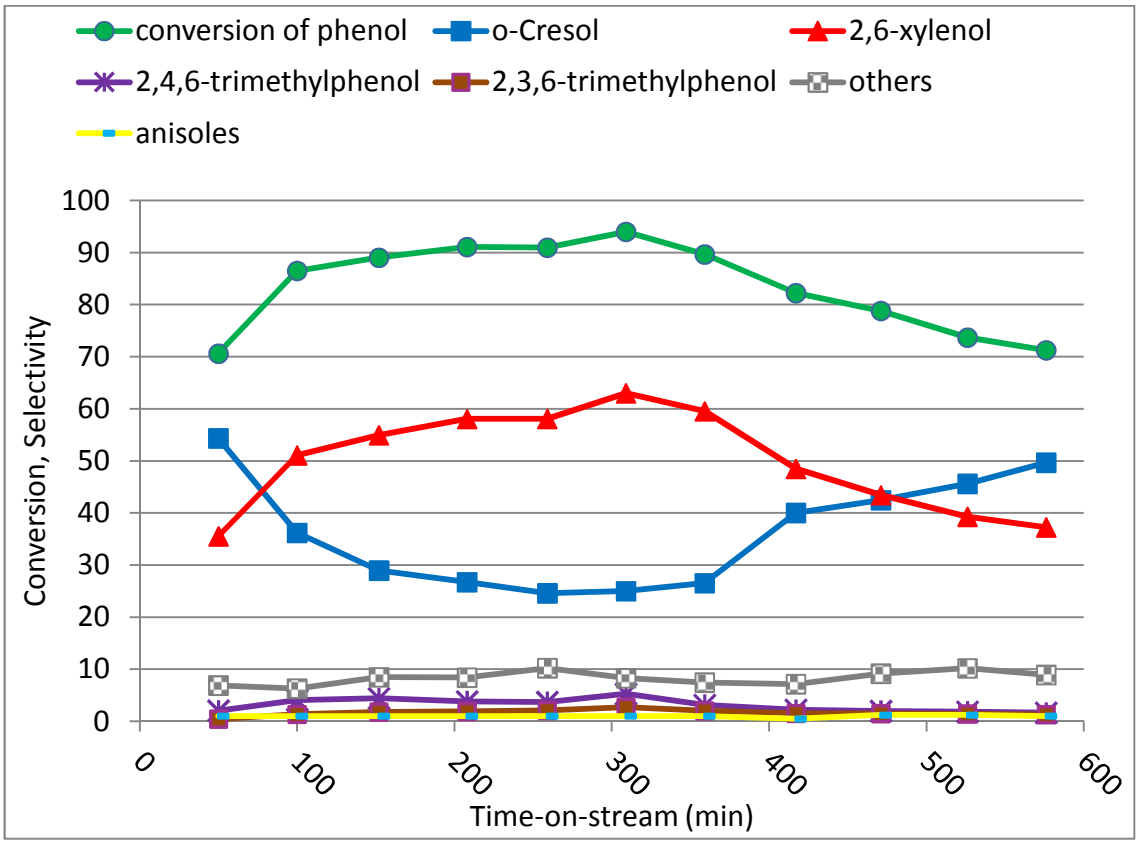

Figure 3.11 Catalytic performance in phenol methylation on $Fe_{0,2}Al_{0,8}VO_4$
in function of time-on-stream at 320°C, residence time 1s; phenol to methanol ratio 1:10.

Summarizing the main effect of iron and aluminum presence ($AlVO_4$, $FeVO_4$) and its proportion ($Fe_{0,8}Al_{0,2}VO_4$, $Fe_{0,6}Al_{0,4}VO_4$, $Fe_{0,2}Al_{0,8}VO_4$) in mixed oxides containing vanadium the behavior reported in the Figure 3.12.

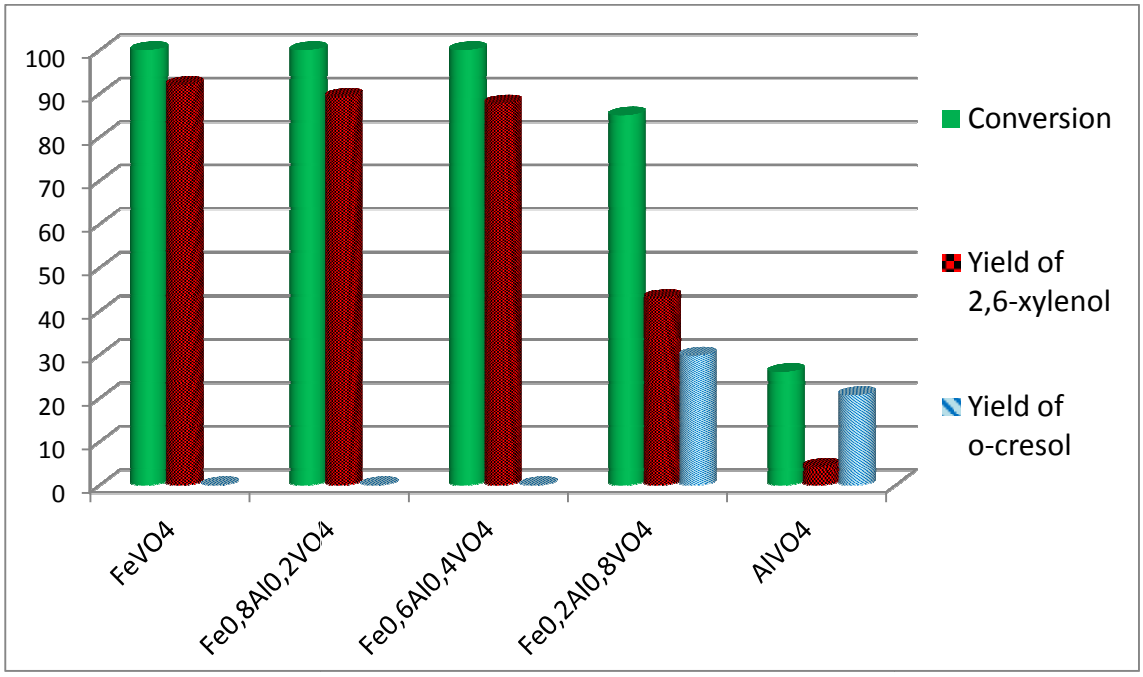

Figure 3.12 Results of catalytic performance in phenol methylation on $FeVO_4$, $Fe_xAl_{1-x}VO_4$, $AlVO_4$ comparing conversion of phenol, yield sum and selectivity to main products.

As it is seen from the Figure 3.12 there is a trend that the higher is amount of iron in mixed oxide, the higher are conversion, yield sum and selectivity to di-methylated product (2,6-xylenol). The opposite is true for aluminum, higher amount of aluminum leads to lower yield sum and higher selectivity to mono-methylated product.

This results lead to hypothesis that differences in both methanol and phenol adsorption on the catalytic surface is very important from the mechanism of adsorption point of view. Also it is essential to understand high regio- and chemoselectivity of catalysts to ortho- and C-methylation respectively.

It is important to mention that in all tests performed, in the beginning there is a slightly different behavior of the catalyst than those after some reaction time. And it was hypothesized that there is some transformation, probably the reduction of the catalyst in the beginning of reaction.

To understand differences in behavior of the catalysts and mechanism of adsorption on catalysts, spectroscopic methods were applied. First of all, central and

useful technique to understand phases, of which catalysts comprise, X-ray powder diffraction was applied.

3.2 X-ray diffraction analysis

In order to characterize catalysts X-ray powder diffraction analysis were done. Results of FeVO4 freshly prepared, exhausted and regenerated samples analyzed by X-ray diffraction were very important for understanding the 'real catalyzing agent'.

Figure 3.13 shows X-ray diffractograms of fresh and exhausted $FeVO_4$ catalyst. Freshly prepared $FeVO_4$ is a homogeneous phase, which peaks suits the database and shows the characteristic features of a triclinic ($P-1$) type of phase.

As it is seen from figure exhausted catalyst possesses a pattern of spinel type phase. The resultant diffractogram of exhausted $FeVO_4$ shows similarities to Fe_3O_4 and Fe_2VO_4 but shifted to the left and to FeV_2O_4 but shifted to the right.

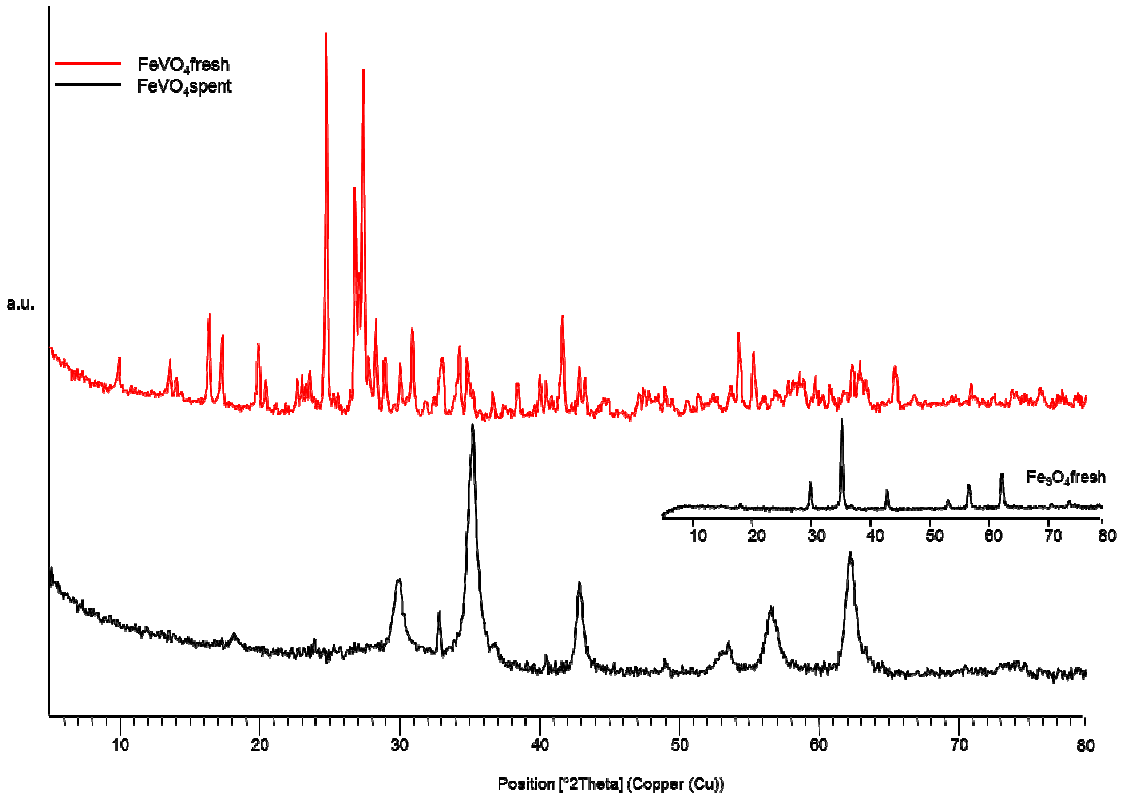

Figure 3.13 X-ray diffractograms of freshly prepared (top) and exhausted (bottom) $FeVO_4$ catalyst. Additional diffractogram of Fe_3O_4 (magnetite).

In Figure 3.14 peaks of FeV_2O_4 and Fe_2VO_4 diffraction pattern from database are shown. Spent $FeVO_4$ located in between the patterns of FeV_2O_4 and Fe_2VO_4, and also shifted from pattern of magnetite. Also some peaks with very low intensity that are related to hematite were found.

Since pattern of spent $FeVO_4$ located in between the patterns of spinels mentioned before, it could be assumed that exhausted $FeVO_4$ possesses characteristics of a spinel phase containing iron and vanadium in unknown stoichiometry. The position of the peaks lead to hypothesis, that during the reaction catalyst modifies to a phase like vanadium-doped magnetite or well mixed FeV_2O_4 and Fe_2VO_4 spinel phase.

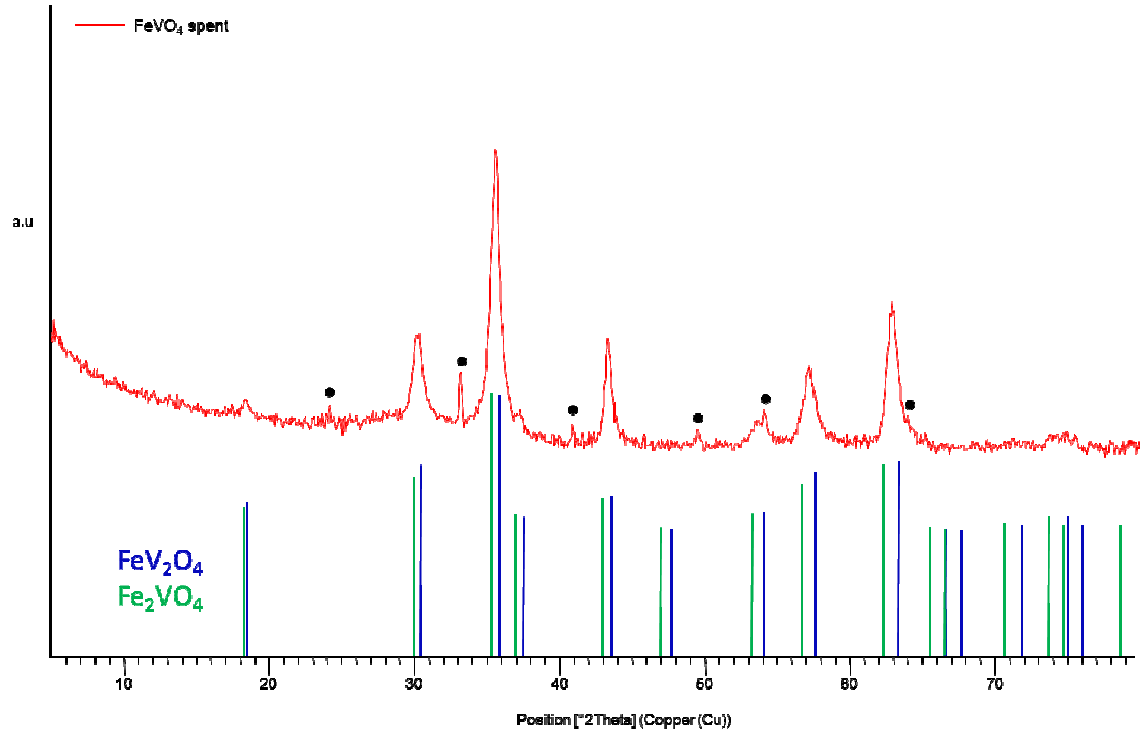

Figure 3.14 X-ray diffractogram of spent $FeVO_4$ (top), peaks of FeV_2O_4 and Fe_2VO_4 diffraction patterns from database, additional peaks (●) of hematite.

Reoxidation of the $FeVO_4$ catalyst was carried out, by air feed at high temperature in same reactor where reaction tests were made. The diffraction pattern of regenerated $FeVO_4$ was similar to fresh catalyst (Figure 3.15). This could be evidence that spent $FeVO_4$ is not consisting of Fe_3O_4, but it has to be mixed Fe_xV_yO4 spinel.

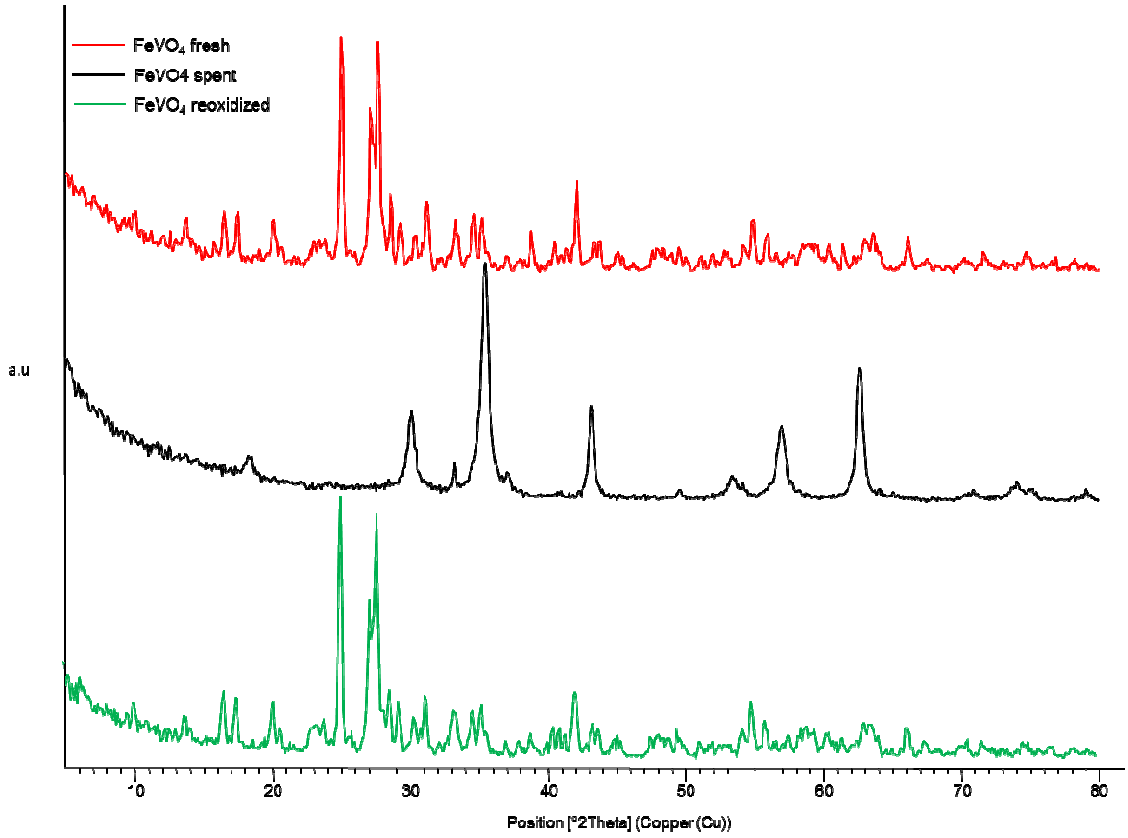

Figure 3.15 X-ray diffractograms of fresh, spent and reoxidized $FeVO_4$ catalysts

In order to corroborate the results of XRD and with the aim of determining the reducing rate of the catalyst, decomposition of methanol tests were done in the same reactor in which experiments were performed. The experiment was done by feeding only methanol and analyzing light products by micro-GC as it is described in experimental part. From the results of decomposition test, reported in Figure 3.16 and Figure 3.17, it is seen that reduction of the catalyst starts from the beginning and stabilizes after 30-35 minutes, with reduction around 25%.

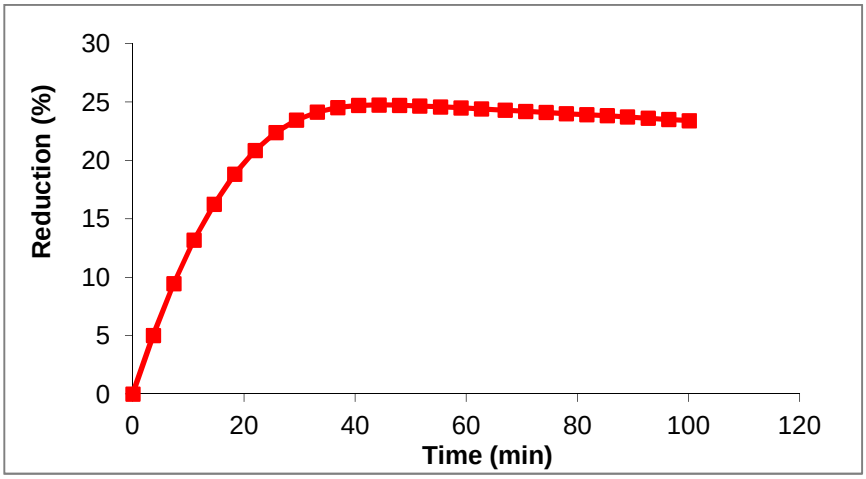

Figure 3.16 Methanol decomposition test on $FeVO_4$ reduction of the catalyst in function of time

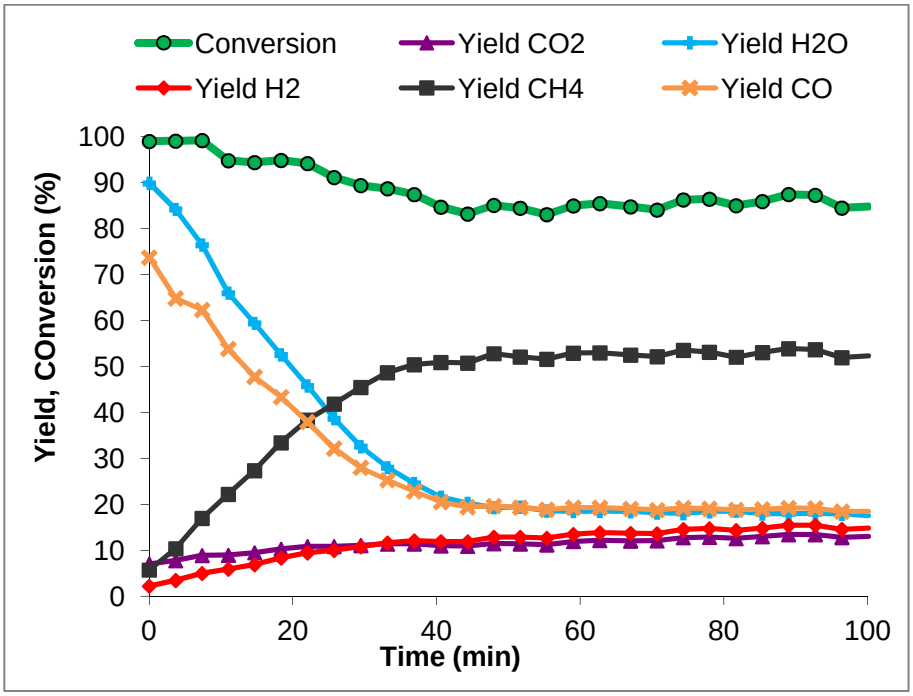

Figure 3.17 Methanol decomposition test on $FeVO_4$ conversion of methanol and yields of light compounds produced.

With the intention of roughly resolving the reduced catalyst composition respective calculations with oxygen balance to possible spinels were done (Table 3.1).

Table 3.1 Examples of possible reduction of $FeVO_4$ catalyst

#	Reduction	Oxygen balance	Reduction grade, %
1	$15FeVO4 \rightarrow 7FeV_2O_4 + Fe_2VO_4 + 3Fe_2O_3$	60O → 41O	≈ 32%
2	$3FeVO4 \rightarrow FeV_2O_4 + Fe_2VO4$	12O → 8O	≈ 33%
3	$17FeVO_4 \rightarrow 8FeV_2O_4 + Fe_2VO_4 + Fe_3O_4 + 2Fe_2O_3$	68O → 46O	≈ 32%
4	$15FeVO4 \rightarrow 7FeV_2O_4 + Fe_2VO_4 + 2Fe_3O_4$	60O → 40O	≈ 33%
5	$6FeVO_4 \rightarrow FeV_2O_4 + Fe_2VO_4 + V_3O_4 + Fe_3O_4$	24O → 16O	≈ 33%
6	$6FeVO_4 \rightarrow 3Fe_2VO_4 + V_3O_4$	24O → 16O	≈ 33%
7	$3FeVO_4 \rightarrow Fe_3O_4 + V_3O_4$	12O → 8O	≈ 33%
8	$6FeVO_4 \rightarrow 3FeV_2O_4 + Fe_3O_4$	24O → 16O	≈ 33%
9	$7FeVO_4 \rightarrow Fe_2VO_4 + 2V_3O_4 + Fe_3O_4 + Fe_2O_3$	28O → 19O	≈ 32%

In all listed cases in Table 3.1 reduction of the catalyst were around 32-33%, which are relatively in respect with experimental values. But first four examples are most possible since they in general match with results of X-ray diffraction. Other examples have much less probability to be correct, due to results of reoxidation test and X-ray diffraction analysis.

Results of X-ray diffraction of freshly prepared and spent V_2O_5 catalyst are presented in Figure 3.18. Fresh catalyst has a very clear pattern of V_2O_5 homogeneous phase. On the other hand diffraction pattern of spent catalyst shows similar pattern of reduced phase of V_2O_5, but not spinel phase. Diffraction pattern of spent catalyst has not match to any pattern from database, thus we could assume that spent catalyst contains of mixed phase of reduced vanadium oxides.

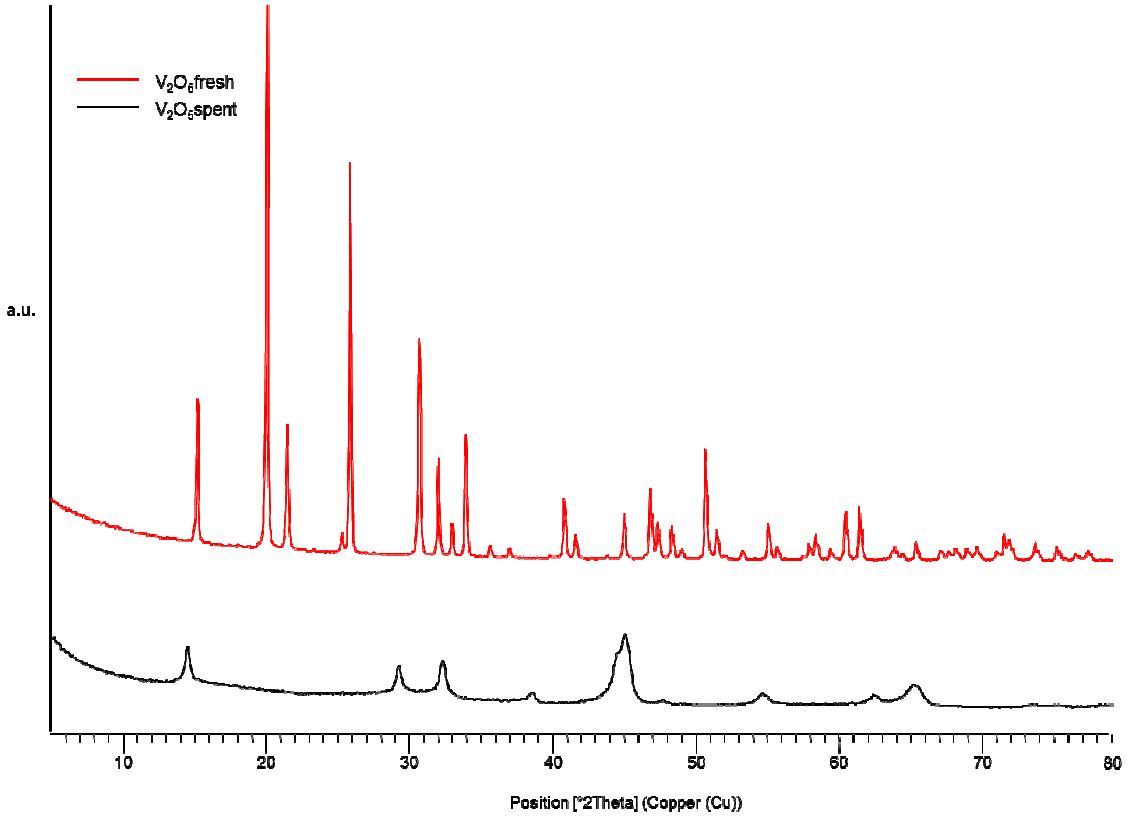

Figure 3.18 X-ray diffractograms of freshly prepared (top) and exhausted (bottom) V_2O_5 catalyst.

Diffraction pattern of fresh $AlVO_4$ show the characteristic features of a triclinic ($P\,-1$) type of phase (Figure 3.19) and has a good match with $AlVO_4$ pattern in database.

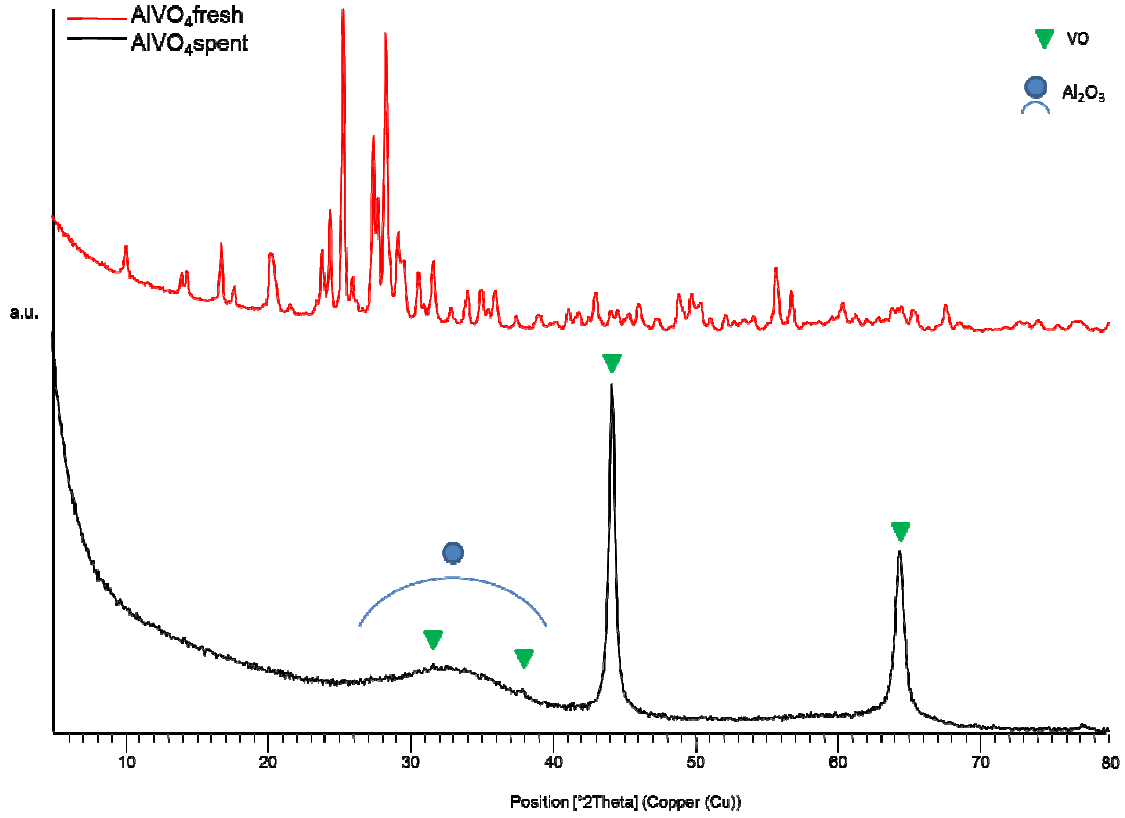

Figure 3.19 X-ray diffractograms of freshly prepared (top) and exhausted (bottom) $AlVO_4$ catalyst

From Figure 3.19 it is well seen that spent $AlVO_4$ catalyst segregates to individual oxide phases. Broad peak from 25-40^o in the used $AlVO_4$ is supposed to be related to amorphous phase of Al_2O_3. Very small peaks at 37^o and 31,5^o, small possibly due to Al2O3 presence, and intense peaks at 45^o and 65^o are related to VO phase and might be with additionally small amount of other reduced vanadium oxides.

With the intention of determining reducing rate of the $AlVO_4$ catalyst and to have a comparison with active $FeVO_4$, decomposition of methanol tests were done on $AlVO_4$ by the same method as with $FeVO_4$.

Reduction of the catalyst rapidly starts from the beginning and then with lower speed after 50-60 minutes, with reduction around 22-30%, but continues to reduce slowly even after 3 hours of reaction (Figure 3.20 and Figure 3.21).

Interesting observation was made, while performing the test; together with same products as in methanol decomposition on $FeVO_4$, in case of AlVO4 dimethyl ether was produced.

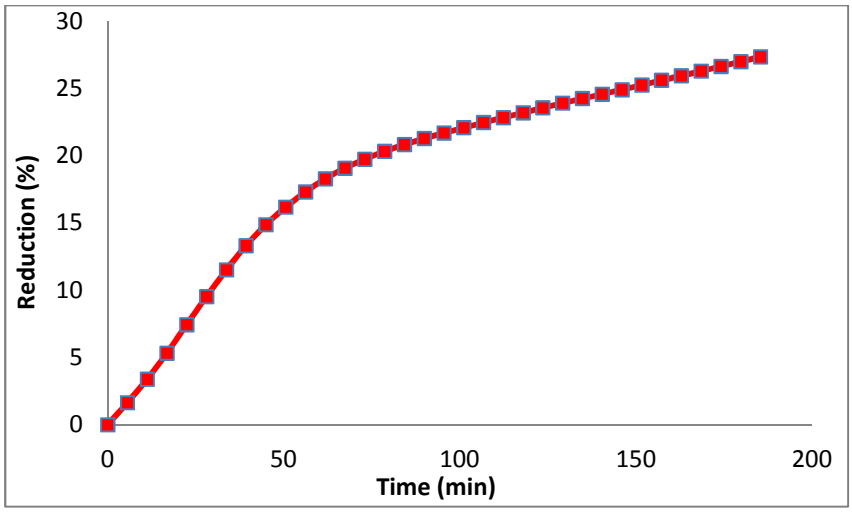

Figure 3.20 Methanol decomposition test on $AlVO_4$. Reduction of the catalyst in function of time

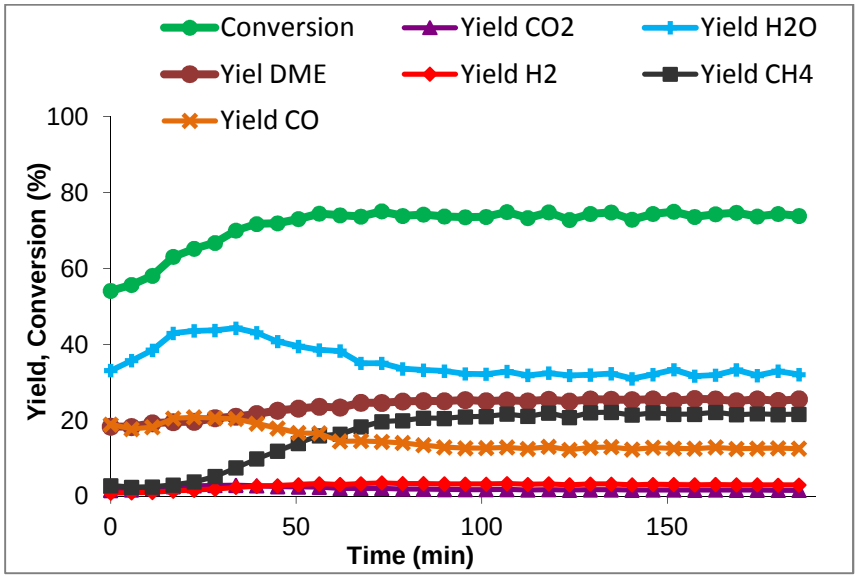

Figure 3.21 Methanol decomposition test on $AlVO_4$. Yields of light compounds produced

In order to approximately determine the reduced catalyst composition and to compare with $FeVO_4$, respective calculations with oxygen balance to possible spinels were done (Table 3.2).

Table 3.2 Examples of possible reduction of $AlVO_4$ catalyst

#	Reduction	Oxygen balance	Reduction grade, %
1	$12AlVO_4 \rightarrow 6AlV_2O_4 + 3Al_2O_3$	(48O → 33O)	≈ 31%
2	$3AlVO_4 \rightarrow AlV_2O4 + Al_2O_3 + VO$	(12O → 8O)	≈ 33%
3	$2AlVO_4 \rightarrow Al_2O_3 + V_2O_4$	(8O → 7O)	≈ 12,5%
4	$2AlVO_4 \rightarrow Al_2O_3 + V_2O_3$	(8O → 6O)	≈ 25%
5	$2AlVO_4 \rightarrow Al_2O_3 + 2VO$	(8O → 5O)	≈ 37,5%
6	$6AlVO_4 \rightarrow Al_2O_3 + V_2O_3 + 4VO$	(24O → 16O)	≈ 33%
7	$6AlVO_4 \rightarrow Al_2O_3 + V_2O_4 + 4VO$	(24O → 17O)	≈ 29%

From listed cases (Table 3.2) first two possibilities are assumed not to be true because there is no presence of this phase in X-Ray diffraction pattern. Examples #3 and #4 are not coincide with results of methanol decomposition test, since low maximum values of reduction. Last three examples of possible reduction of the catalyst were around 29-37,5%, which are relatively in respect with experimental values and could be explained through X-ray diffraction pattern.

The catalysts $FeVO_4$, $Fe_xAl_{1-x}VO_4$ (x=0.2, 0.6, 0.8) and $AlVO_4$ were characterized by XRD both as synthesized and after use in phenol methylation. The XRD patterns of the freshly prepared samples are displayed in Figure 3.22. As it was mentioned, $FeVO_4$ and $AlVO_4$ samples show the characteristic features of a triclinic ($P-1$) type of phase, isostructural with $FeVO_4$ and $AlVO_4$. Freshly prepared $Fe_{0.6}Al_{0.4}VO_4$ catalyst seems to be segregated FeVO4 and AlVO4 phases. In the other mixed $Fe_xAl_{1-x}VO_4$ catalysts, with increasing amount of aluminum, we witness change in unit cell and it is possible to observe a shifts.

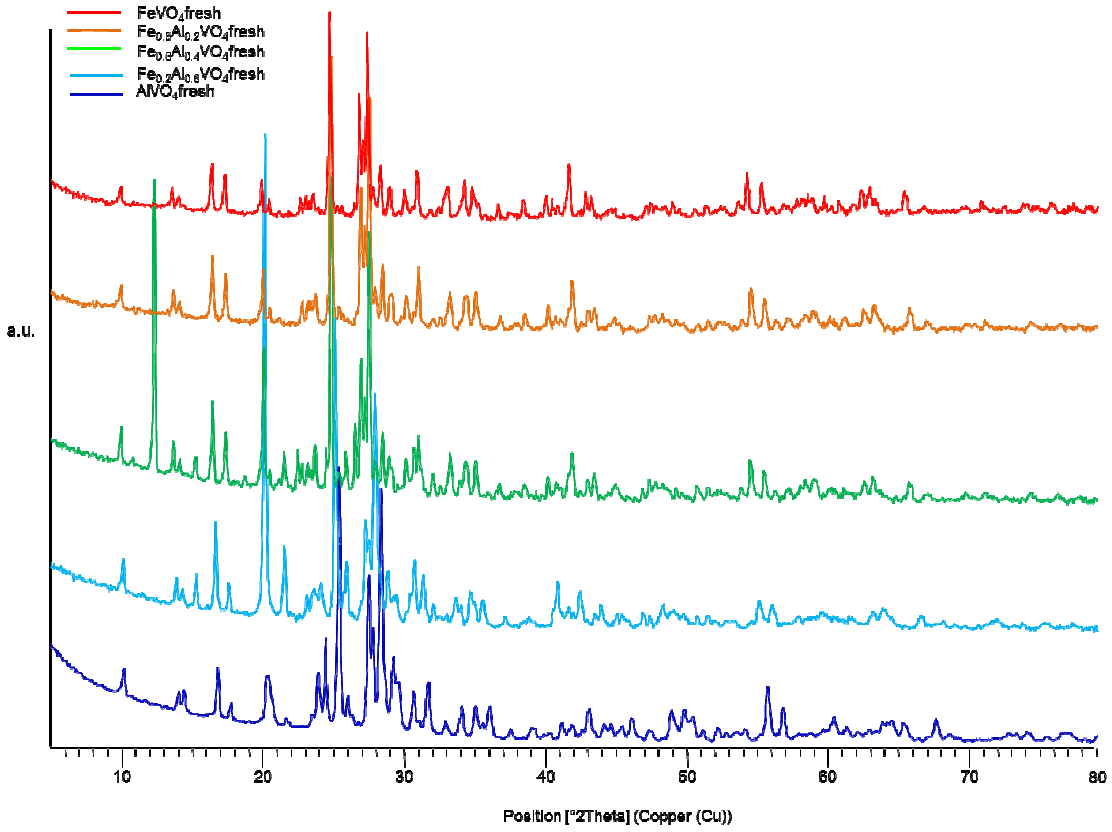

Figure 3.22 X-ray diffractograms of freshly prepared $FeVO_4$, $Fe_{0,8Al0,2VO4}$, $Fe_{0,6}Al_{0,4}VO_4$, $Fe_{0,2}Al_{0,8}VO_4$ catalysts

The XRD patterns of the used samples are displayed in Figure 3.23. Comparing this figure with Figure 3.22 clearly shows that the used catalysts possess spinel-type phases, which are different from fresh catalysts.

From $FeVO_4$ to $AlVO_4$ there is a tendency that peaks possibly related to mixed spinel phases of FeV_2O_4, Fe_2VO_4 are broadened and shifted except $Fe_{0.6}Al_{0.4}VO_4$ which had a different characterization after preparation.

In $FeVO_4$ catalyst there are not intense peaks which could be related to hematite (Fe_2O_3). These peaks are also present, but with lower intensity, in $Fe_{0.8}Al_{0.2}VO_4$. Then with lowering iron in composition of catalyst these peaks disappear and very broad peak related to Al_2O_3 appears. Diffraction pattern of $Fe_{0.2}Al_{0.8}VO_4$ more similar to spent $AlVO_4$ pattern with segregated oxides of aluminum and vanadium(II).

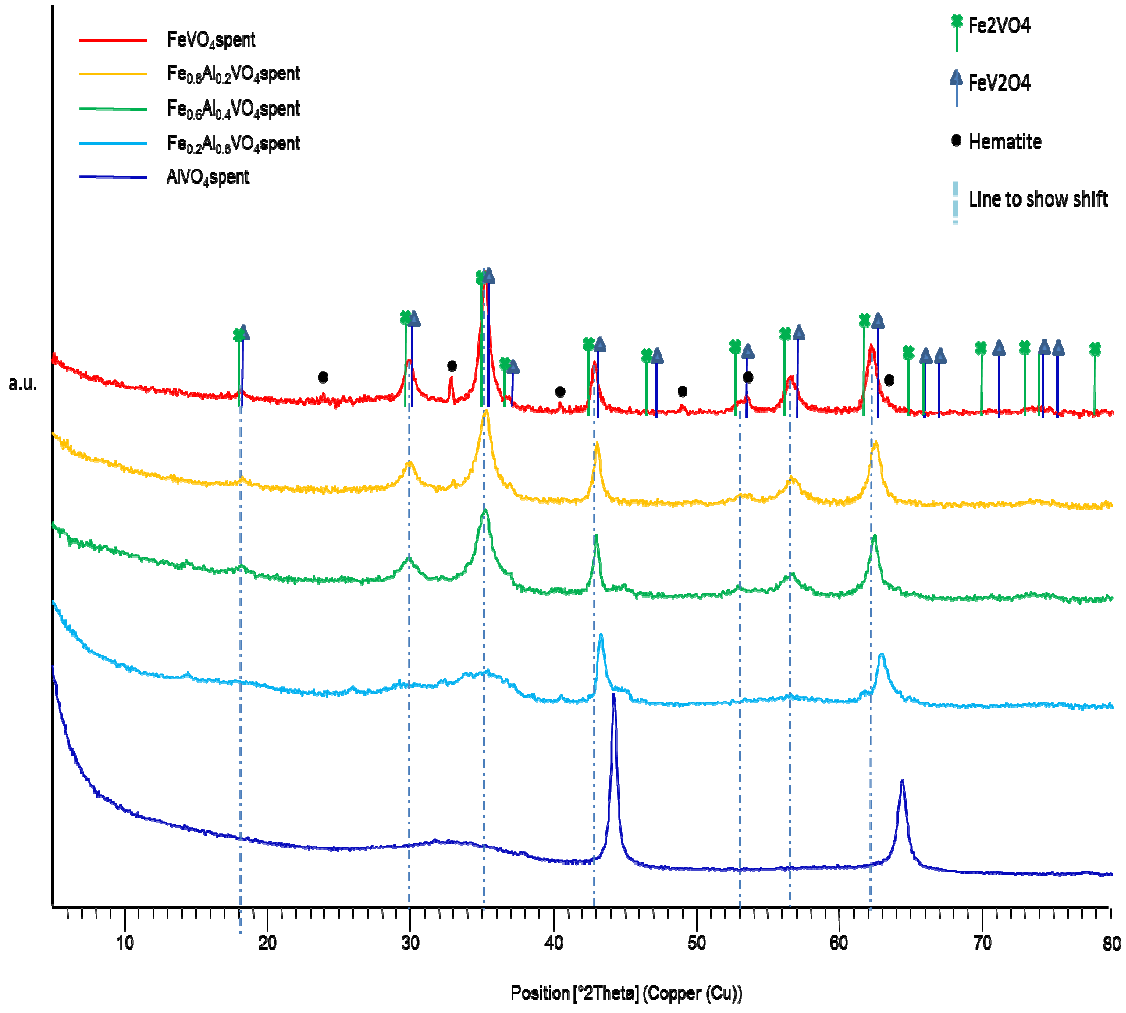

Figure 3.23 X-ray diffractograms of spent $FeVO_4$, $Fe_{0,8Al0,2VO4}$, $Fe_{0,6}Al_{0,4}VO_4$, $Fe_{0,2}Al_{0,8}VO_4$ catalysts

From X-Ray powder diffraction analysis we understood that $FeVO_4$ catalyst reduces during the reaction to mixed spinel phase containing Fe_2VO_4 and FeV_2O_4 as major phases probably with small amount of magnetite and hematite. After the reoxidation the catalyst has a similar pattern characteristic of $FeVO_4$, which is proof of an almost full evolution of the catalyst back to former fresh phase and thus spent catalyst is reversible.

On the other hand AlVO4 catalyst is segregating to Al_2O_3 and VO during the reaction, which leads to deactivation of it.

Mixed $Fe_xAl_{1-x}VO_4$ catalysts have properties similar to either $FeVO_4$ or $AlVO_4$ depending on the amount of according element.

Observed high activity of $Fe_{0,6}Al_{0,4}VO_4$ similar to $FeVO_4$ might be due to segregation of $FeVO_4$ and $AlVO_4$ during synthesis. Thus, $FeVO_4$ part in this segregated catalyst mostly played important role in successful reaction.

Vanadium (V) oxide reduces during the reaction, and does not form spinel type phase. The spent catalyst consists of mixed reduced phases of vanadium oxides of different oxidation states.

3.3 Raman Spectroscopic studies

Raman spectroscopy was used to examine the metal oxide phases present in the synthesized catalysts. Raman spectra of freshly prepared and spent $FeVO_4$ catalyst are presented in Figure 3.24. The Raman spectrum of the dehydrated $FeVO_4$ mixed metal oxide contains bands at 971, 936, 910, 900, 850, 836, 773, 738, 664, 634, 370, and 327 cm-1 characteristic of the bulk $FeVO_4$ phase. The absence of Raman bands from crystalline R-Fe_2O_3 or V_2O_5 nanophases demonstrate that the bulk FeVO4 mixed metal oxide is phase pure.

The spectrum of spent $FeVO_4$ appears similar to fresh one, but with poorer resolution and shifted in the regions were V-O bands are present. Bands corresponding to V-O-Fe and Fe-O not shifted or shifted not significantly. This could be due to temperature, since vanadium species (crystals) increase in volume.

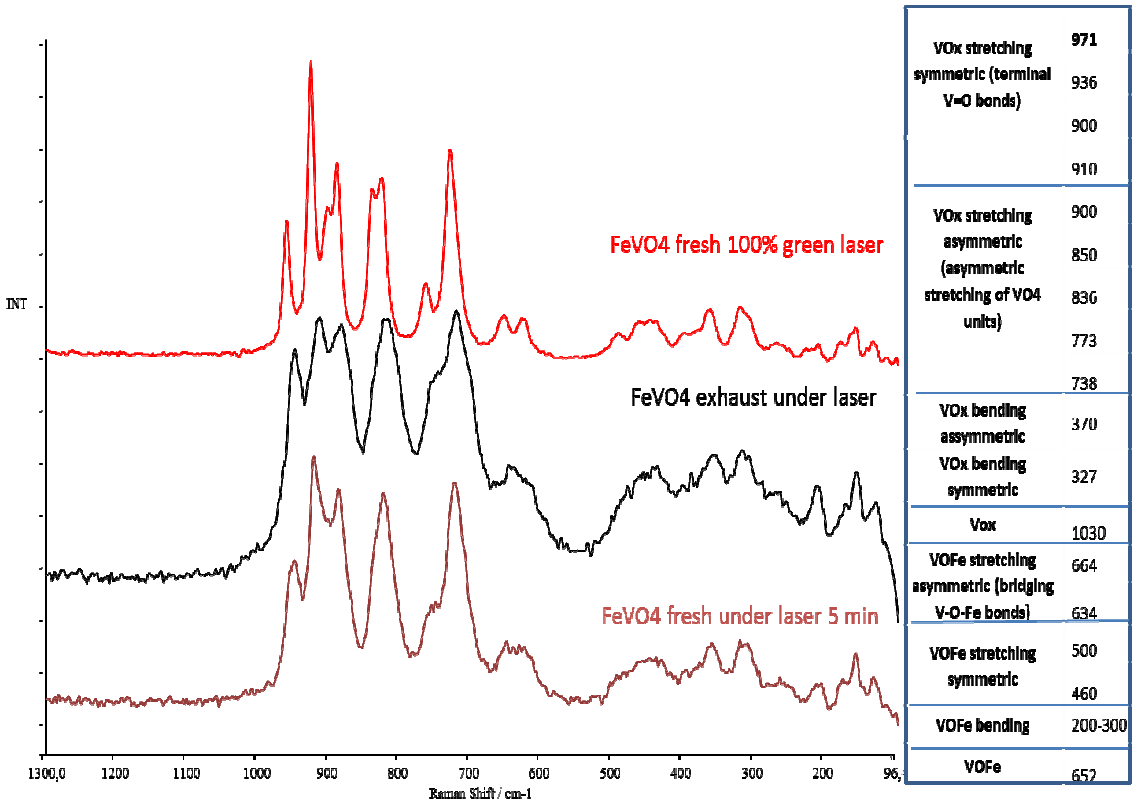

Figure 3.24 Raman analysis of freshly prepared and exhausted $FeVO_4$ under green Ar laser. Additional table of $FeVO_4$ vibrational modes

The reason why spectra of fresh and spent catalyst look similar possibly due to reoxidation of spent catalyst because of laser excitation. In order to prove this theory, analysis with lower laser power was performed. Figure 3.25 concludes spectra taken with lower and different laser power. First attempt with 1% laser power was not enough to resolve peaks successively, but it was enough to notice some broad peak about 660 cm^{-1}. Therefore same laser power was applied and we observed spectra more typical to spinel type. For comparison in Figure 3.25 spectra of typical spinel freshly prepared Fe_3O_4 are shown.

After applying 5% laser, broad intense peaks similar to freshly prepared $FeVO_4$ started to form. Once more spectrum with 5% laser was taken, and this time broad peaks of freshly prepared $FeVO_4$ was observed clearly (Figure 3.25).

It is worth mentioning that magnetite under the laser also reoxidize to hematite.

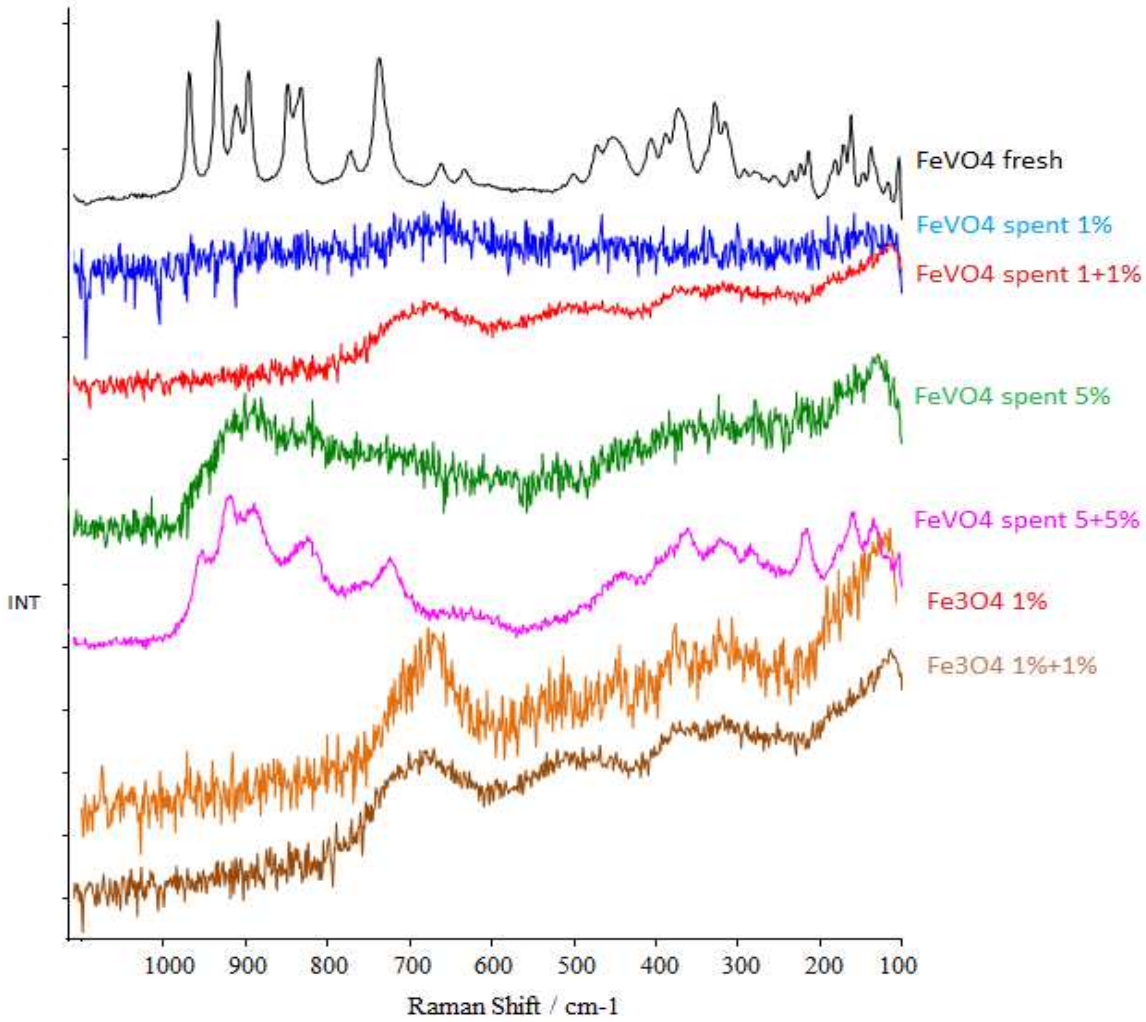

Figure 3.25 Raman spectra of freshly prepared, spent $FeVO_4$ and freshly prepared Fe_3O_4 under different power of laser

In Figure 3.26 Raman spectroscopic analysis of fresh and exhausted V_2O_5 catalyst are demonstrated. In this experiment same behavior as in $FeVO_4$ catalyst's analysis was found. When applying 1% laser power catalyst spectra possess reduced vanadium oxide characteristic bands. After increasing the laser power catalyst regenerates by laser heat, however with some shift of the peaks from spectra of the fresh catalyst. Possibly due to the laser heat, unit cell of vanadium oxide crystal increase in volume.

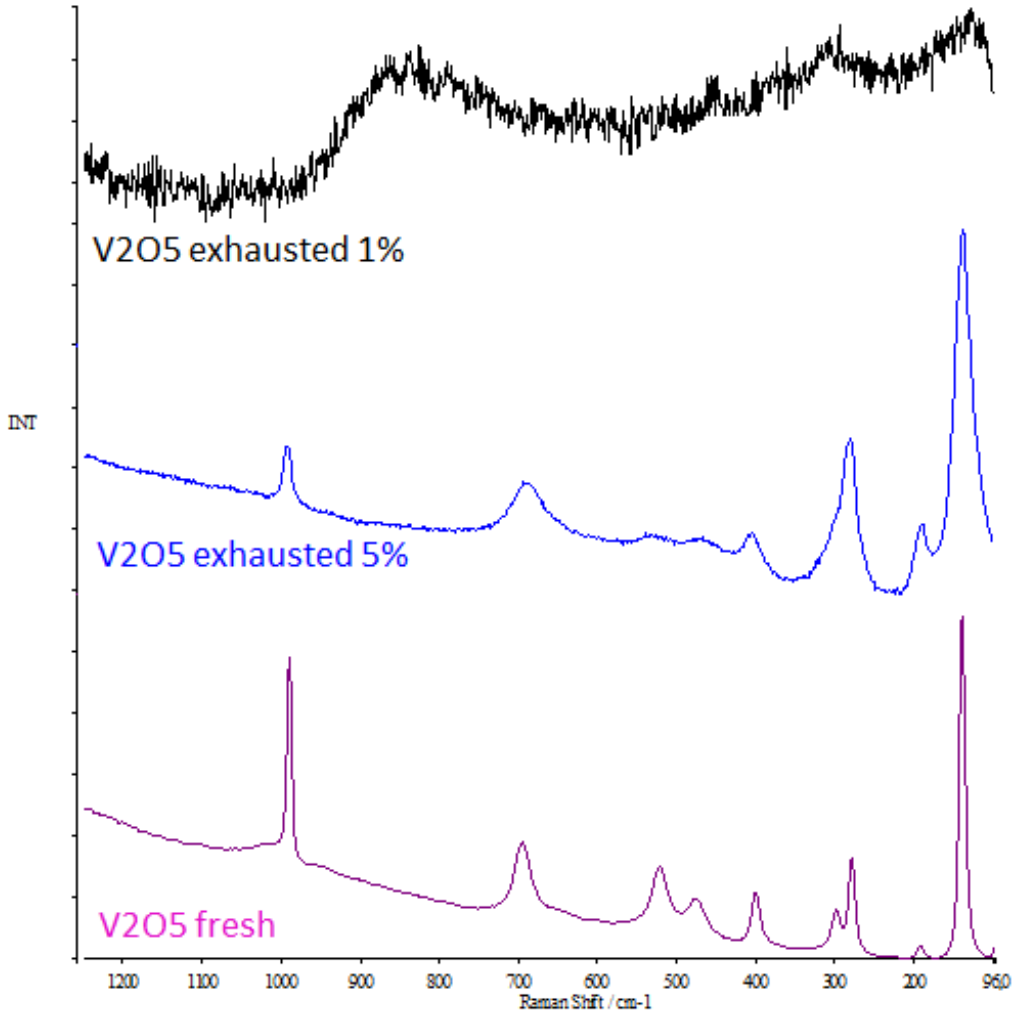

Figure 3.26 Raman analysis of exhausted V_2O_5 1% laser power, 5% laser power, freshly prepared V_2O_5

Interesting results was obtained when Raman spectra of fresh and exhausted $AlVO_4$ was taken. Resultant spectrum of fresh $AlVO_4$ is matching with literature data with a small exception of lower resolution of peaks that are characteristic of Al-V-O_4 (Figure 3.27).

Spectra of exhausted $AlVO_4$ look similar to spectra of fresh V_2O_5 and with broad band between 950-750cm-1 which could correspond to Al_2O_3. Characteristic behavior of vanadium oxides, is that spectra of oxides of vanadium with different oxidation states show almost same peaks with some shifts. In other words, similarity of the bands proves that exhausted $AlVO_4$ segregates to Al_2O_3 and VO.

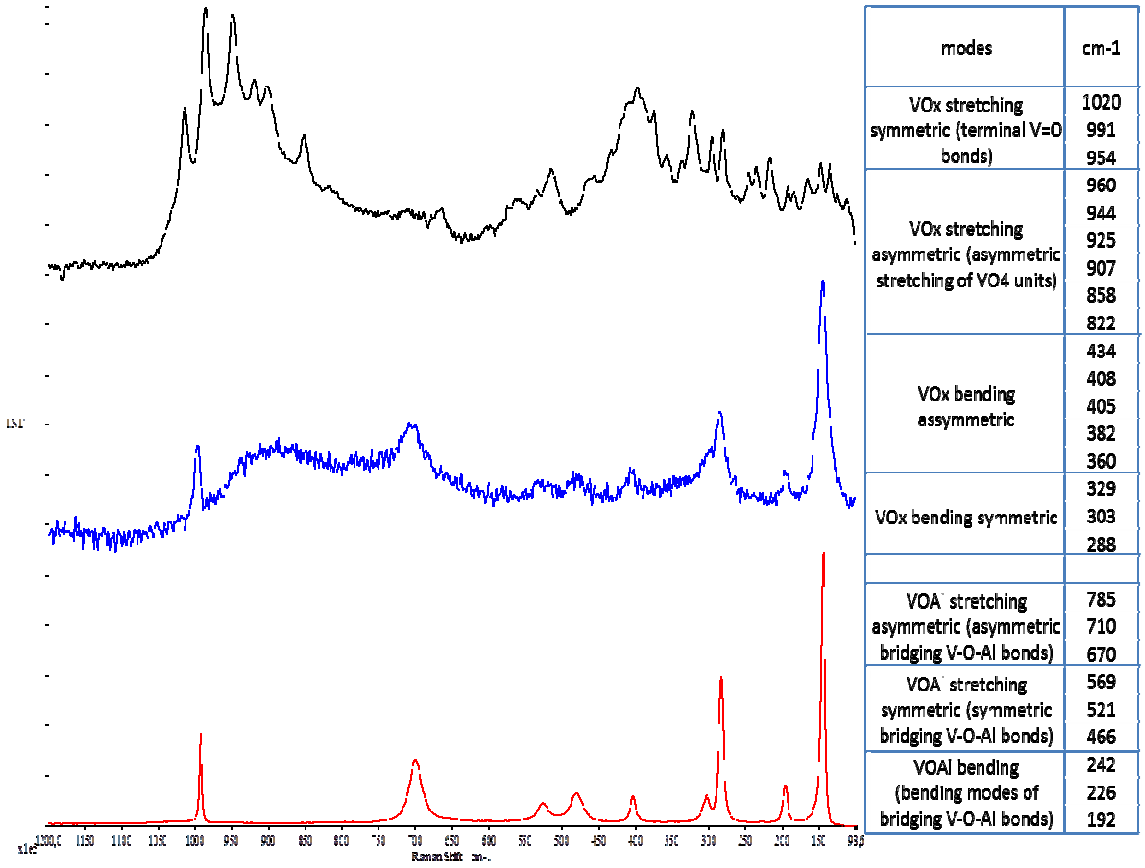

modes	cm-1
VOx stretching symmetric (terminal V=O bonds)	1020 991 954
VOx stretching asymmetric (asymmetric stretching of VO4 units)	960 944 925 907 858 822
VOx bending assymmetric	434 408 405 382 360
VOx bending symmetric	329 303 288
VOA stretching asymmetric (asymmetric bridging V-O-Al bonds)	785 710 670
VOA stretching symmetric (symmetric bridging V-O-Al bonds)	569 521 466
VOAl bending (bending modes of bridging V-O-Al bonds)	242 226 192

Figure 3.27 Raman analysis of freshly prepared and exhausted $AlVO_4$ and freshly prepared V_2O_5. Additional table of $AlVO_4$ vibrational modes.

When applying X-ray diffraction on $Fe_{0,6}Al_{0,4}VO_4$ there was a deviation from a trend. After applying Raman analysis it was found that $Fe_{0,6}Al_{0,4}VO_4$ catalyst consisted of two segregated phases, dark and bright parts (Figure 3.28). From Raman data attempt was made in order to assign those phases, results are present on Table 3.3.

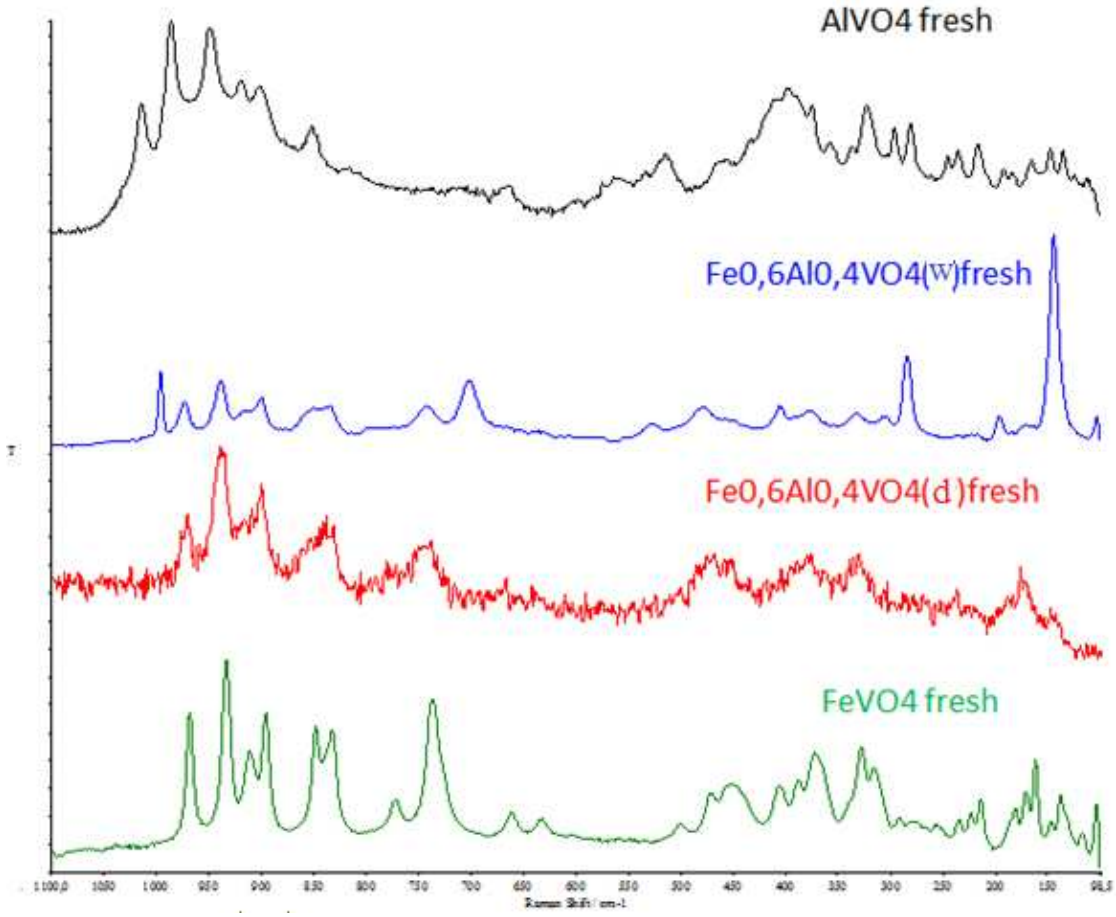

Figure 3.28 Raman analysis of freshly prepared $AlVO_4$, $Fe_{0,6}Al_{0,4}VO_4$ bright part (w), $Fe_{0,6}Al_{0,4}VO_4$ dark part (d), $FeVO_4$ catalysts

Table 3.3 Assignment of Raman shifts of $FeVO_4$, $AlVO_4$ and $Fe_{0,6}Al_{0,4}VO_4$ catalysts

Raman analysis $Fe_{0,6}Al_{0,4}VO_4$

FeVO4		AlVO4		Fe0.6Al0.4VO4			
					Dark		Bright
VOx stretching symmetric (terminal V=O bonds)	971m	VOx stretching symmetric (terminal V=O bonds)	1020m	Vox stretching symm	974		969
	936s		991s		936		992
	900		954s		900		936
VOx stretching asymmetric (asymmetric stretching of VO4 units)	910s	VOx stretching asymmetric (asymmetric stretching of VO4 units)	960	Vox stretching asymm			915
	900s		944		900		898
	850s		925s		845		846
	836s		907m		835		834
	773m		858w				
	738s		822w		746		740
VOx bending assymmetric	370w	VOx bending assymmetric	434m	VOx bending asymm	376		
			408s				
			405s				402
			382m				374
			360m				
VOx bending symmetric	327w	VOx bending symmetric	329m	VOx bending symm	331		331
			303m				303
			288m				282
Vox	1030						
VOFe stretching asymmetric (bridging V-O-Fe bonds)	664w	VOAl stretching asymmetric (asymmetric bridging V-O-Al bonds)	785w				
			710w				700
	634w		670w				
VOFe stretching symmetric	500	VOAl stretching symmetric (symmetric bridging V-O-Al bonds)	569w		481-446		
			521m				526
	460		466m				477
VOFe bending	200-300	VOAl bending (bending modes of bridging V-O-Al bonds)	242m		276		194
			226m		+174		*+172
			192m		+169		*+167 *+143
VOFe	652						

As it is seen from the Table 3.3 bands of the dark part of the $Fe_{0,6}Al_{0,4}VO_4$ catalyst corresponds to $FeVO_4$ and the bright part corresponds mostly to $AlVO_4$ and VO (or V_2O_5).

3.4 In situ Raman Spectroscopy in the cell

With the purpose of simulating the reaction, study the catalysts when methanol is adsorbed on surface, in-situ Raman spectroscopy analysis on reaction conditions were performed.

Figure 3.29 demonstrates in situ Raman analysis of methanol adsorption on $FeVO_4$ catalyst carried out by method described in experimental part. At room temperature we see vibration modes of $FeVO_4$. After increasing the temperature spectra lowers in intensity and also we observe a shift of the bands of V-O, confirming the hypothesis that the volume of unit cell of vanadate crystal increase with temperature. On the other hand bands related to V-O-Fe is not shifted or negligibly shifted. As it is seen from the figure, the bands of the catalyst lowers in the intensity and shifts a little, due to the methanol adsorption too.

The interesting observation was made when performing this experiment: reduction of the catalyst is not observed, but the point where laser pointed to the catalyst sample became black after 1 hour of experiment (about 15-20 min of continuous laser light), also the whole surface of the catalyst became a bit darker.

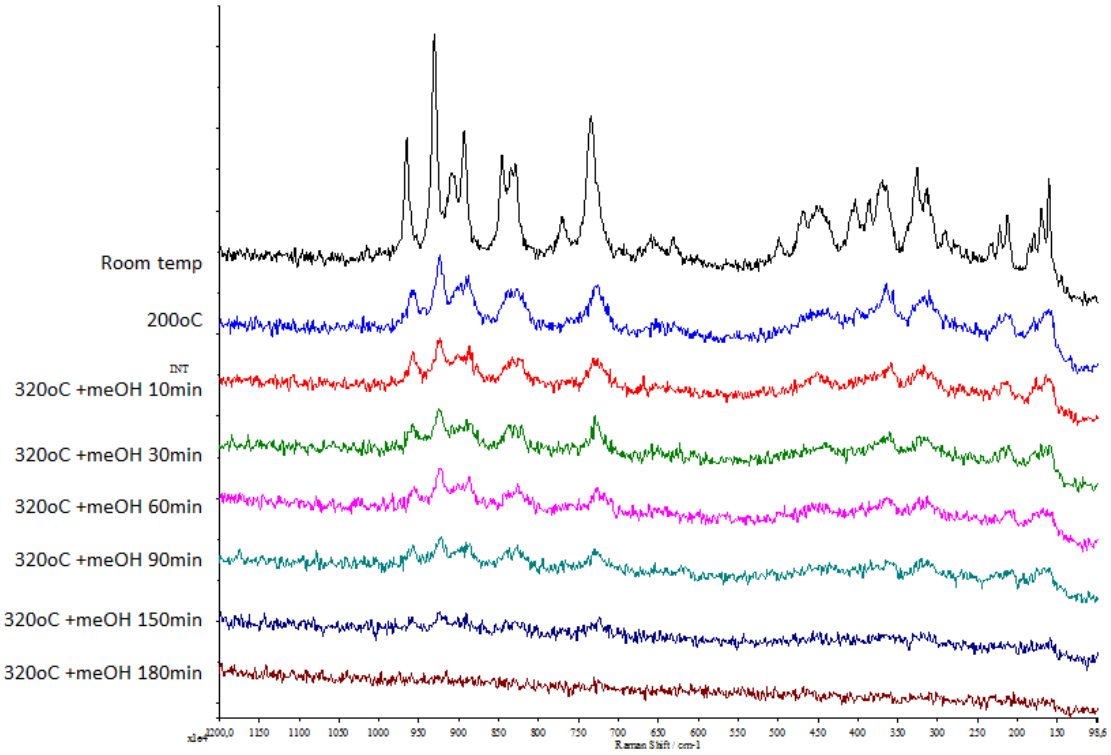

Figure 3.29 In situ Raman analysis of $FeVO_4$ catalyst

Same experiment in-situ Raman was performed with methanol adsorption on $AlVO_4$ catalyst. Figure 3.30 shows results of the analysis. Similar behavior to $FeVO_4$ was observed under the laser, temperature increase and time of methanol adsorption. Bands of the catalyst lower in the intensity and shift a little during the heat and adsorption. The difference from previous experiment with $FeVO_4$ is that the surface of catalyst became dark faster; there was no black point were the laser pointed; intensity of the bands lowered faster.

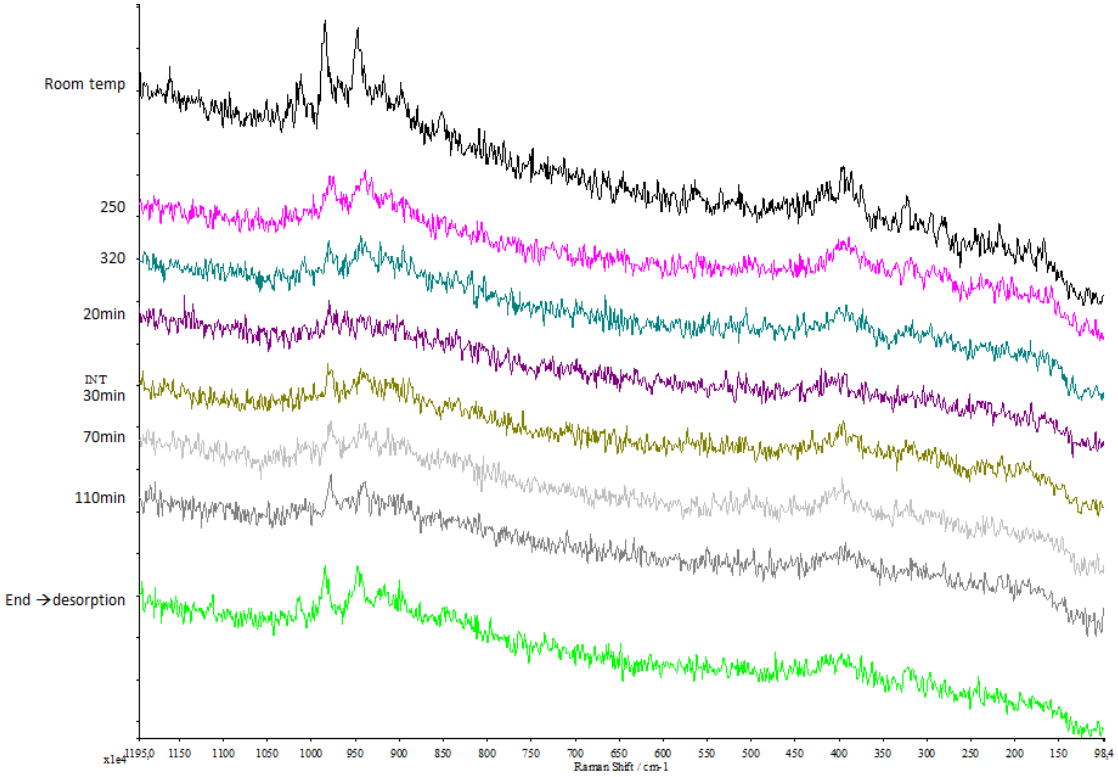

Figure 3.30 In situ Raman analysis of $AlVO_4$ catalyst

The in-situ Raman experiment with $Fe_{0,6}Al_{0,4}VO_4$ was carried out by same method as previous. When applying X-ray diffraction and conventional Raman analysis it was found that $Fe_{0,6}Al_{0,4}VO_4$ catalyst consisted of two segregated phases, dark and bright parts.

Since, in-situ Raman investigation for adsorption of methanol on $Fe_{0,6}Al_{0,4}VO_4$ catalyst was performed twice pointing different phases.

In-situ Raman analysis carried out for dark part showed almost identically same behaviour as FeVO4 catalyst, a little shift due to heat and decrease of the intensity (Figure 3.31).

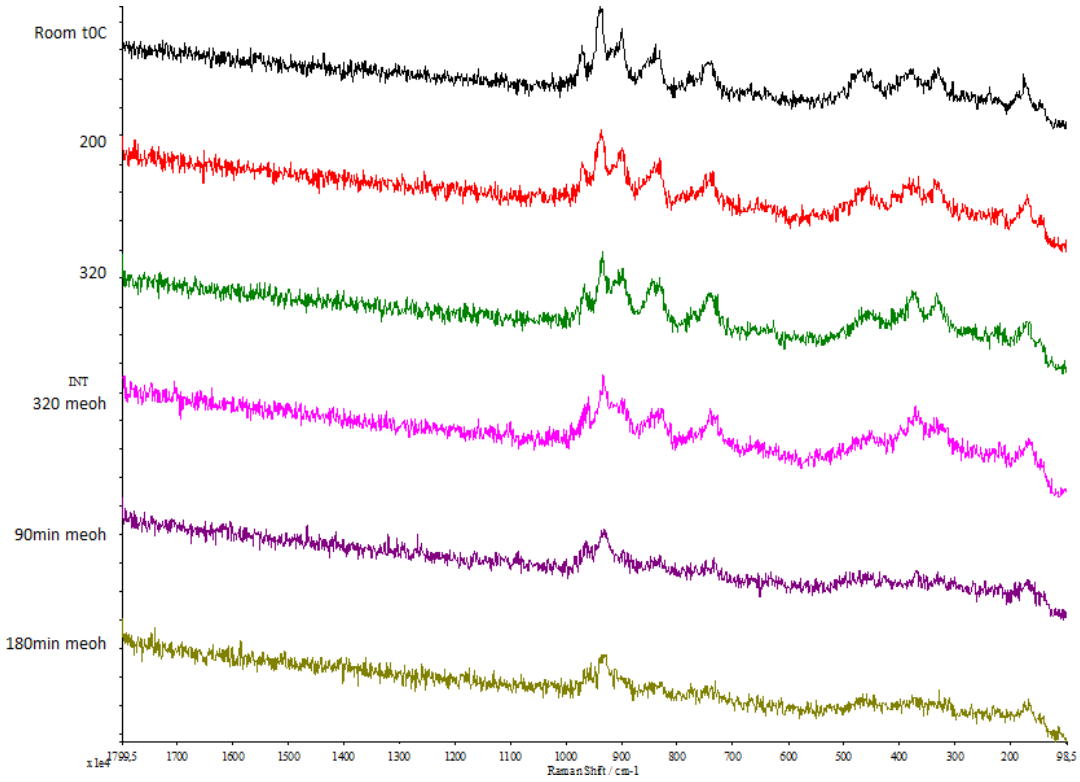

Figure 3.31 In situ Raman analysis of dark part of $Fe_{0,6}Al_{0,4}VO_4$ catalyst

In situ Raman of the bright part of $Fe_{0,6}Al_{0,4}VO_4$ catalyst demonstrated in Figure 3.32 and Figure 3.33 showed more interesting results. When heating the sample and at first 20 min of methanol feeding the spectra of the catalyst showed intensity decrease and a little shift as in previous experiments (Figure 3.32).

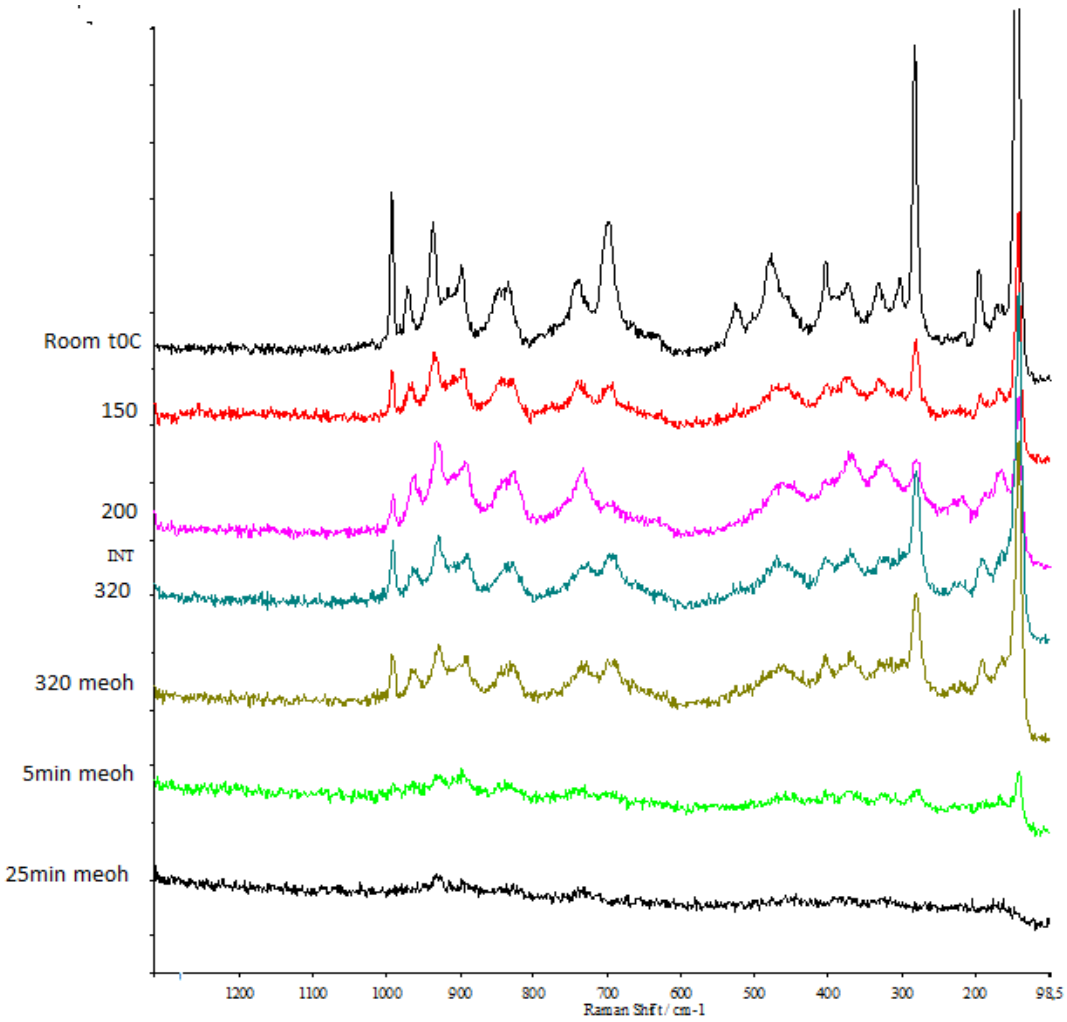

Figure 3.32 In situ Raman analysis of bright part of $Fe_{0,6}Al_{0,4}VO_4$ catalyst until 25 min. feeding methanol

However, after 20-25 min feeding methanol under the reaction temperature very intense bands probably corresponding to V_2O_5 (or V_xO_y) decreased in the intensity and disappeared, while bands most likely corresponding to $FeVO_4$ and $AlVO_4$ decrease in the intensity, but still present (Figure 3.33).

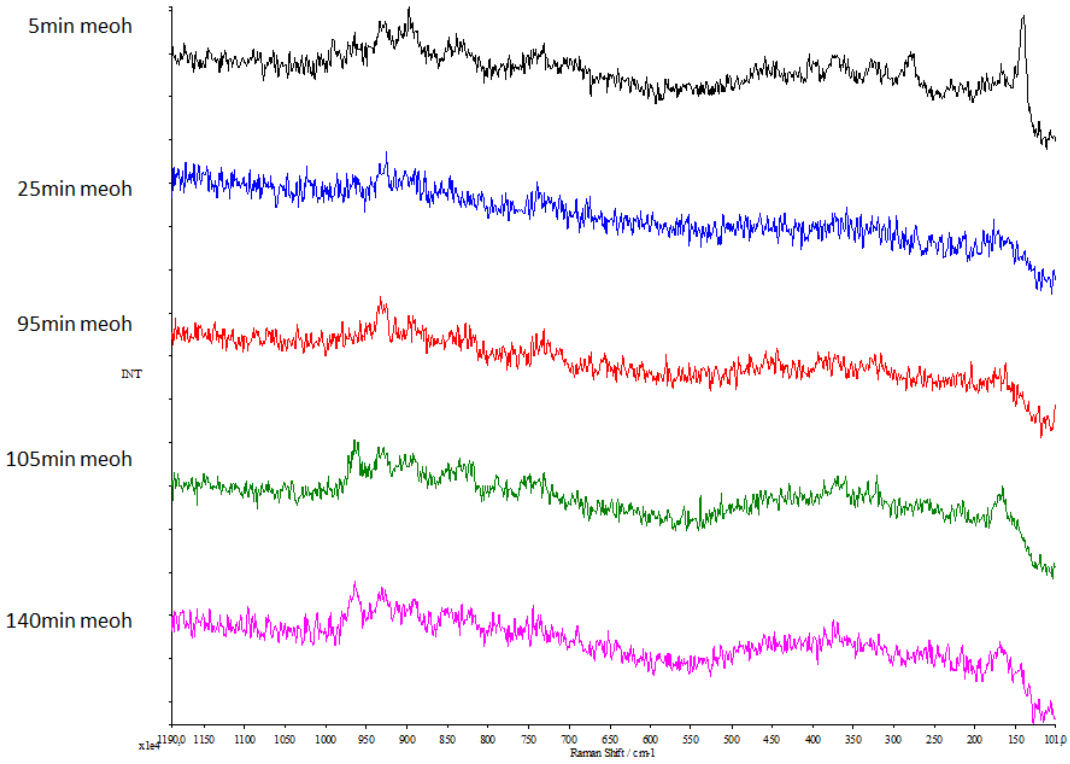

Figure 3.33 In situ Raman analysis of bright part of $Fe_{0,6}Al_{0,4}VO_4$ catalyst, after 25 min feeding methanol

With the aim of having a full picture for comparison of catalysts behavior same method of in-situ Raman was performed for methanol feeding on V_2O_5 catalyst. Figure 3.34 shows that there is an intensity decrease, as in previous catalysts analysis, however there is almost no or very insignificant shift due to the heat and laser light heat.

Main difference of experiment with V_2O_5 from previous catalysts is that when feeding methanol about 20 min, catalyst became fully black and any signal on the spectra disappeared.

In order to check if this behavior somehow relates to Raman cell, the catalyst sample was taken out of the cell and conventional Raman with low power laser was done. The resultant spectra was similar to exhausted catalyst, in other words we observe reduction of the catalyst.

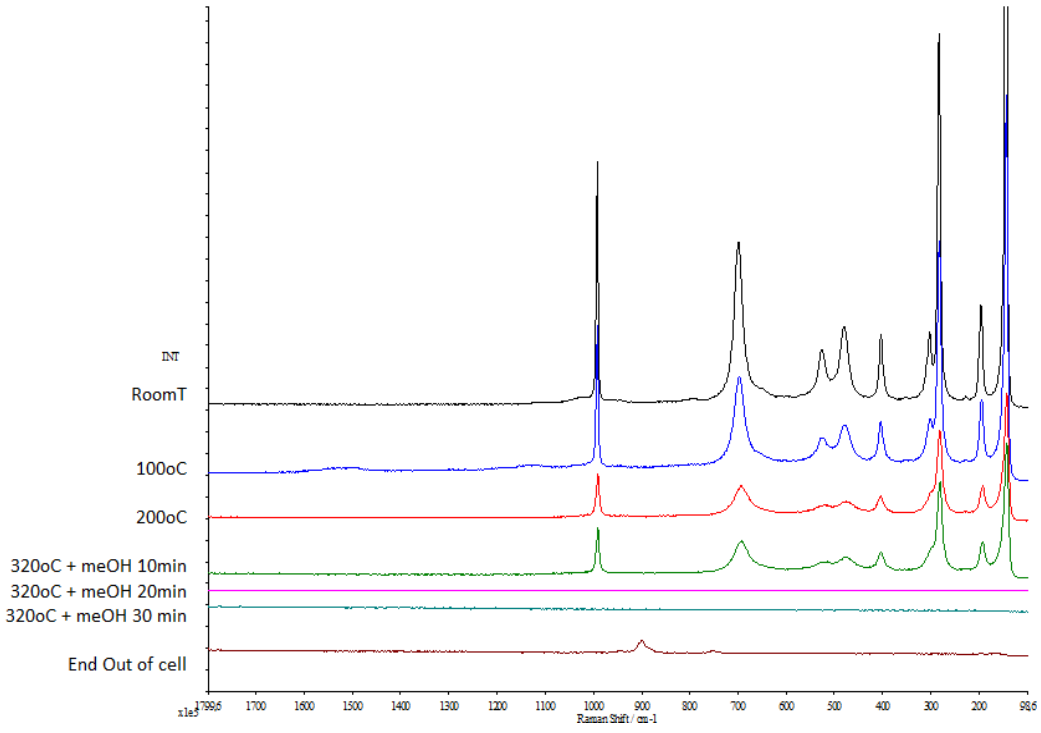

Figure 3.34 In situ Raman analysis of V_2O_5 catalyst

After performing test with V_2O_5 we could hypothesize that reduction of the catalyst happens on all the catalysts that were tested. But the reduction of the catalysts appears on the entire surface except the point where laser is directing. In the other words the point where the laser is focused stays reoxidezed by laser. Therefore with Raman spectroscopy it is impossible to study the reduction of the catalyst and other changes that could happen due to methanol adsorption.

3.5 Diffuse Reflectance Infrared Fourier Transform Spectroscopy investigations

Another technique to study the reaction of phenol methylation, Diffuse Reflectance Infrared Fourier Transform Spectroscopy (DRIFTS) was applied in order to presume the behavior of the catalyst and to identify adsorbed species on the surface of the catalysts.

The DRIFTS spectra after methanol adsorption at 85^{o}C on the $FeVO_4$ catalyst are presented in Figure 3.35. The IR spectra prior to the CH_3OH adsorption on the dehydrated catalyst sample in the He environment have been subtracted from that of methanol exposed surfaces to isolate the surface vibrations resulting from methanol adsorption. Both surface CH_3O* and intact surface CH_3OH* species, with the molecular methanol bound to Lewis acid surface sites (L-CH3OH), are observed on catalyst. Predominantly surface CH_3O* species are observed at 2930 and 2828 cm-1, along with a smaller signal for the intact surface CH_3OH* species at 2956 and 2852 cm-1. The surface CH_3O* vibrations on $FeVO_4$ match the vibrations of the surface V-OCH_3 assuming that bulk $FeVO_4$ phase is surface enriched with VO_x species.

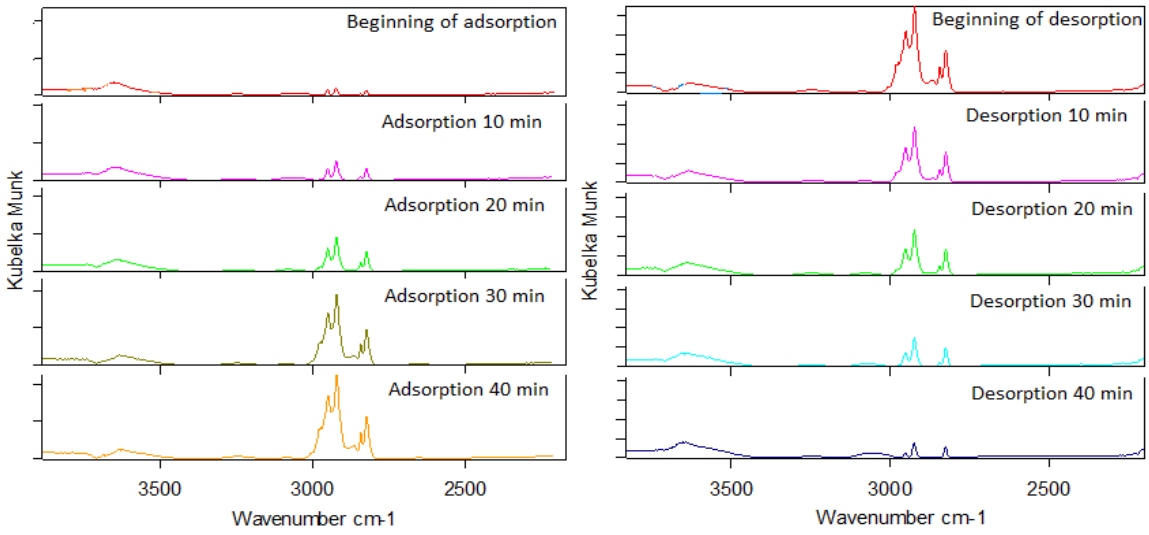

Figure 3.35 DRIFTS analysis of $FeVO_4$ catalyst adsorption (left) and desorption (right) at 85^{o}C

As it is shown in the Figure 3.35 adsorption appears rapidly after beginning of feeding methanol. After 40 minutes of feeding there were no significant changes in spectra. Desorption spectra shows that most of the species are physically adsorbed. There

is also some presence of –OH species identified by broad peak at around 3700 cm^{-1} and some not significant peak of formate species are present during desorption.

DRIFTS spectra at phenol methylation reaction temperature (320^{o}C) with only methanol adsorption on the $FeVO_4$ catalyst are presented in Figure 3.36 and Figure 3.37. The spectra after CH_3OH adsorption were subtracted from the dehydrated catalyst spectra in the He environment. Both surface CH_3O* and intact surface CH_3OH* with the molecular methanol bound to Lewis acid surface sites (L-CH3OH) species are present as in spectra of 85^{o}C adsorption (CH_3O* at 2930 and 2828 cm-1, along with CH_3OH* at 2956 and 2852 cm-1).

The main difference from spectra observed at 85^{o}C is that there is a reduction of catalyst. The proof of reduction is observed with increase of background at 2078 cm^{-1} which is V^{4+}-O bond vibration, and decrease of V^{5+} - O at 2020 cm^{-1} (Figure 3.36). Also very important difference from the spectra obtained at 85 ^{o}C that methoxy species appear in the beginning of feeding and then disappear, while broad bands related to formate species remain on the surface and increase in intensity. This observation could be assumed as one of the evidences of $FeVO_4$ activity in producing formaldehyde and in methylation of phenol.

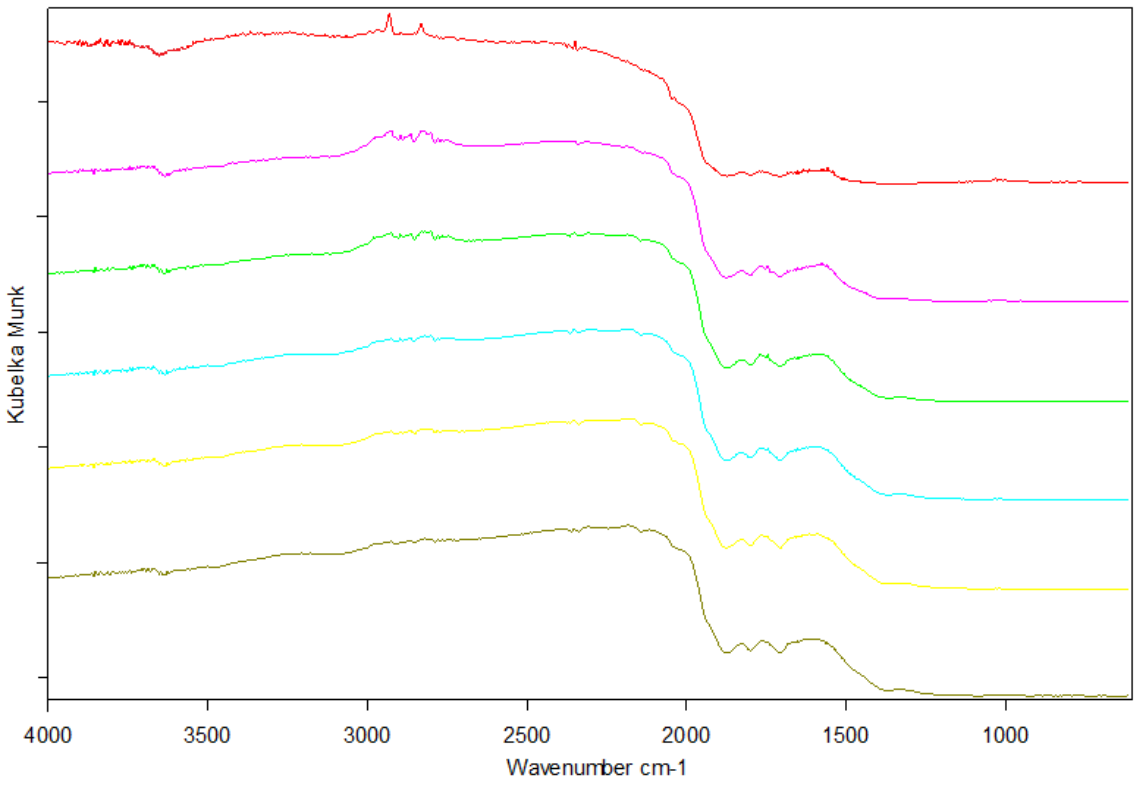

Figure 3.36 DRIFTS analysis of methanol adsorption at 320^{o}C on $FeVO_4$ catalyst

From spectra of methanol desorption at 320°C on $FeVO_4$ we observe that broad bands at 1670–1500 cm^{-1} ; 1350– 1300 cm^{-1} and at 1713-1772 cm^{-1}, which are correspond to formate species and C-O vibrations probably from molecular form of H_2CO, are strongly adsorbed and remain unchanged in intensity. Some other weak bands attributed to -CH 1473 and 1454 cm^{-1} could be present, masked under the broad band of formate species, but we observe a shoulder on broad band (Figure 3.37).

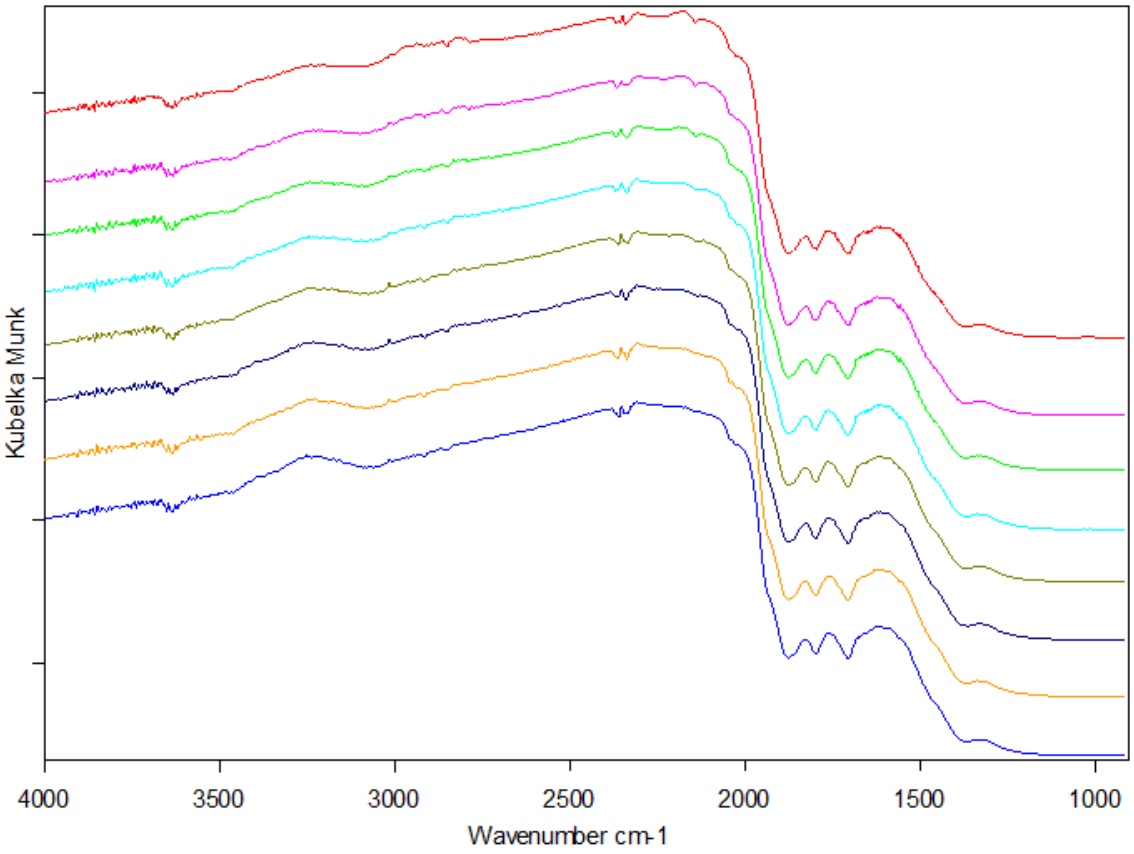

Figure 3.37 DRIFTS analysis of methanol desorption at 320°C on $FeVO_4$ catalyst

DRIFTS at 85°C and 320°C with methanol adsorption were carried out on the $AlVO_4$ catalyst. Figure 3.38 shows the spectra obtained after methanol adsorption and desorption at 85°C, both subtracted from dehydrated catalyst spectra at same temperature. As it is demonstrated both surface CH_3O* and intact surface CH_3OH* with the molecular methanol bound to Lewis acid surface sites (L-CH3OH) species, are present in spectra of 85°C adsorption and desorption (CH_3O* at 2930 and 2828 cm-1, along with CH_3OH* at 2956 and 2852 cm-1), similar to $FeVO_4$ catalyst. Likewise $FeVO_4$ spectra there is a presence of –OH bond vibrations at 3700cm^{-1}.

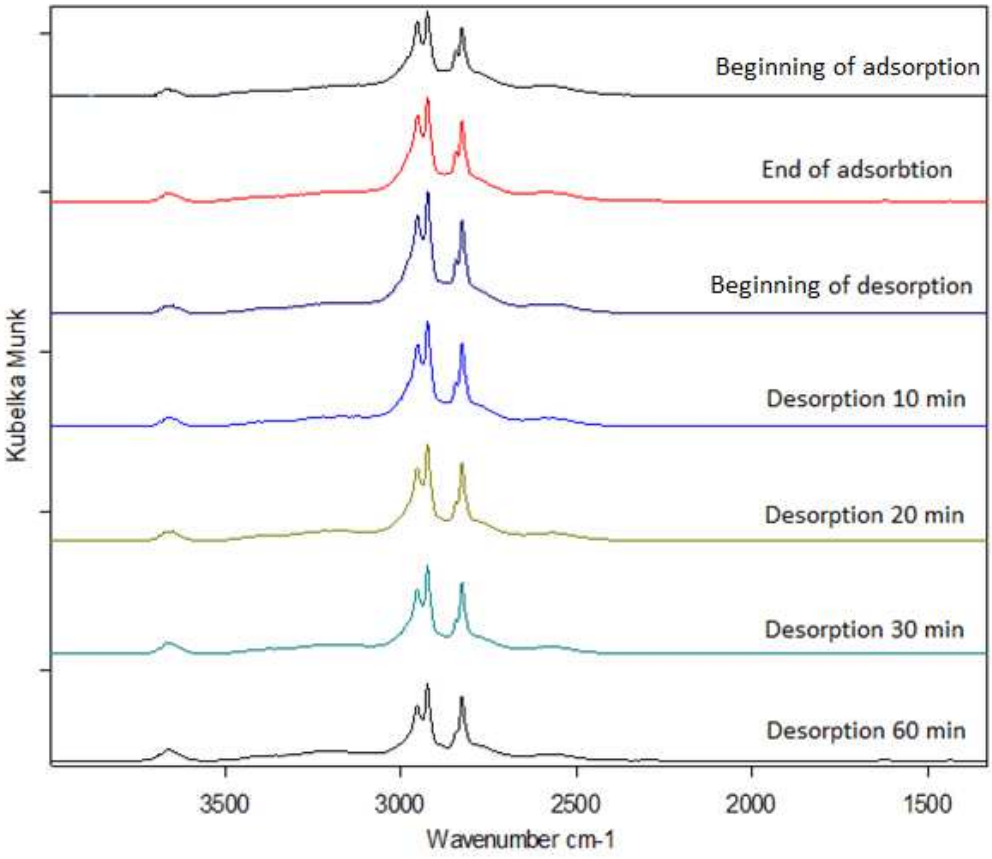

Figure 3.38 DRIFTS analysis of $AlVO_4$ catalyst, adsorption and desorption of methanol at 85°C

In Figure 3.39 DRIFTS spectra of adsorption of methanol on $AlVO_4$ at 320°C, subtracted from pure $AlVO_4$ spectra at same temperature are displayed. As in the case of $FeVO_4$ surface CH_3O* (2930 and 2828 cm^{-1}) and intact surface CH_3OH* (2956 and 2852 cm-1) species are present. Also increase of background at 2078 cm^{-1} which is V^{4+}-O bond vibration, and decrease of V^{5+}- O at 2020 cm^{-1} during the adsorption suggests the reduction of the catalyst. There are also presence of broad bands at 1500-1600 cm^{-1} which correspond to formate species and C-O vibrations probably from molecular form of H_2CO at 1713-1772 cm^{-1}.

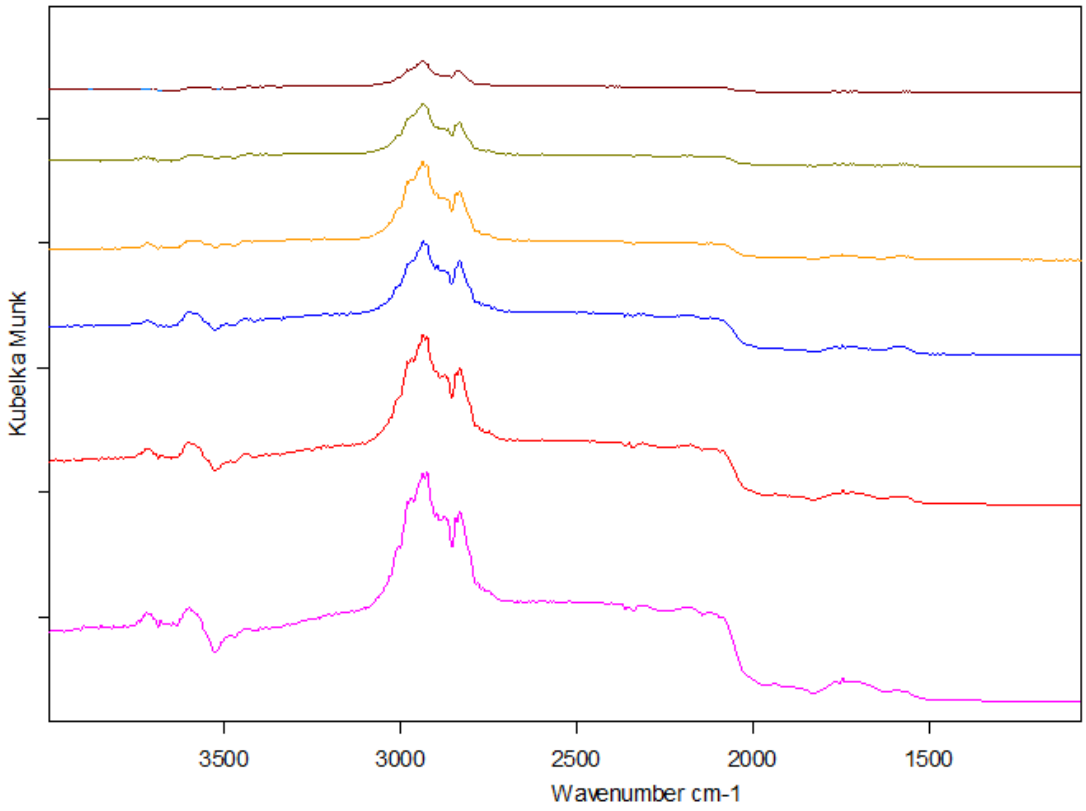

Figure 3.39 DRIFTS analysis of $AlVO_4$ catalyst, adsorption of methanol at 320°C

In Figure 3.40 DRIFTS spectra of desorption of methanol on $AlVO_4$ at 320°C illustrated, spectra of adsorption also subtracted from pure $AlVO_4$ spectra. Surface CH_3O* (2930 and 2828 cm^{-1}) and intact surface CH_3OH* (2956 and 2852 cm-1) species are decreasing in intensity very rapidly until almost disappear. On the other hand there are nearly no changes in intensity of broad peaks corresponding to –OH vibration at about 3700 cm^{-1}, formate species at 1500-1600 cm^{-1} and C-O vibrations probably from molecular form of H_2CO at 1713-1772 cm^{-1}.

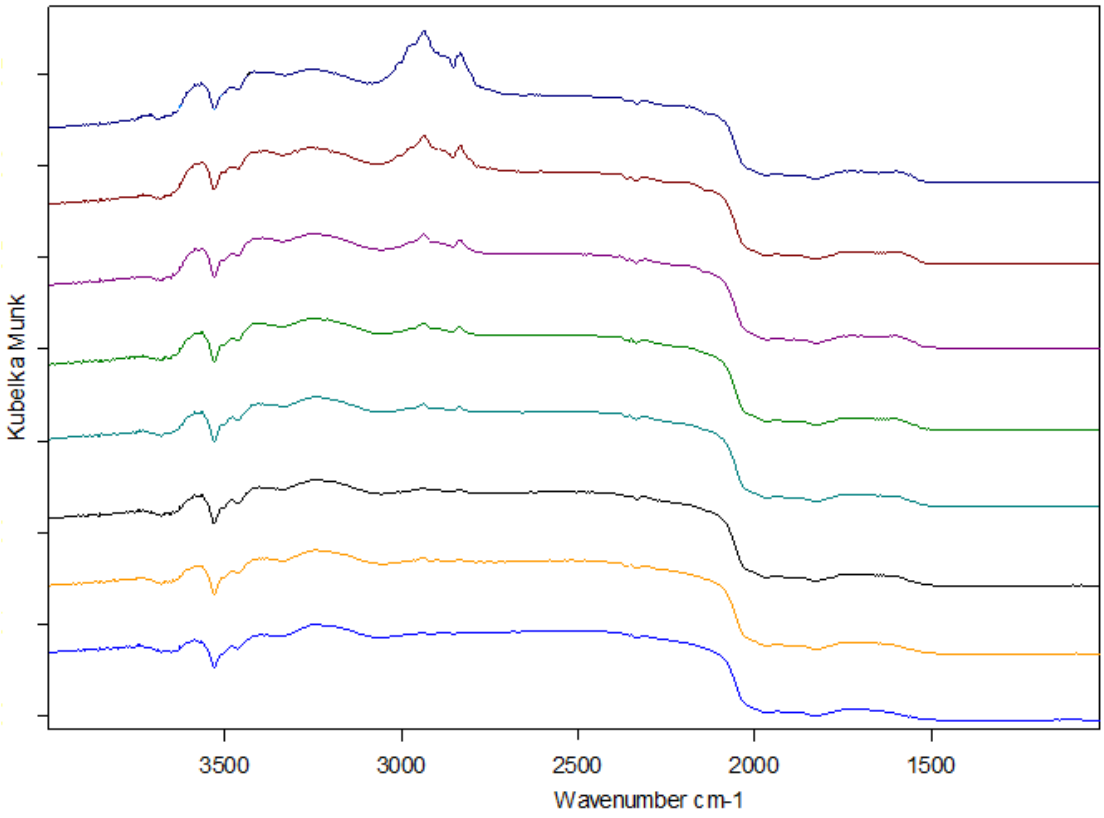

Figure 3.40 DRIFTS analysis of $AlVO_4$ catalyst, desorption of methanol at 320°C

In Figure 3.41 and 3.42 DRIFTS spectra obtained with V_2O_5 in-situ at 85°C are shown. In order to have a better observation of the changes produced in the catalyst IR spectra, the adsorption of methanol spectra were subtracted from dehydrated catalyst spectra. When methanol is introduced in the DRIFTS cell, several bands characteristic of adsorbed methoxy groups appear. Those bands in the 3030–2800 cm^{-1} region discussed before (in $FeVO_4$ and $AlVO_4$); three observed at 1055, 1030 and 1005 cm^{-1} are due to –CH, C–O of adsorbed methoxy species; bands between 3700 and 3600 cm^{-1} are assigned to -OH of V–OH groups; some other weak bands attributed to -CH 1473 and 1454 cm^{-1}; CH of H CO species at 1278 cm^{-1} and formate species at 1670–1500 cm^{-1} and 1350–1300 cm^{-1} are also observed. There is also some reduction of the catalyst due to decrease of V^{+5}-O at 1971 and 2020 cm^{-1} and increase of V^{4+}-O at 2078 cm^{-1}.

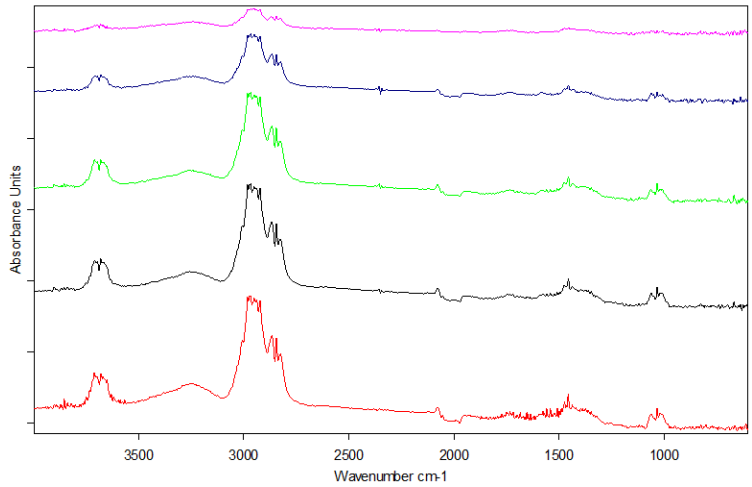

Figure 3.41 DRIFTS analysis of methanol adsorption at 85°C on V_2O_5 catalyst

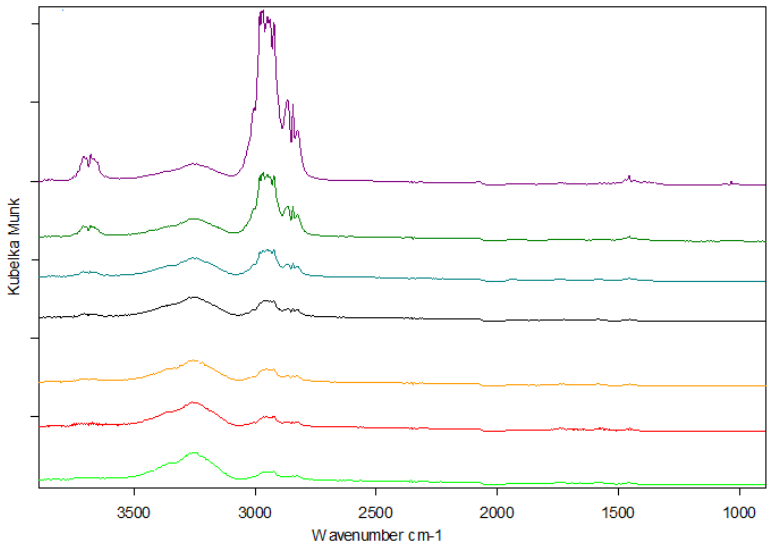

Figure 3.42 DRIFTS analysis of methanol desorption at 85°C on V_2O_5 catalyst

After increase of temperature of the system (Figure 3.43 and Figure 3.44), a decrease in the intensity of the bands due to the V^{+5}-O at 1971 and 2020 cm^{-1} observed much more dramatically as in the experiments with previous catalysts. Since that and because of greater increase of background at 2078 cm^{-1} (V^{4+}-O), the presence of reduction of the catalyst is assumed.

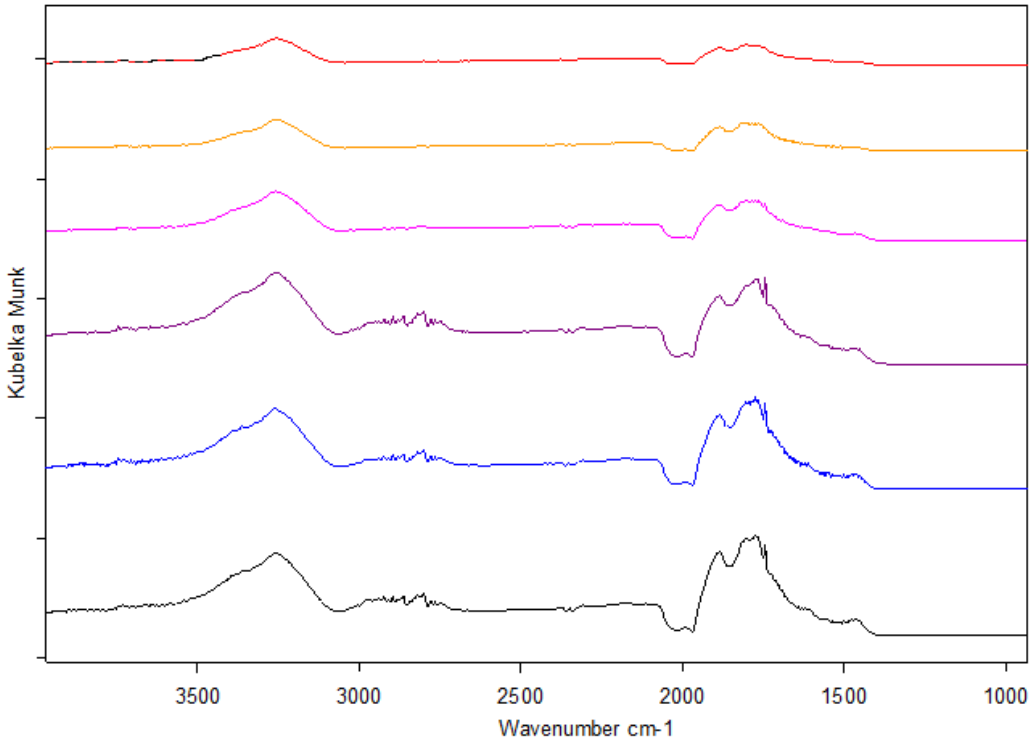

Figure 3.43 DRIFTS analysis of V_2O_5 catalyst adsorption at 320°C

Also on raising the temperature there is a much higher intensity of weak bands in the 1650–1500 and 1350–1300 cm^{-1} regions, which are assigned to formate species; intense broad bands due to C--O 1772, 1745 and 1713 cm^{-1}; and C–-H species 2803 and 2760 cm^{-1} were found (Figure 3.43 and Figure 3.44). On the other hand, bands due to methoxy species (between 3030–2800 cm^{-1}), which were observed at lower temperatures and at same temperature on previous catalysts, disappear or masked.

Broad bands of C-O (1713-1772cm^{-1}) assigned to a perturbed molecular form of HCO_2 probably coordinated on Lewis acid sites.

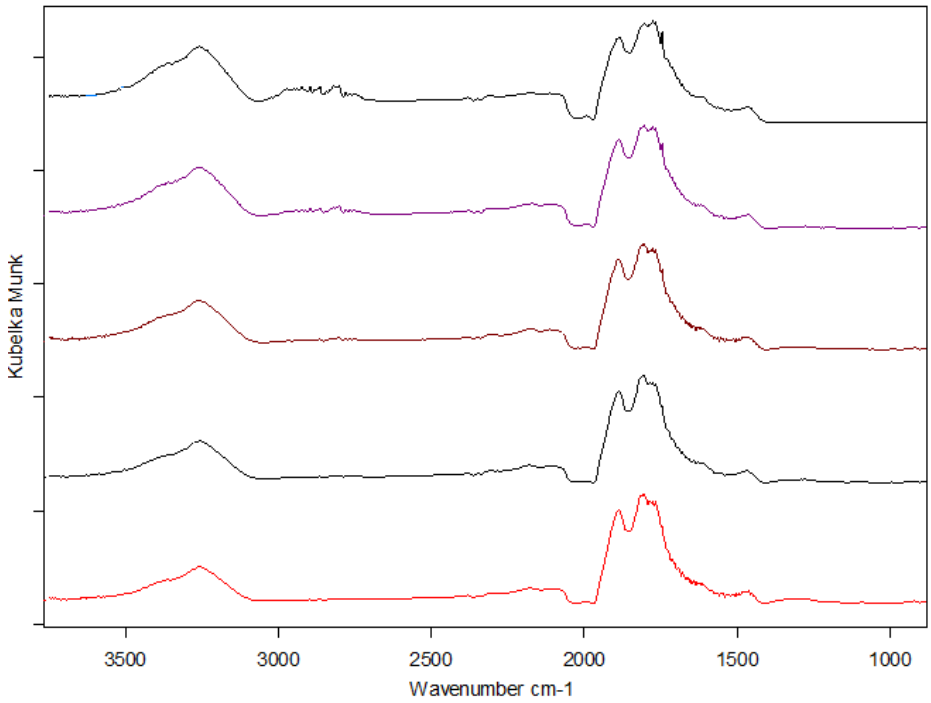

Figure 3.44 DRIFTS analysis of V_2O_5 catalyst adsorption at 320^oC

DRIFTS results show that a large number of OH groups are formed in this process at the same time that a reduction of surface vanadium atoms is produced V^{5+} to V^{4+}. Besides this, molecular water is also produced, probably as a result of hydroxyl condensation.

The DRIFTS instrument that was used for abovementioned tests equipped with MASS spectrometer. The main results taken from MASS data of methanol adsorption at 320°C on $FeVO_4$ and $AlVO_4$ are shown in Figure 3.45 and Figure 3.46 respectively. The main difference noticed is that on $AlVO_4$ there is a high formation of m/z=46 (di-methyl ether), which is not produced on $FeVO_4$. Both catalysts produce formaldehyde, CO, CO_2 and other species that were also produced during methanol decomposition test.

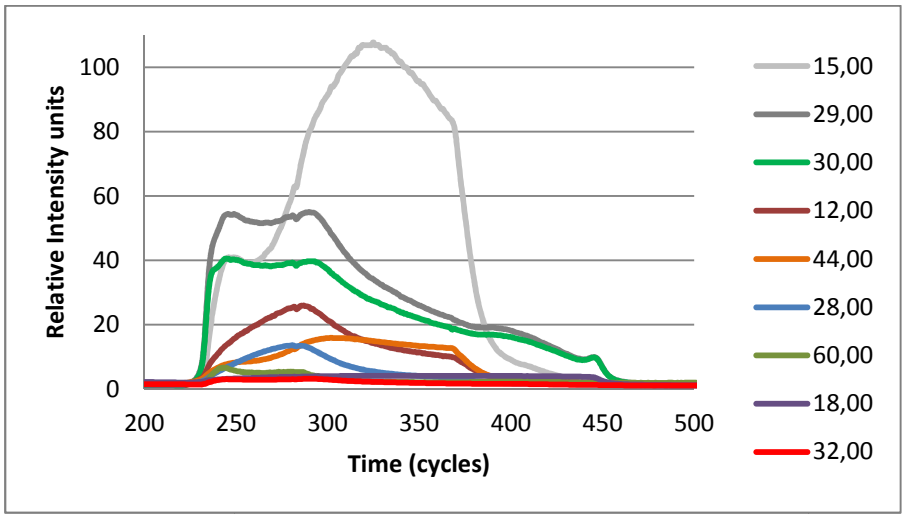

Figure 3.45 DRIFT-MASS data taken during methanol adsorption and desorption on $FeVO_4$ catalyst at 320°C. Note: numbers (lines) correspond to m/z value.

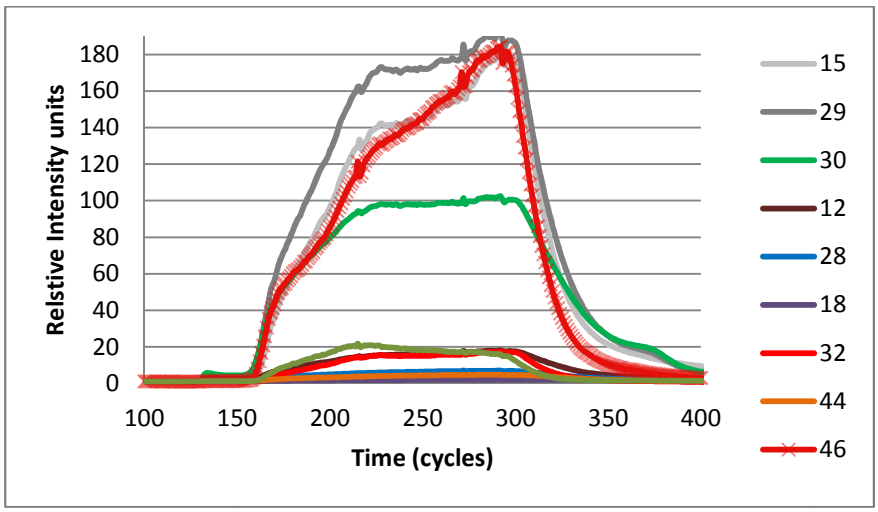

Figure 3.46 DRIFT-MASS data taken during methanol adsorption and desorption on $AlVO_4$ catalyst at 320°C. Note: numbers (lines) correspond to m/z value

Concluding DRIFTS part of this work we could hypothesize that one of the reasons of the high activity of $FeVO_4$ and V_2O_5 comparing with $AlVO_4$ is because the spectra demonstrates that the FeVO4 catalyst is very active in dehydrogenation of methanol to produce formaldehyde; the latter may either react with phenolate or form the formate species because of the oxidizing properties of the catalyst. Therefore, in any case the development of the formate species highlights the ready formation of formaldehyde.

On $AlVO_4$ catalyst there is relatively lower formation of formate species comparing with formation of methoxy species. At reaction temperature, relatively strong adsorption of methoxy species observed only on $AlVO_4$.

Another reason of lower activity is that $AlVO_4$ possess some acid characteristics, which is proved by formation of dimethyl ether in a relatively big amount.

We observed how methanol adsorbed on the surface of $FeVO_4$, $AlVO_4$ and V_2O_5, but not only methanol adsorbs on the surface of the catalyst during the phenol methylation reaction, also the phenol is a substrate. Another way to explicate the reactivity of the catalysts, is a phenol adsorption on the surface.

3.6 In-Situ Infrared spectroscopy in vacuum

In order to perform Infrared spectroscopy analysis with phenol adsorption plant specially made for in-situ Infrared spectroscopy in vacuum was performed. The tests were carried out as it is described in experimental part.

Results of in-situ Infrared spectroscopy analysis of phenol adsorption and desorption on $FeVO_4$ catalyst are displayed in Figure 3.47. Despite that intensities of the bands are low, from the spectra of phenol adsorption we are able to identify O-H, C-H, C-C, C-O stretching bands.

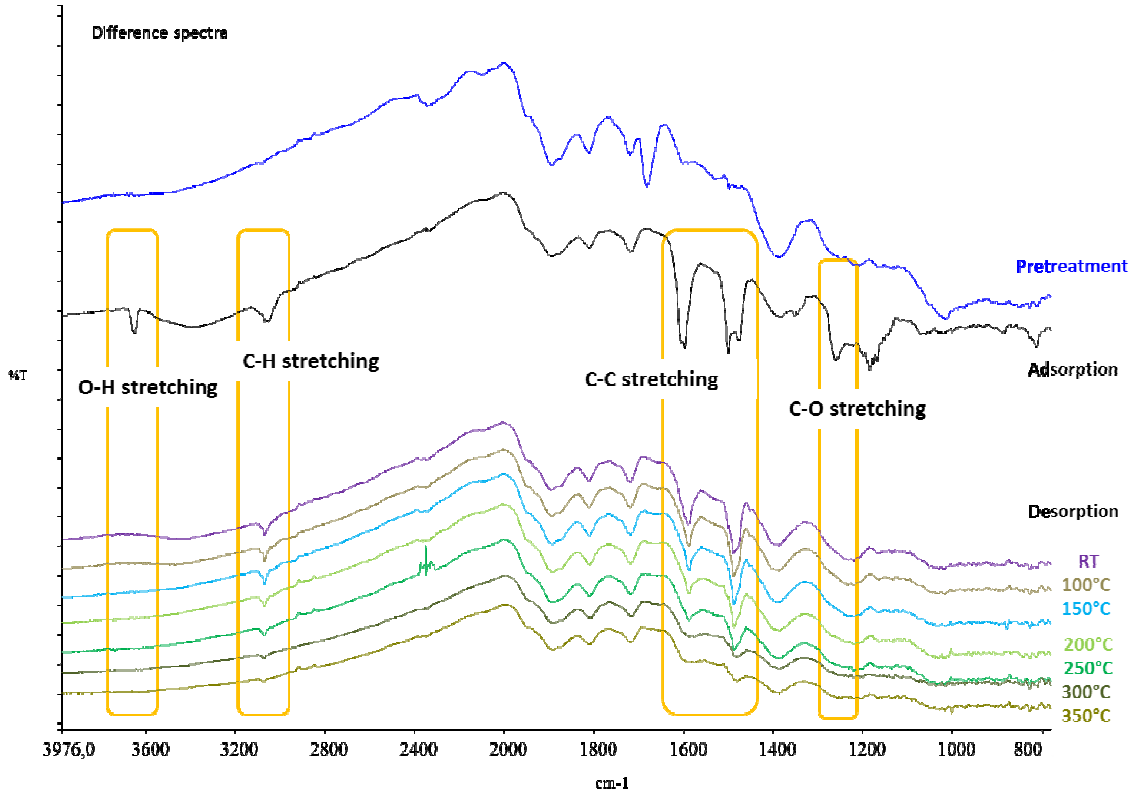

Figure 3.47 In-situ IR spectroscopy in vacuum. Spectra of pretreatment at 500°C, phenol adsorption and desorption of phenol on $FeVO_4$ at increasing temperatures

When start to perform desorption, at room temperature in vacuum O-H stretching band disappear immediately. This is the evidence that no phenol remains on the surface of the catalyst, therefore there is low energy of adsorption, and most amount of phenol is physisorbed. But on the same time we observe the presence of C-H, C-C and C-O stretching modes, consequently phenol chemisorbed in the form of phenate species. C-H and C-C modes of aromatic ring are not shifted, that could be proof of orthogonal

adsorption of phenate onto the surface, and explains regioselectivity to ortho positions. It is noticeable that band of C-O is perturbed, because C-O band shifts when transformed from –C-O-H form to -C-O-surface form (Figure 3.47). The adsorption of phenate species is strong, since the presence of mentioned bands even after increasing the temperature to 350°C. This could be the reason why FeVO4 is selective to dimethylated products.

Same experiment, in-situ IR in vacuum, was done on phenol adsorption and desorption on $AlVO_4$ catalyst. After adsorption of phenol we observe isolated O-H, broad band of interacting O-H, C-H, C-C and C-O stretching modes of phenol on the surface of the catalyst (Figure 3.48).

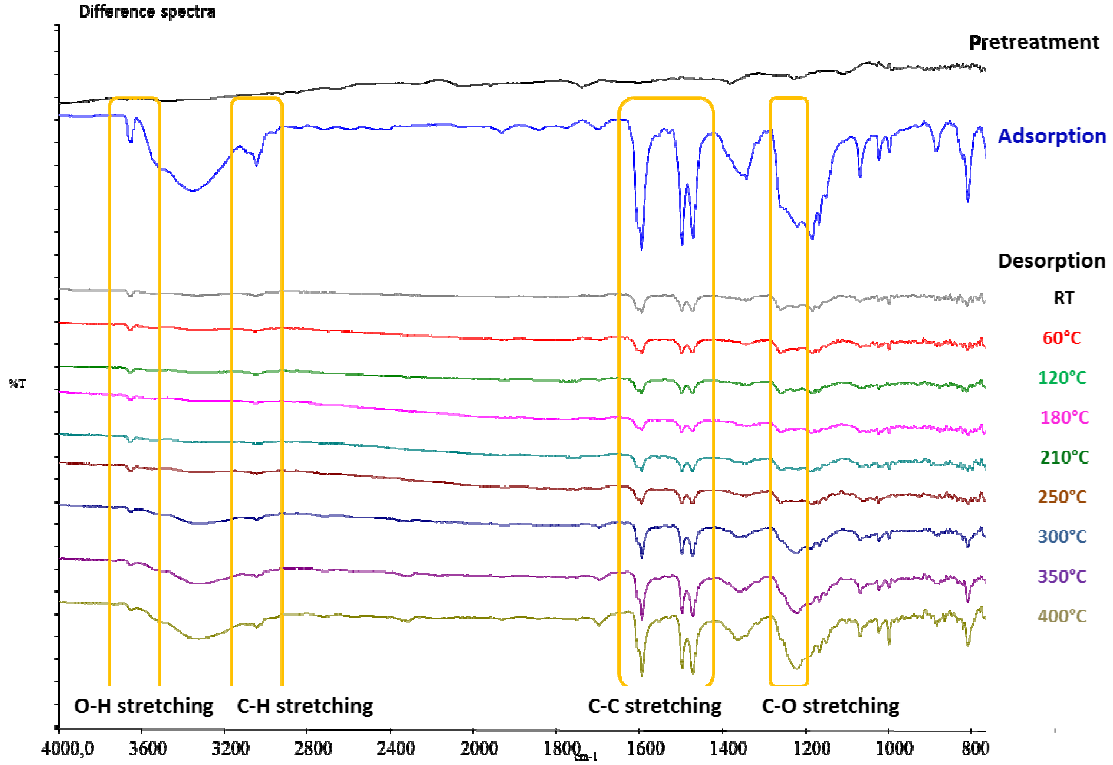

Figure 3.48 In-situ IR spectroscopy in vacuum. Spectra of pretreatment at 500°C, phenol adsorption and desorption of phenol on $AlVO_4$ at increasing temperatures.

After the start of desorption at room temperature and during the increase of temperature until 400°C there is a presence of all listed bands observed (Figure 3.48). It seems that low amount of phenol remains on the surface of the catalyst, because of the presence of isolated –OH band that is present during desorption. Phenol adsorbs

orthogonally on the surface since C-C and C-H bands are almost at the same wavelength during adsorption and desorption.

Band related to C-O stretching mode is very broad while adsorption, so it is difficult to be sure, but it seems that both phenol and phenate species adsorbed on the surface.

After desorption at 300^{o}C, probably due to some acidity of catalyst, there are increase of broad bands of surface -OH (≈3300cm^{-1}), and some increase of intensity in the area of C-O stretching.

Concerning V_2O_5 catalyst, it was impossible to perform in-situ Infrared spectroscopy analysis, because catalyst became black during pretreatment and adsorption of phenol on surface.

CONCLUSIONS

The aim of this work was to investigate the reactivity of metal oxide catalysts for the gas-phase phenol methylation with methanol.

Particular attention was devoted to the comprehension of the interaction of reactant and active phase in order to explicate the role of each character involved in the reaction.

$FeVO_4$ showed the best catalytic performance, leading to the formation of 2,6-xylenol with high selectivity and yield at the optimized reaction conditions (320°C and feed ratio methanol:phenol=10:1).

Bulk V_2O_5 showed a similar reactivity compared to $FeVO_4$ instead Fe_3O_4 is almost not active. This demonstrated that the real active phase for the adsorption and activation of phenol and methanol by dehydrogenation to formaldehyde is a V-containing phase.

On the other hand, $AlVO_4$ lead to formation of mono-methylated product with low yield and low conversion of phenol. Moreover it is rapidly deactivate during the reaction time.

This behavior of the catalysts was explained both by XRD and Raman analysis, which are evidenced that $FeVO_4$ reduce to a mixed spinel that is the real active phase and could be easily reoxidated to the original triclinic vanadate form. In opposite, $AlVO_4$ during the reaction segregates to alumina and reduced vanadium oxide, which are possessing low catalyzing characteristics and could not be reoxidated.

In addition we have found that in the in-situ Raman spectroscopy during methanol adsorption, reduction of the catalysts appears on the entire surface of the catalyst, but the area of the catalyst where laser is focused reoxidized to the higher oxidation state.

Furthermore, DRIFTS and in-situ IR analysis evidenced the interaction and the activation respectively of methanol and phenol on the surface of the catalysts. Adsorption of methanol on $FeVO_4$ benefits with high amount of formate species, while on $AlVO_4$ adsorption appears with low amount of formate species, high amount of physisorbed methoxy species and also formation of dimethyl ether.

From in situ IR in vacuum we confirm that phenol adsorbs on $FeVO_4$ orthogonal and by strongly adsorbed phenate formation, which lead to the very active ortho-di-methylation. In contrast, $AlVO_4$ has a low adsorption energy of phenol and phenate, alumina presence lead to acidity and this help the easily desorption of phenol.

REFERENCES

1. Horsley LH (1952, 1962) Azeotropic Data I and II. American Chemical Society, Washington D.C.
2. Naumann HJ, Schaefer H, Oberender H, Timm D, Meye H, Pohl G (1977) Chem. Techn, Heft 1, p 38.
3. U.S. 4,092,360 Pat (March 30, 1978).
4. Fiege H (2005) Cresols and Xylenols. In: Ullmann's encyclopedia of industrial chemistry, 7th edn, VCH, Weinheim.
5. Weber M, Weber M, Kleine-Boymann M (2004) Phenol. In: Ullmann's encyclopedia of industrial chemistry, 7th edn, VCH, Weinheim.
6. D. Mc Neil, "Cresols", in Kirk-Othmer, Encyclopedia of Chemical Technology, Interscience, New York, 2nd Ed., Vol. 6, pp. 434 - 444 (1965).
7. G. Moon, W. Bohringer, C.T. O'Connor, Catal. Today, 97 (2004) 291.
8. K.E. Clonts, and R.A. McKetta, "Cresols and cresylic acids", in: Kirk - Othmer, Encyclopedia of Chemical Technology, Interscience, New York, 3rd ed., Vol. **3**, pp. 212 - 227 (1978).
9. "Cresols, xylenols and cresylic acid" in: Chemical Economics Handbook, SRI International, pp. 637.5000 B - 637.5002 M (1994).
10. K. Alive, R.A. Venkataraman, and P. Ratnasamy, US Patent No. 5,811,599 (1998).
11. G.N. Vayssiloc, Z. Popova, S. Bratinova, and A. Tuel, Stud. Surf. Sci. Catal., **110** (3rd World Congress on Oxidation Catalysis, Elsevier Science B.V., 1997), 909 - 918 (1997).
12. Z. Popova, G. Vayssilov, and K. Genov, God. Sofii. Univ., Khim. Fak., **90**, 221 - 236 (1998).
13. P. Wu, T. Komatsu, and T. Yashima, J. Phys Chem., ACS ASAP AmChemSoc (1998).
14. R. Kumar, and A. Bhaumik, Microporous Mesoporous Material., **21** (4-6), 497 - 504 (1998).
15. K. Bahranowski, M. Gasior, A. Kielski, J. Podobinski, E.M. Serwicka, L.A. Vartikian, K. Wodnicka, Clay Minerals., **34** (1), p 79-87 (1999).
16. P.R. Singh, G.P. Tercho, J.N. Wentz, J.r., and K.R. Olewine, PCT Inter. Appl., World-wide Patent Applicat ion No. 9,925,666 **A2** (1999).

17. K.M. Dear, Catalyzed Oxidations using Peroxygen Reagents, Interox Widness, UK, p. 356 (1996).
18. T.M. Barnhart, and A.W. Hug hes, US patent 5,912,391 (1997).
19. N. Ballarini, F. Cavani, L. Maselli, A. Montaletti, S. Passeri, D. Scagliarini, C. Flego, C. Perego, J. Catal. 251 (2007) 4238.
20. Mukhopadhyay A.K. and others, Industrial Chemical Cresols and Downstream Derivatives, 2005.
21. G. Sarala Devi, D. Giridhar, B.M. Reddy, J. Molec. Catal., 181 (2002) 173.
22. B.M. Reddy, G. Sarala Devi, P.M. Sreekanth, Res. Chem. Int., 28(6) (2002) 595.
23. F.M. Bautista, J.M. Campelo, A. Garcia, D. Luna, J.M. Marinas, A. Romero, J.A. Navio, M. Macias, Appl. Catal., A, 99 (1993) 161.
24. V. Durgakumari, S. Narayanan, L. Guczi, Catal. Lett., 5 (1990) 377.
25. R. Pierantozzi, A.F. Nordquist, Appl. Catal., 21 (1986) 263.
26. F. Nozaki, I. Kimura, Bull. Chem. Soc. Japan, 50(3) (1977) 614.
27. J.M. Campelo, A. Garcia, D. Luna, J.M. Marinas, M.S. Moreno, Stud. Surf. Sci. Catal., 41 (1988) 249.
28. L. Calzolari, F. Cavani, T. Monti, C.R. Acad. Sci. Paris, Serie IIc, Chimie, 3 (2000) 533.
29. F. Cavani, T. Monti, in “Catalysis of Organic Reactions”, M.E. Ford (Ed.), Marcel Dekker, New York (2000), p. 123.
30. F. Cavani, T. Monti, D. Paoli, Stud. Surf. Sci. Catal., 130 (2000) 2633.
31. F. Cavani, T. Monti, P. Panseri, B. Castelli, V. Messori, WO Patent 74,485 (2001), assigned to Borregaard Italia.
32. L. Gilbert, M. Janin, A.M. Le Govic, P. Pommier and A. Aubry, in “The Roots of Organic Development”, J.R. Desmurs and S. Ratton (Eds.), Elsevier, Amsterdam (1996), p. 48.
33. Y. Shiomi, Y. Nakamura, T. Manabe, S. Furusaki, M. Matsuda and M. Saito, US Patent 5,248,835 (1993), assigned to UBE Ind.
34. E. Santacesaria, D. Grasso, D. Gelosa, S. Carra, Appl. Catal., 64 (1990) 83 and 101.
35. R. Tleimat-Manzalji, D. Bianchi, G.M. Pajonk, Appl. Catal. A, 101 (1993) 339.
36. Y. Fu, T. Baba, Y. Ono, Appl. Catal. A, 166 (1998) 419 and 425.
37. Y. Fu, T. Baba, Y. Ono, Appl. Catal. A, 178 (1998) 219.

38. L. Kiwi-Minsker, S. Porchet, R. Doepper, A. Renken, Stud. Surf. Sci. Catal. 108 (1997) 149.
39. S. Porchet, L. Kiwi-Minsker, R. Doepper, A. Renken, Chem. Eng. Sci., 51(11) (1996) 2933.
40. L. Kiwi-Minsker, S. Porchet, P. Moeckli, R. Doepper, A. Renken, Stud. Surf. Sci. Catal. 101 (1996) 171.
41. M.C. Samolada, E. Grigoriadou, Z. Kiparissides, I.A. Vasalos, J. Catal., 152 (1995) 52.
42. M. Renaud, P.D. Chantal, S. Kaliaguine, Can. J. Chem. Eng. 64 (1986) 787.
43. S.C. Lee, S.W. Lee, K.S. Kim, T.J. Lee, D.H. Kim, J.Chang Kim, Catal. Today, 44 (1998) 253.
44. M. Marczewski, G. Perot, M. Guisnet, Stud. Surf. Sci. Catal., 41 (1988) 273.
45. M. Marczewski, J.-P. Bodibo, G. Perot, M. Guisnet, J. Molec. Catal., 50 (1989) 211.
46. L. Garcia, G. Giannetto, M.R. Goldwasser, M. Guisnet, P. Magnoux, Catal. Lett., 37 (1996) 121.
47. S. Balsama, P. Beltrame, P.L. Beltrame, P. Carniti, L. Forni, G. Zuretti, Appl. Catal., 13 (1984) 161.
48. P. Beltrame, P.L. Beltrame, P. Carniti, A. Castelli, L. Forni, Appl. Catal., 29 (1987) 327.
49. R.F. Parton, J.M. Jacobs, H. van Ooteghem, P.A. Jacobs, Stud. Surf. Sci. Catal., 46 (1989) 211.
50. S. Namba, T. Yashima, Y. Itaba, N. Hara, Stud. Surf. Sci. Catal., 5 (1980) 105.
51. Z.-H. Fu, Y. Ono, Catal. Lett., 21 (1993) 43.
52. M.D. Romero, G. Ovejero, A. Rodriguez, J.M. Gomez, I. Agueda, Ind. Eng. Chem. Res., 43 (2004) 8194.
53. J.B. Moffat, Catal. Rev. Sci. Eng., 18 (1978) 199.
54. Jacobs et al, Stud. Surf. Sci. Catal., 41 (1989) 228.
55. A. Corma, H. Garcia, J. Primo, J. Chem. Res. (S) (1988) 40.
56. P.D. Chantal, S. Kaliaguine, J.L. Grandmaison, Stud. Surf. Sci. Catal., 19 (1984) 93.
57. L.B. Young, N.J. Skillman, US Patent 4,371,714 (1983), assigned to Mobil Oil Co.

58. K. Tanabe, T. Nishizaki, Proceed. 6th ICC, G.C. Bond et al. (Eds), The Chemical Society, London (1977), p. 863.
59. US Patent 3,855,318 (1974), assigned to Asahi Chem.
60. JP 58208244, assigned to Mitsui Toatsu.
61. US Patent 3,446,856 (1964), assigned to General Electric.
62. T. Kotanigawa, K. Shimokawa, Bull. Chem. Soc. Japan, 47 (1974) 950 and 1535.
63. T. Mathew, M. Vijayaraj, S. Pai, B.B. Tope, S.G. Hegde, B.S. Rao, C.S. Gopinath, J. Catal., 227 (2004) 175.
64. F. Cavani, L. Dal Pozzo, C. Felloni, L. Maselli, D. Scagliarini, C. Flego, C. Perego, in “Catalysis of Organic Reactions”, J.R. Sowa Jr., Ed., Taylor & Francis, Boca Raton, p. 347 (2005).
65. F. Cavani, L. Maselli, D. Scagliarini, C. Flego, C. Perego, Stud. Surf. Sci. Catal., 155, 167 (2005).
66. K. Tanabe, Stud. Surf. Sci. Catal., 20 (1985) 1.
67. J. Shabtai, L.H. Klemm, D.R. Taylor, J. Org. Chem. 35 (1970) 1075.
68. J. Shabtai, L.H. Klemm, D.R. Taylor, J. Org. Chem., 33 (1968) 1489.
69. L.H. Klemm, C.E. Klopfenstein, J. Shabtai, J. Org. Chem., 35 (1970) 1069.
70. L.H. Klemm, D.R. Taylor, J. Org. Chem., 35 (1970) 3216.
71. L.H. Klemm, R. Zell, J.S. Shabtai, J. Org. Chem., 39 (1974) 698.
72. L.H. Klemm, D.R. Taylor, J. Org. Chem., 45 (1980) 4320.
73. L.H. Klemm, D.R. Taylor, J. Org. Chem., 45 (1980) 4326.
74. H. Hattori, K. Shimazu, N. Yoshii, K. Tanabe, Bull. Chem. Soc. Japan, 49 (1976) 969.
75. H. Grabowska, W. Mista, L. Syper, J. Wrzyszcz and M. Zawadzki, J. Catal., 160 (1996) 134.
76. H. Grabowska, W. Kaczmarczyk, J. Wrzyszcz, Appl. Catal., 47 (1989) 351.
77. R. Sokoll, H. Hobert, J. Catal., 125 (1990) 285.
78. S. Scire, C. Crisafulli, R. Maggiore, S. Minico, S. Galvagno, Appl. Surf. Sci., 93 (1996) 309.
79. R.F. Parton, J.M. Jacobs, D.R. Huybrechts and P.A. Jacobs, Stud. Surf. Sci. Catal., 46 (1989) 163.
80. J.M. Campelo, A. Garcia, D. Luna, J.M. Marinas, M.S. Moreno, Bull. Soc. Chim. France, 2 (1988) 283.

81. R.F. Parton, J.M. Jacobs, H. van Ooteghem, P.A. Jacobs, Stud. Surf. Sci. Catal., 46 (1989) 211.
82. M. Barteau, Chem. Rev., 96 (1996) 1413.
83. G. Busca, Catal. Today, 27 (1996) 457.
84. J.C. Lavalley, Catal. Today, 27 (1996) 377.
85. US Patent 4,933,509 (1989), assigned to General Electric.
86. US Patent 4,041,085 (1975), assigned to General Electric.
87. V. Durgakumari, S. Narayanan, J. Molec. Catal. 65 (1991) 385.
88. S. Sato, K. Koizumi, F. Nozaki, J. Catal. 178 (1998) 264.
89. K.-T. Li, I. Wang, K.-R. Chang, Ind. Eng. Chem. Res. 32 (1993) 1007.
90. J. Kaspi, G.A. Olah, J. Org. Chem. 43(16) (1978) 3142.
91. P.D. Chantal, S. Kaliaguine, J.L. Grandmaison, Appl. Catal. 18 (1985) 133.
92. R.C. Greenler, J. Chem. Phys. 37 (1962) 2094.
93. R.O. Kagel, J. Phys. Chem. 71 (1967) 844.
94. L.J. Burcham, L.E. Briand, I.E. Wachs, Langmuir 17 (2001) 6164 and 6175.
95. N.D. Lazo, D.K. Murray, M.L. Kieke, J.H. Haw, J. Am. Chem. Soc. 114 (1992) 8552.
96. P. Mars, J.J. Scholten, P. Zwietering, Adv. Catal. 14 (1963) 35.
97. C. Di Valentin, A. Del Vitto, G. Pacchioni, S. Abbet, A.S. Worz, K. Judai, U. Heiz, J. Phys. Chem. B 106 (2002) 11961.
98. M. Ziolek, J. Kujawa, O. Saur, J.C. Lavalley, J. Phys. Chem. 97 (1992) 9761
99. X.D. Peng, M.A. Barteau, Langmuir 5 (1989) 1051.
100. G. Patermarakis, Appl. Catal. A 252 (2003) 231.
101. T. Yumura, T. Amenomori, Y. Kagawa, K. Yoshizawa, J. Phys. Chem. A 106 (2002) 621.
102. K.S. Kim, M.A. Barteau, Langmuir 4 (1988) 945.
103. D.E. Fein, I.E. Wachs, J. Catal. 210 (2002) 241.
104. P. Forzatti, E. Tronconi, A.S. Elmi, G. Busca, Appl. Catal. A 157 (1997) 387.
105. T. Kim, I.E. Wachs, J. Catal. 255 (2008) 197.
106. G. Deo, I.E. Wachs, J. Catal. 146 (1994) 323.
107. S. Lim, G.L. Haller, Appl. Catal. A 188 (1999) 277.
108. I.E. Wachs, L.E. Briand, US Patent 7 193 117 B2, 2007, to Lehigh University.
109. R. Malin´ ski, React. Kinet. Catal. Lett. 5 (1976) 265.
110. R. Malin´ ski, M. Akimoto, E. Echigoya, J. Catal. 44 (1976) 101.

111. L.E. Briand, J.-M. Jehng, L. Cornaglia, A.M. Hirt, I.E. Wachs, Catal. Today 78 (2003) 257.
112. G.V. Isaguliants, I.P. Belomestnykh, Catal. Today 100 (2005) 441.
113. A. Bielan´ ski, J. Haber, Oxygen in Catalysis, Dekker, New York, 1991.
114. R. Haggblad et al,. Journal of Catalysis 258 (2008) 345–355
115. US patent 3937669, assigned to Asahi Kasei Kogyo Kabushiki Kaisha
116. J. W. Niemantsverdriet, Spectroscopy in Catalysis. Weinheim, Germany: Wiley-VCH Verlag GmbH & Co. KGaA, 2007.
117. Paula, Peter Atkins, Julio de (2009). Elements of physical chemistry (5th ed. ed.). Oxford: Oxford U.P. p. 459.
118. B. Stuart, Infrared Spectroscopy: Fundamentals and Applications. John Wiley & Sons, 2004, p. 217.
119. Z. M. Khoshhesab, "Reflectance IR Spectroscopy," in Infrared Spectroscopy - Materials Science, Engineering and Technology, T. Theophile, Ed. INTECH, 2012, p. 510.
120. Gardiner, D.J. (1989). Practical Raman spectroscopy.
121. T. Armaroli, T. Bécue, and S. Gautier, "Diffuse Reflection Infrared Spectroscopy (Drifts): Application to the in Situ Analysis of Catalysts," Oil & Gas Science and Technology, vol. 59, no. 2, pp. 215–237, Mar. 2004.